DEVELOPMENT OF A RAY TRACING MODEL FOR ULTRASONIC WAVE PROPAGATION IN COMPOSITE MATERIALS

By

Nitesh Jain

DEPARTMENT OF MECHANICAL ENGINEERING

Indian Institute of Technology Kanpur

FEBRUARY, 2002

DEVELOPMENT OF A RAY TRACING MODEL FOR ULTRASONIC WAVE PROPAGATION IN COMPOSITE MATERIALS

A Thesis Submitted

in Partial Fulfillment of the Requirements

for the Degree of

MASTER OF TECHNOLOGY

by

NITESH JAIN

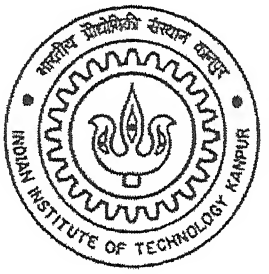

to the

DEPARTMENT OF MECHANICAL ENGINEERING

INDIAN INSTITUTE OF TECHNOLOGY, KANPUR

FEBRUARY, 2002

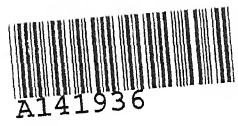

CERTIFICATE

It is certified that the work contained in the thesis entitled **"DEVELOPMENT OF A RAY TRACING MODEL FOR ULTRASONIC WAVE PROPAGATION IN COMPOSITE MATERIALS"**, by NITESH JAIN, has been carried out under our supervision and that this work has not been submitted elsewhere for a degree.

Dr. P. Munshi
(Professor)
Department of Mechanical Engg.
Indian Institute of Technology, Kanpur.

Dr. N. N. Kishore
(Professor & Head)
Department of Mechanical Engg.
Indian Institute of Technology, Kanpur.

Dedicated to

MY PARENTS

Who sacrificed their dreams

so that mine could come true

ACKNOWLEDGEMENTS

I wish to express my deep sense of gratitude to my ever-cherished guides Dr. N.N. Kishore and Dr. P. Munshi for their guidance, invaluable suggestions and constant encouragement. I am sincerely thankful for their valuable suggestions in my academic as well as personal life.

I am paying my great regards to Dr. Bishakh Bhattacharya and Dr. P.M. Dixit for giving me invaluable exposure to composite materials and numerical techniques respectively.

I wish to express my special thanks to Dr. Atul Kumar Agrawal and Mr. S. K. Rathore for their invaluable suggestions and constant encouragement towards completion of my work.

I appreciate and extend my thanks to my lab mates Sqn.Ldr.Sarin, Sajay, Shashi, Samuel, Pradipta and daliraju for their suggestions while I was developing the code.

I would like to thank all my friends IIT friends, Ayush Jha, Ashish Gupta, Gajendra Pandey for making my stay at IITK very enjoyable and memorable. I will cherish the moments forever.

I wish to express my heartful thanks to my sister Harsha and my friend Alankrita for their endless love and care.

Finally, I am grateful to the Almighty and my family for what I am today.

Indian Institute of Technology, Kanpur. -Nitesh Jain

February, 2002

Abstract

The simulation of ultrasonic wave propagation is one of the emerging fields of research in non-destructive testing & evaluation. Looking at the underlying physics, the challenging problems in ultrasonic NDT are on one hand, caused by micro and macrostructural material characteristics as inhomogeneity and anisotropy, and on the other hand by the presence of complex component defect geometries. Both can lead to considerable problems in testing performance and in the interpretation of inspection results. Straightforward solutions like experience-based adaptation in the experimental set-up are in general insufficient, insecure and cost-intensive. The better choice is to combine practical experience with theoretical modeling.

In ultrasonic nondestructive testing (NDT) use is made of the properties of elastic waves propagation in solids in order to detect the defects and materials inhomogeneities. However, modern materials mostly exhibit anisotropic elastic behavior leading to complicated wave propagation phenomenon. To ensure the reliability of ultrasonic inspection techniques, these material properties as well as the influence of microstructural inhomogeneities and the effects of non-planar surfaces and interfaces on ultrasonic wave propagation have to be taken in to account.

In the present work a numerical model has been developed for understanding the ultrasonic wave propagation in composite materials. Typically wave speed, energy flux deviation have been the primary parameters. From this model direction of low inspection sensitivity and also the regions of material to which no ultrasound penetrates can be predicted. The relevance of this work to the ultrasonic non-destructive testing of composite material has been discussed, concluding that care is needed over the choice of wave modes, probe angels and receiver position, to ensure sensitive inspection of the whole component.

CONTENTS

List of Figures

Chapter 1
Introduction

1.1 Introduction

The search for ever lighter, stiffer, and tougher substances from which to construct aerospace vehicles has led inexorably towards more highly engineered, lower density materials like composite materials. The novelty and expense of composite materials has meant, historically, that they are thoroughly inspected prior to use, typically using ultrasonic non-destructive testing.

Ultrasonic materials characterization is the most important application of ultrasonics in aerospace engineering and engineering mechanics. Historically, ultrasonic nondestructive testing (NDT) has been used almost exclusively for detecting macroscopic discontinuities in structures after they have been in service for some time. It has become increasingly evident that it is practical and cost effective to expand the role of ultrasonic NDT testing to include all aspects of materials production and application. Research efforts are being directed at developing and perfecting NDT capable of monitoring (i) material production processes, (ii) material integrity following transport, storage and fabrication, and (iii) the amount and rate of degradation during service. In addition, efforts are underway to develop techniques capable of quantitative discontinuity sizing, permitting determination of material response using fracture mechanics analysis, as well as techniques for quantitative materials characterization to replace the qualitative techniques used in the past. Ultrasonic techniques play a prominent role in these developments because they afford useful and versatile methods for evaluating microstructures, associated mechanical properties, as well as detecting microscopic and macroscopic discontinuities in solid materials.

But, the strong, almost pathological, anisotropy of a composite laminate has significant implications for its elastic behavior and for the propagation of ultrasound. For this reason the use of ultrasonic waves to characterize the mechanical condition of composites has presented engineers inspecting these advanced materials with special challenges. The main objective in this thesis is to study the behavior of ultrasonic wave propagation in composite materials and its use in their nondestructive characterization.

From the beginning, Ultrasonics has been the tool of choice to inspect composites, since the likely defects and important material properties are most easily, and inexpensively, uncovered in ultrasonic nondestructive testing. In ultrasonic NDE, real materials with more complex elastic properties (anisotropy, inhomogeneity, nonlinearity, attenuation, dispersion, temperature-dependence, etc.) are considered. The primary purpose of ultrasonic NDE is to understand the wave-material interaction and assess the desirable material properties from the observed deviation in the ultrasonic response from that of an ideal, defect-free medium.

The growing need for their proper testing of composites/composite laminates raised considerable interest in studying elastic wave propagation in anisotropic media. The main problem of ultrasonic testing methods used in the field of quantitative nondestructive evaluation arises from the difference of wave propagation direction and direction of energy flow. Complex microstructure, macrostructure, or both present in many of today's structural component lead to complicated ultrasound paths due to beam profile distortion and beam path bending. Further in composite materials the direction of wave vector and direction of energy flow is not the same, which lead to beam skewing effects. In this respect mathematical modeling has evolved as an important tool providing assisting analysis and has optimized experimental setups. A particular interest exists in the propagation of pulses as applied in ultrasonic testing, where proper understanding and modeling promises optimized and effective application.

1.2 Literature Survey

Theoretical studies on the elastic wave propagation found in literature are manifold, most of which dealing with isotropic media, only a few are concerned with wave propagation in

anisotropic material. Extending the scope of interest to the wave scattering problem in anisotropic materials for purpose of location and classification of defects and other inhomogeneities, respective studies are approximate in character and mostly restricted to particular geometries and materials symmetries. The theory presented is obtained by applying a coordinate free approach, which had been first used by Chen [1], making it useful in dealing with lay structures.

Synge [2] developed the theory of slowness surfaces after that Musgrave [3] first introduced the idea of superimposing the slowness surface on the geometric space, which contains the incident and emerging waves.

Previously, modeling techniques for inhomogeneous materials have been developed with emphasis on inspection of austenitic welds and claddings. Although the numerical based methods such as finite difference, finite element or finite integration provide good results, they suffer from the requirement of large computation times and hardware requirements. Computationally advantageous analytical ray tracing method developed in this work is very useful in explaining certain phenomenon and in optimizing ultrasonic inspection techniques.

In the literature, only a few ray-tracing algorithm for wave propagation in anisotropic inhomogeneous materials are discussed. Silk [4] divides the austenitic weld region into a number of quadrilateral regions, each with a fixed direction of grain crystals. Ogilvy [5] defined the inhomogeneity of the weld by empirical analytic function that describes the orientation of grain crystals continuously.

Leander [6] developed the relation between the wavefront speed, which is the speed of propagation of a front of a pulse and group velocity concept. Crandell's [7] work was based on use of slowness diagrams to represent wave reflections.

Very few quantitative results have been published on the reflection and refraction of plane elastic waves from an interface between anisotropic media. Musgrave and Fedorov [8] summarized the general theoretical results for the reflection- refraction problem in their comprehensive books. Auld [9] discussed several examples for planes of symmetry. Henneke [10] and McNiven et al [11] reviewed Fedorov's method and discussed critical- angle

phenomena for the elastic waves at an interface. These works mainly focused on finding reflection-refraction angles using geometrical plotting on slowness surfaces. Vandenbossche et al. [12] studied the mode transition in unidirectional composites.

More recently, Rokhlin et al. [13] have described a unified approach to the numerical solution of the reflection-refraction problem for generally anisotropic media. Ogilvy [14] also studied the influence of austenitic weld geometry and manufacture on ultrasonic inspection of weld joints. Ogilvy [15,16] was the first to purpose a ray-tracing model for ultrasonic NDT in austenite welds. Schmitz et al. [17] modified the Ogilvy's model and proposed a new model for austenite materials to follow the longitudinal, horizontal and vertical polarized shear wave propagation from the base material through the cladding in three dimension.

Harker et al. [18] presented full numerical solution of wave equation and showed that ray tracing method gives similar and consistent results. Spies [19] studied elastic wave propagation in general anisotropic media using Green's function and elastodynamic holography.

1.3 Present Work

The nature of wave propagation in anisotropic and inhomogeneous media is significantly different from that in isotropic media. The basic difference may be formulated in the following manner:

(1) For an arbitrarily selected direction in an anisotropic material, the propagation of three elastic wave modes is possible. These three are pure transverse, quasi-transverse and quasi-longitudinal. For special directions called acoustic axes the velocity of two transverse waves coincide.

(2) The displacement direction for each of the wave is uniquely determined by the direction of wave propagation. Only for the propagation along acoustic axes can the transverse wave be arbitrarily polarized as in an isotropic material.

(3) Each of these waves has different phase and group (ray or energy) velocities. The ray velocity is greater than or equal to the phase velocity and its direction does not coincide with wave normal.

To ensure the reliability of ultrasonic inspection techniques, these complex material properties as well as the influence of microstructural inhomogeneities and the effects of non-planar surfaces and interfaces on ultrasonic wave propagation have to be taken in to account. In this respect, simulation and optimization in ultrasonic testing have gained a considerable importance, where mathematical modeling provides a simple method of assisting analysis. In this presentation a ray-tracing model is developed to follow quasi-longitudinal and quasi-shear wave propagation in composite materials for various phase angle.

This dissertation presents a general study of elastic wave propagation in inhomogeneous and anisotropic media. For the present work transversely isotropic symmetry assumption is used, which is the macroscopic symmetry of unidirectional fiber composites, extruded metal matrix composites, as well as ideally structured columnar-grained steels. The results are most general in that they are derived for arbitrary orientation of the rotational symmetry axis which-for the sake of simplicity-will in the following to be referred as the fiber direction. The theory presented is obtained by applying a coordinate free approach making it useful in dealing with lay structures. Subsequent chapters will deal with the plane wave solution of the equation of motion, which is characterized by the respective wave velocity, polarization, and group velocity vectors, the fiber direction being a variable. Then reflection and refractions of plane wave at an interface between two arbitrarily oriented homogeneous transversely isotropic layers are considered. Finally an algorithm to numerically simulate the path of the refracted wave is developed.

An analytical ray tracing method has been developed which is very useful in explaining certain phenomenon and in optimizing ultrasonic inspection techniques. This ray tracing algorithm can be used to trace the ultrasonic wave propagation from the search unit through the composite base material and various inhomogeneities. The algorithm calculates the direction of the sound field, but does not render any amplitude information. Both travel path and travel time information can be inferred from these model. This model can be used to

calculate; the slight deviation which occurs in the direction of wave vector and direction energy flow, and to determine the ray behavior at an interface between two regions of different material properties. Presently a two dimensional analysis has been done and this can be extended to three dimensions with some modifications. Within this region, several defective regions may exist, those being circular, rectangular and elliptical etc. Interfaces between different regions are treated as locally planar.

1.4 Thesis Organization

Chapter II gives the fundamentals of elastic wave propagation in anisotropic media. It describes the equation of motion and plane wave solution of this equation. It discusses the fundamental equation of wave propagation in inhomogeneous and anisotropic media called as Christoffel's equation. Various terms associated with the elastic wave propagation in anisotropic media like phase and group velocity, slowness, energy flux and critical angle are discussed in this chapter. Beam divergence and Beam Skewing associated with elastic waves are also discussed.

In Chapter III refraction and reflection properties of elastic waves are discussed. Snell's law for isotropic has been discussed and it is extended for the anisotropic case. The use of slowness diagrams for determining the reflected and refracted wave properties has been discussed in this chapter.

Chapter IV provides the mathematical formulation for the elastic wave propagation in arbitrarily oriented transversely isotropic media.

Chapter V presents the ray-tracing model, which has been proposed to simulate the ultrasonic wave paths in an inhomogeneous and anisotropic media.

In chapter VI various results of the ray-tracing model developed in the work have been presented and these results are compared with the experimentally obtained results.

Chapter VII presents the conclusion and scope of future work.

Chapter 2
Basics of Ultrasonic wave propagation in anisotropic media

2.1 Introduction

Ultrasonics involves the propagation of acoustic waves. Therefore, it is necessary to understand the basic features of propagating waves and some of the mathematical equations governing wave propagation. Acoustics is the study of time-varying deformations, or vibrations in elastic media. It is concerned with material particles that are small but yet contain many atoms. Within each particle the atoms move in unison. Therefore, acoustics deals with macroscopic phenomena and is formulated as if matter were a continuum.

Propagation of ultrasonic waves in isotropic media has been well studied and can be predicted theoretically with good results. The problem is defined by two constants for the medium, such as λ and μ, the Lame constants and, the incident wave speed and direction. For anisotropic media the problem becomes considerably more complicated, as the elastic constants determining the wave propagation are then directionally dependent.

In general, for a given propagation direction, the wave equation has three solutions with differing speeds corresponding to three different polarization. A plane wave solution to the wave equation describes the possibility of three different wave modes with different phase velocities. These wave modes are not in general, purely longitudinal or transverse, but quasi wave modes.

The effect of anisotropy on ultrasonic wave propagation can be very marked as wave velocities become directionally dependent; group and phase velocities are no longer necessarily parallel or equal in magnitude. These effects lead to beam distortion with in the material, unexpected beam propagation directions, 'favoured' propagation directions,

alteration in spatial profiles and, for inhomogeneous media, beam paths which become curved as the beam propagates through the material. It is therefore important to be able to predict such effects to ensure that beam energy (which travels in the group velocity direction) is directed to the required region for inspection purpose.

2.2 Equations of Motion

The static equilibrium of an arbitrary, three-dimensional solid body occupying volume V that has both surface and body forces requires that the resultant force vector vanish, this gives

$$\frac{\partial \sigma_{ij}}{\partial x_j} + \rho b_i = 0 \tag{2.1}$$

The term b_i is the body force density vector and the result is sometimes referred to as Euler's first relation. This is a static result, however, and to describe the dynamical motion of a continuum, an inertial term accounting for the particle acceleration must be included,

$$\frac{\partial \sigma_{ij}}{\partial x_j} + \rho b_i = \rho \frac{\partial^2 u_i}{\partial t^2}, \tag{2.2}$$

It is also called Cauchy's equation. If body force b_i vanishes for free, unforced motion, it gives

$$\frac{\partial \sigma_{ij}}{\partial x_j} = \rho \frac{\partial^2 u_i}{\partial t^2}, \tag{2.3}$$

and this gives dynamical equation of equilibrium for the elastic continuum. Using constitutive relations Eq. 2.3 can be written as

$$C_{ijkl} \frac{\partial \varepsilon_{kl}}{\partial x_j} = \rho \frac{\partial^2 u_i}{\partial t^2}, \tag{2.4}$$

where C_{ijkl} is the elastic coefficient tensor. It is symmetric and positive definite in the sense that

$$C_{ijkl} n_{ij} n_{kl} \geq 0$$

for all symmetric n_{ij} where equality is satisfied only when $n_{ij} \equiv 0$

By inserting for the strain ε_{kl} its linearized equivalent in terms of the displacement gradient,

$$\varepsilon_{kl} = \frac{1}{2}\left[\frac{\partial u_k}{\partial x_l} + \frac{\partial u_l}{\partial x_k}\right], \tag{2.5}$$

Eq. (2.4) can be written as

$$\frac{1}{2} C_{ijkl} \frac{\partial}{\partial x_j}\left[\frac{\partial u_k}{\partial x_l} + \frac{\partial u_l}{\partial x_k}\right] = \rho \frac{\partial^2 u_i}{\partial t^2}, \tag{2.6}$$

This can be written as

$$C_{ijkl} \frac{\partial^2 u_k}{\partial x_l \partial x_j} = \rho \frac{\partial^2 u_i}{\partial t^2} \tag{2.7}$$

Equation (2.7) is the equation of motion for an infinite linear elastic medium in three dimensions.

2.3 Plane Wave Propagation in Bulk Materials

The plane harmonic wave solution of Eq. (2.7) can be expressed either in index notation or in vector notation as

$$\mathbf{u}(\mathbf{r},t) = A_0 \mathbf{p} \exp i(\mathbf{k}.\mathbf{r} - \omega t) \tag{2.8}$$

$$u_j(x_m,t) = A_0 p_j \exp i(k_m x_m - \omega t) \tag{2.9}$$

where A_0 is the amplitude of the wave, $\mathbf{p}$ (p_j) is the polarization unit vector and ω is the angular frequency. The wavevector $\mathbf{k}$ or (k_m) is given by

$$\mathbf{k} = k\mathbf{n}, \qquad k = \frac{2\pi}{\lambda} \tag{2.10}$$

where $\mathbf{n}$ is a unit vector in the direction of wave propagation, and λ is the wavelength. The phase of the wave ϕ is given by

$$\phi = \mathbf{k} \cdot \mathbf{r} - \omega t \tag{2.11}$$

For points of constant phase on the wave is

$$\mathbf{k} \cdot \mathbf{r} - \omega t = const. \tag{2.12}$$

Taking differential and rearranging gives

$$\mathbf{k} \cdot \frac{d\mathbf{r}}{dt} = \omega \tag{2.13}$$

Substituting $\mathbf{k}$ from Eq. (2.10) and let ξ be the projection of the wavefront position vector $\mathbf{r}$ on the direction of wave propagation ($\xi = \mathbf{n} \cdot \mathbf{r}$), as shown in Fig. 2.1,

$$k\mathbf{n} \cdot \frac{d\mathbf{r}}{dt} = \omega \tag{2.14}$$

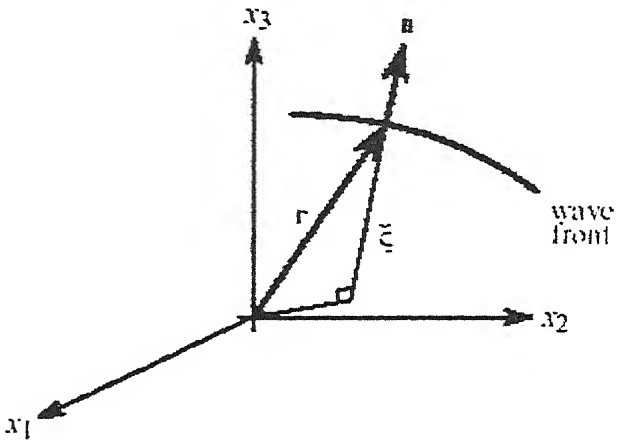

Figure 2.1 Wavefront moving in a rectangular coordinate system

and the propagation of a point of constant phase proceeds with phase velocity V given by

$$V = \frac{d\xi}{dt} = \frac{\omega}{k} \tag{2.15}$$

in vectorial form

$$\mathbf{V} = V\mathbf{n} = \frac{\omega}{k}\mathbf{n}. \tag{2.16}$$

Substituting the plane harmonic wave solution (2.9) into the equation of motion (2.7) gives

$$\rho\omega^2 u_i = C_{ijlm} k_j k_l u_m, \tag{2.17}$$

Or

$$C_{ijlm} n_j n_l u_m - \rho V^2 p_i = 0, \tag{2.18}$$

By using $p_i = \delta_{im} p_m$, the above equation can be rewritten as

$$\left(C_{ijlm} n_j n_l - \rho V^2 \delta_{im}\right) p_m = 0. \tag{2.19}$$

where δ_{im} is the Kroneker delta. In order to have a nontrivial solution for p_m, the determinant of the coefficients for the linear equation Eq. (2.18) must vanish, leading to the following well known eigenvalue equation, also known as Christoffel's equation,

$$\left|C_{ijlm} n_j n_l - \rho V^2 \delta_{im}\right| = 0. \tag{2.20}$$

if $\lambda_{il} = C_{ijlm} n_j n_l$ and $\eta = \rho V^2$

Eq. (2.19) can also be written as

$$(\lambda_{il} - \eta\delta_{im})\, p_m = 0 \tag{2.21}$$

From the properties of C_{ijlm}, it follows that λ_{il} is also symmetric and positive definite. Therefore, all the eigen values of λ_{il} are real and positive and their corresponding eigenvectors are orthogonal.

This can be interpreted as that a for a given direction of wave propagation **n** there will be three phase velocities, and three corresponding displacement vectors will be orthogonal. These three waves are pure shear, quasi-longitudinal and quasi shear wave.

Pure longitudinal mode (the polarization vector **p** is parallel to the propagation direction m, l, n are the direction cosines of propagation direction) is obtained only when $p_i=n_i$ (i = 1,2,3). Pure shear mode (the polarization vector **p** is normal to the propagation direction **n**) are obtained only when $p_1n_1+p_2n_2+p_3n_3=0$ (i.e. $\mathbf{p}\cdot\mathbf{n}=0$) In all other cases, either quasi-longitudinal or quasi-shear modes can only propagate. It can also be noted that any general wave propagation can be split in three modes: pure shear (S), quasi-longitudinal (QL) and quasi-shear (QS). In a elaborate form Eq.(2.21) can be written as

$$\begin{bmatrix} \lambda_{11}-\rho V^2 & \lambda_{12} & \lambda_{13} \\ \lambda_{12} & \lambda_{22}-\rho V^2 & \lambda_{23} \\ \lambda_{13} & \lambda_{23} & \lambda_{33}-\rho V^2 \end{bmatrix} \begin{Bmatrix} p_1 \\ p_2 \\ p_3 \end{Bmatrix} = \begin{Bmatrix} 0 \\ 0 \\ 0 \end{Bmatrix} \tag{2.22}$$

where λ in terms of elastic constants can be given as

$$\begin{aligned}
\lambda_{11} &= \ell^2 C_{1111}+m^2 C_{1212}+n^2 C_{1313}+2mnC_{1312}+2n\ell C_{1113}+2m\ell C_{1112} \\
\lambda_{22} &= \ell^2 C_{1212}+m^2 C_{2222}+n^2 C_{2323}+2mnC_{2223}+2n\ell C_{2312}+2m\ell C_{2212} \\
\lambda_{33} &= \ell^2 C_{1313}+m^2 C_{2323}+n^2 C_{3333}+2mnC_{3323}+2n\ell C_{3313}+2m\ell C_{2313} \\
\lambda_{12} &= \ell^2 C_{1112}+m^2 C_{2212}+n^2 C_{2313}+mn(C_{2312}+C_{2213})+n\ell(C_{1123}+C_{1312})+m\ell(C_{1122}+C_{1212}) \\
\lambda_{13} &= \ell^2 C_{1113}+m^2 C_{2312}+n^2 C_{3313}+mn(C_{2313}+C_{3312})+n\ell(C_{1133}+C_{1313})+m\ell(C_{1123}+C_{1312}) \\
\lambda_{23} &= \ell^2 C_{1312}+m^2 C_{2223}+n^2 C_{3323}+mn(C_{2323}+C_{2233})+n\ell(C_{3312}+C_{2313})+m\ell(C_{2213}+C_{2312})
\end{aligned} \tag{2.23}$$

m, l, n are the direction cosines of propagation direction

2.4 Phase and Group Velocity

Phase velocity is defined as the velocity with which plane wave crests and troughs travel through a medium and is expressed as the ratio of the frequency of vibration and the wave number (i.e. the number of wavelengths per unit distance normal to the wavefronts). Group

velocity, also known as ray or energy velocity, is defined as the velocity with which the energy of the wave propagates.

An additional complication in anisotropic media is that the wave normal does not necessarily coincide with the propagation direction of the energy (ray direction). An arbitrary wave is dependent on time and spatial coordinates as $f = f(\omega t - k x)$. In dispersive media, where the velocity is dependent on frequency, the acoustic energy of a narrow-band tone-burst propagates at the group velocity V_g. The phase velocity is simply

$$V = \frac{\omega}{k}, \tag{2.24}$$

and the group velocity is given as

$$V_g = \frac{\partial \omega}{\partial k} \tag{2.25}$$

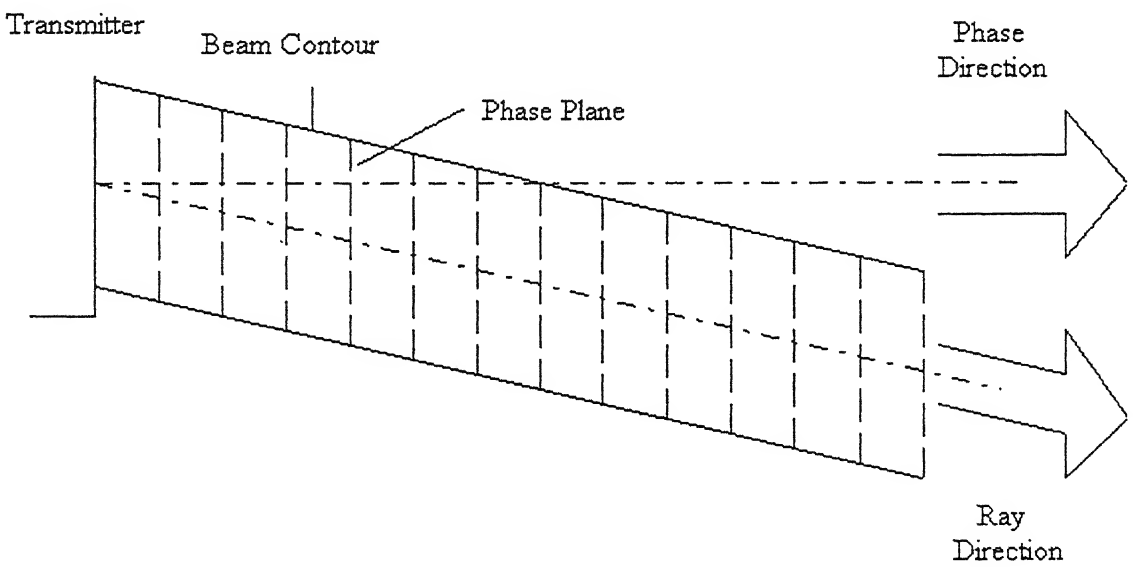

Figure 2.2 Deviaiton between phase direction and ray direction

In the symmetry directions only pure modes propagate and the phase and ray directions are necessarily parallel. This is because deviation from a symmetry direction in any direction

must have the same effect as an equal deviation in the opposite direction. This also means that the velocities of pure waves are either maxima or minima for that particular mode. In any other directions the beam becomes skewed as illustrated in Figure 2.2. Needless to say that this skewing effect makes it more difficult to align the ultrasonic transducers for optimal inspection in highly anisotropic materials such as unidirectional composite laminates. The same effect is also responsible for the lateral shift of the transmitted ultrasonic beam through anisotropic plates that occurs even at normal incidence.

2.5 Energy Flux and Group Velocity

For acoustic waves propagating in elastic solids, the kinetic T and strain U energy densities are given as

$$T = \frac{1}{2}\rho \dot{u}^2, \tag{2.26}$$

$$U = \frac{1}{2} C_{iklm} \varepsilon_{ik} \varepsilon_{lm}, \tag{2.27}$$

Both T and U are scalar quantities. The total energy contained in a volume V is given by

$$E = \int_V (T + U) dV \tag{2.28}$$

and the rate of change of energy with respect to time is given by

$$\dot{E} = \frac{dE}{dt} = \int_V \frac{\partial (T+U)}{\partial t} dV. \tag{2.29}$$

Using Eqs. (2.26) and (2.27) and the chain rule in the derivatives, Eq. (2.29) can be written as

$$\dot{E} = \int_V (\rho \dot{u}_i \ddot{u}_i + \frac{\partial U}{\partial \varepsilon_{ik}} \dot{\varepsilon}_{ik}) dV \tag{2.30}$$

a slight mathematical treatment and use of Gauss' theorem will give

$$\dot{E} = \int_V \dot{u}_i \left[\rho \ddot{u}_i - \frac{\partial \sigma_{ik}}{\partial x_k} \right] dV + \oint \sigma_{ik} \dot{u}_i dS_k, \qquad (2.31)$$

From equation of motion

$$\rho \ddot{u}_i - \frac{\partial \sigma_{ik}}{\partial x_k} = 0, \qquad (2.32)$$

Eq. (2.31) reduces to

$$\dot{E} = \oint \sigma_{ik} \dot{u}_i dS_k$$

Here by introducing the vector of energy flow density **P**, that is often called the acoustic Poynting vector, as follows

$$P_k = -\sigma_{ik} \dot{u}_i. \qquad (2.33)$$

P is directed towards the local direction of energy transfer. Finally, from Eq. (2.32)

$$\dot{E} + \oint \mathbf{P}.d\mathbf{S} = 0, \qquad (2.34)$$

where dS denotes the elementary surface area vector that is everywhere normal to the surface S which encloses the volume V .

Using the plane harmonic wave solution (2.9) the kinetic and strain energy densities can be given as

$$T = \frac{1}{2} \rho \dot{u}^2 = \frac{1}{2} \rho \omega^2 A_0^2 \sin^2 (k_n x_n - \omega t) \qquad (2.35)$$

and

$$U = \frac{1}{2} C_{ijkl} k_j k_l A_0^2 p_i p_k \sin^2(k_n x_n - \omega t) \tag{2.36}$$

respectively, where it is exploited that the polarization vector is defined as a unit vector. From the equation of motion,

$$\rho \omega^2 u_i = C_{ijkl} k_j k_l u_m . \tag{2.37}$$

Multiplying both sides of the equation by u_i gives,

$$\rho \omega^2 u^2 = C_{ijkl} k_j k_l u_m u_i , \tag{2.38}$$

which leads to the conclusion that the kinetic and strain energy densities of a propagating plane wave are always equal

$$T = U \tag{2.39}$$

Propagating waves exhibit spatial and temporal invariances that require that the kinetic and potential components maintain the same balance everywhere and all the time. In terms of energy density this means that the two components must be equal, i.e., they rise and fall together everywhere and all the time. It is a consequence of the Reciprocity Theorem, which requires that the transfer efficiency between two coupled forms in which energy can exist must be the same in both directions. Under these conditions, balance is feasible only if the kinetic and strain energies are equal.

The time-averaged total energy density $\overline{E}$ and energy flow density vector $\overline{P_i}$ are given as

$$\overline{E} = \frac{1}{2} \rho \omega^2 A_0^2 \tag{2.40}$$

$$\overline{P_i} = \frac{1}{2} C_{ijlm} k_l \omega A_0^2 p_m p_j \tag{2.41}$$

Finally, the energy flow velocity Vg is defined as

$$V_{gi} = \frac{\overline{P}_i}{\overline{E}} = \frac{C_{ijlm} k_l p_m p_j}{\rho \omega}. \tag{2.42}$$

2.6 Relation Between the Phase and Group Velocities

The group velocity can be written in terms of phase velocity as

$$V_{gi} = \frac{C_{ijlm} n_l p_m p_j}{\rho V} \tag{2.43}$$

In order to find the relation between $\mathbf{V}_g$ and $\mathbf{V}$ a vector $\mathbf{Q}$ is defined here as follows

$$Q_i = C_{ijlm} n_l p_m p_j \tag{2.44}$$

group velocity can be written as

$$V_{gi} = \frac{Q_i}{\rho V} \tag{2.45}$$

From the equation of motion (2.36)

$$C_{ijlm} n_j n_l p_m p_i - \rho V^2 = 0. \tag{2.46}$$

This can be written as

$$Q_i n_i = \rho V^2 \tag{2.47}$$

Finally, from Eqs. (2.46) and (2.48),

$$V_{gi} n_i = V \tag{2.48}$$

Or

$$Vg\cos\gamma = V, \tag{2.49}$$

where γ is the angle between $\mathbf{V_g}$ and $\mathbf{V}$. This relation indicates that $\mathbf{V}$ is the projection of $\mathbf{V_g}$ in the direction of wave propagation

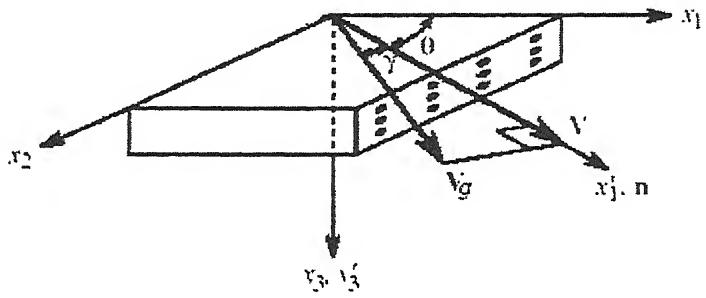

Figure 2.3 Relation beween Phase velocity vector Group velocity vector

2.7 Slowness Surface

An extremely useful insight of the effects of anisotropy can be obtained by examination of the slowness surfaces of a material. The correct interpretation of these surfaces can aid in the prediction of beam profiles in anisotropic materials.

The slowness vector of a wave, **m**, is defined as

$$\mathbf{m} = \frac{\mathbf{n}}{V} \tag{2.50}$$

Hence **m** has magnitude given by the reciprocal of the phase velocity. Since, for an anisotropic material, a wave's phase velocity magnitude is dependent on the phase velocity direction, it can be said that $|\mathbf{m}|$ is a function of **n**, i.e.

$$\mathbf{m} = \mathbf{m}(\mathbf{n}) \tag{2.51}$$

If the value of **m** is plotted for all possible values of **n**, i.e. all phase velocity direction, then a three-dimensional surface mapped out by the end points of the slowness vectors, is called slowness surface. Since there are three modes of wave propagation in anisotropic materials there exists three slowness surfaces corresponding to the three wave modes.

For an isotropic material each surface, corresponding to a wave polarization, will be a sphere since m is independent of **n** (i.e. phase velocity is independent of direction in isotropic materials)

Figure 2.6 shows a slice through the slowness surface for transversely isotropic. There are several points to notice from the figure

1. Each slowness surface is not a circle, indicating departure from isotropy.

2. The three slowness surfaces, one for each mode, are of different shapes. This immediately indicates that no two wave modes will behave in the same manner with in the composite.

A further use of slowness surface arises in depicting group velocity i.e. energy direction. Theory shows that for any phase velocity direction **n**, the normal to slowness surface for that particular value of **n** is in the direction of the group velocity.

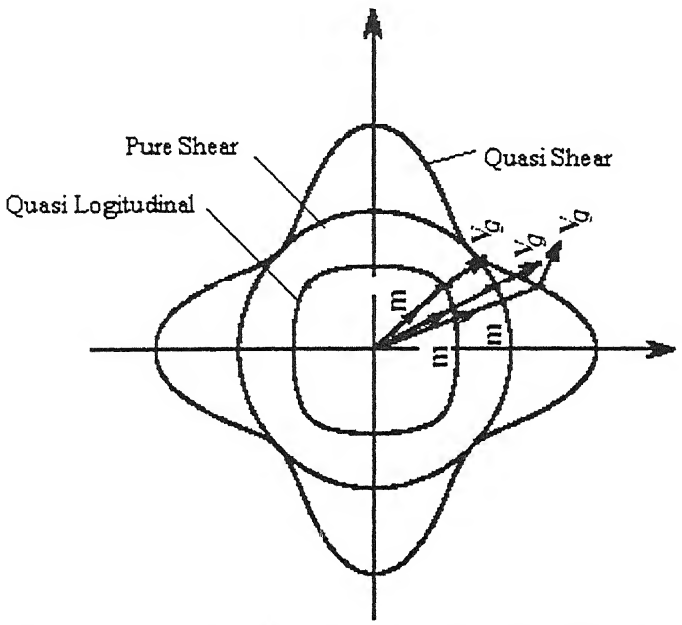

Figure 2.4 A general slowness diagram for an anisotropic material

The usefulness of this unusual parameter than conventional velocity, lies in the nature of anisotropy itself. In many cases (e. g., refraction at a plane interface or diffraction from a periodic structure) the wave direction is determined by the wave speed. For example, according to the well-known Snell's law, the refraction angles of all reflected and transmitted waves are determined by the incident angle θ_i and incident velocity V_i as follows

$$\frac{\sin\theta_r}{V_r}=\frac{\sin\theta_i}{V_i} \tag{2.52}$$

where the subscript r represents any of the refracted waves. This simple explicit relation for θ_r becomes an implicit one for anisotropic cases

$$\frac{\sin\theta_r}{V_r(\theta_r)}=\frac{\sin\theta_i}{V_i(\theta_i)}. \tag{2.53}$$

With slowness instead of velocity, the above condition becomes

$$m_r(\theta_r)\sin\theta_r=m_i(\theta_i)\sin\theta_i, \tag{2.54}$$

i.e., the projections of the slownesses of all waves are the same on the interface. This feature can be readily exploited to determine the refraction angles in a graphical way. At first the horizontal slowness projection $m=m_i(\theta_i)\sin\theta_i$ is determined from the angle of incidence. Then, for each particular refracted wave the refraction angle is determined from the intersection point of the slowness diagram with the same vertical line representing m. A special case in which the vertical line does not intersect a particular mode's slowness diagram then that mode will no longer exist in propagation.

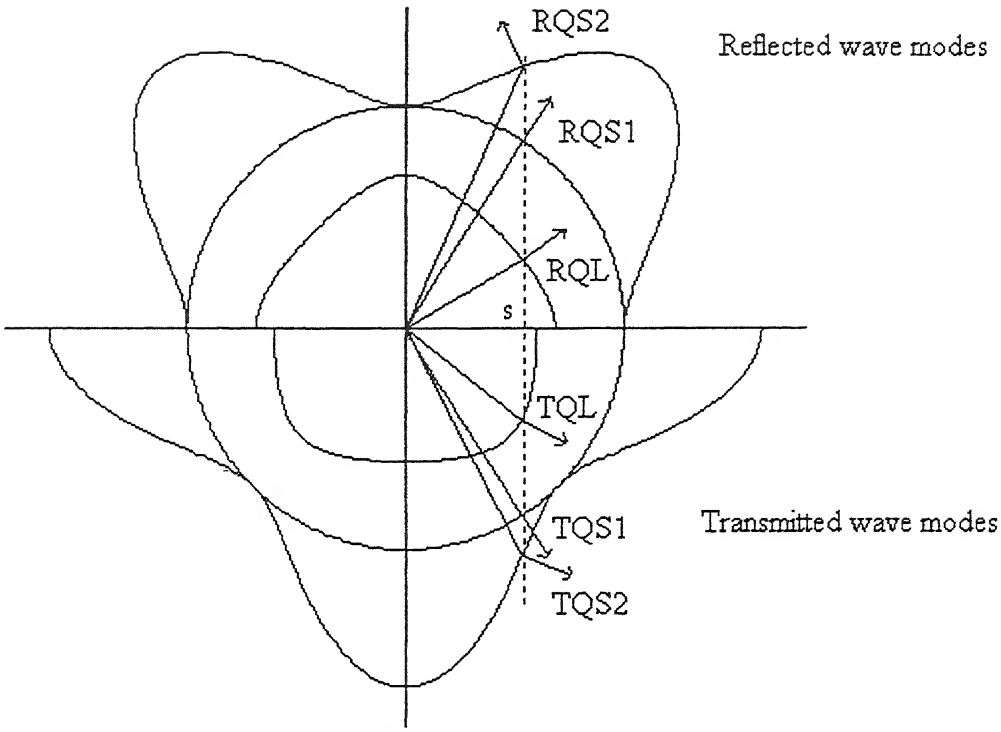

Figure 2.5 representation of reflected/transmitted wave modes using slowness diagram

2.8 Beam Divergence

Beam divergence is measure of how fast the energy within the beam is spreading as the beam travels. For example, if wave has zero divergence then the spatial beam width remains constant along the beam path and the associated energy will be highly concentrated. Conversely, a large beam divergence leads to wide beams with a diffuse energy spread. A good measure of beam divergence is obtained by considering a small change in phase velocity direction, $\Delta\theta_p$, and finding the associated change in group velocity direction, $\Delta\theta_g$. The modulus of the ratio of these two gives beam divergence

$$D = \left| \frac{\Delta\theta_g}{\Delta\theta_p} \right| \tag{2.55}$$

If D=1 (as is always the case for waves in isotropic materials), then beam widths are as expected for a given transducer. However, if D>1, then for a transducer whose frequency, dimensions, etc. are known, then angular speed of beam will be much larger then expected.

This arises because adjacent layers in beam, of only slightly different phase velocity direction, have widely group velocity (or energy propagation) directions. Therefore, the beam spread from a conventional transducer when injecting ultrasound into anisotropic material will be much wider and hence more diffuse then would be case for isotropic material. Conversely, when D<1 it is find that an ultrasonic beam injected into anisotropic material will be narrower and hence more concentrated in energy, than it would be in an isotropic material.

A good indication of beam divergence behavior as a function of propagation direction (i.e. phase velocity direction) can be obtained by examination of the slowness surface of a material. The local radius of curvature at any point on the slowness surface is a measure of beam divergence as this controls the rate of change of the surface normal with distance along the surface. Since the surface normal is the direction of group velocity, and distance along the surface is proportional to change in phase velocity direction (**m**), it gives

$$\left|r_c(\theta_p)\right| = \left|\mathbf{m}(\theta_p)\right| \left|\frac{\Delta\theta_p}{\Delta\theta_g}\right| \tag{2.56}$$

Here, $r_c(\theta_p)$ is the radius of the curvature of the surface.

The beam divergence is given by

$$D = \left|\frac{\Delta\theta_g}{\Delta\theta_p}\right| = \frac{1}{\left|r_c(\theta_p)\right|}\left|\mathbf{m}(\theta_p)\right| \tag{2.57}$$

A larger radius of curvature leads to small beam divergence and vice versa. Inspection of the slowness surface can give a good quantitative feel for beam divergence.

To illustrate the beam divergence effects discussed above, let us consider the situation shown in fig 2.6, where a transducer fires ultrasound into a homogeneous transversely isotropic medium. By varying the angle of transducer beam the effect of probe direction on beam width can be illustrated. It is the shape of beam emerging at the bottom. To understand

the location of the emergent beam, which is not always directly under the transmitter, consideration of beam skewing is required.

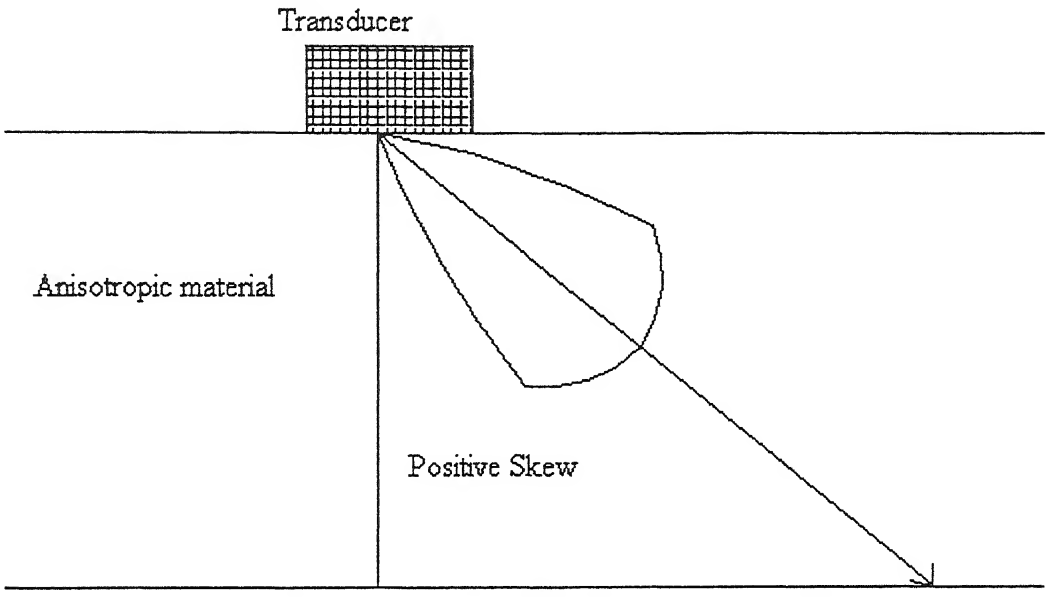

Figure 2.6 Beam divergence and Beam skew

2.9 Beam skewing

The beam skew is defined as the difference between the group angle and phase angel. A positive skew angel signifies that the group angel is larger than the phase angel. Hence for all wave mode and phase angel combination having non-zero skew angel, in addition to change in beam profiles (due to beam divergence), the emerging beam's positions will be altered from where it would be if the block were of isotropic material.Beam skew,ψ, can be given as

$$\psi = \theta_g - \theta_p \tag{2.58}$$

giving

$$D = \frac{d\theta_g}{d\theta_p} = \frac{d\psi}{d\theta_p} + 1 \tag{2.59}$$

From this relation it can be clearly seen that beam divergence is very low when rate of change of skew is ≈ -1. Conversely divergence is high when the rate of change skew is large.

2.10 Closure

In this Chapter fundamentals of ultrasonic wave propagation in anisotropic media have been presented. The fundamental equation of wave propagation in inhomogeneous and anisotropic media called as Christoffel's equation has been discussed. Various terms associated with the elastic wave propagation in anisotropic media like phase and group velocity, slowness, energy flux and critical angle has been discussed. Beam divergence and Beam Skewing associated with elastic waves has been also discussed.

Chapter 3
Reflection and Refraction of Waves at a Planar Interface

3.1 Introduction

Nondestructive ultrasonic testing of inhomogeneous and composite materials is affected by several special features of wave propagation that arise from the strong anisotropy and inhomogeneity of these materials. The resulting complexity requires re-examination of old testing methodologies and development of new ones. One of the most fundamental phenomena in ultrasonic NDE is the reflection-refraction of ultrasonic waves at a plane interface. Even the simplest test procedure requires understanding of mode conversion and knowledge of elastic wave reflection and transmission coefficients and refraction angles. Reflection-refraction phenomena, while straightforward and well documented for isotropic materials, are much more complicated for anisotropic materials. In anisotrpic case Incident and reflected/refracted waves can no longer be thought of as purely longitudinal or transverse with the appropriate directionally constant wave speeds. In addition, the direction of maximum energy flow does not, in general, coincide with the direction of the wave normal.

3.2 Fundamentals of Reflection and Refraction

The simplest situation is depicted in Figure 3.1a, where a wave encounters a boundary at right angle or normal incidence. The interaction only involves reflection of some of the wave and transmission of a portion, with the amount of energy in each part depending on the material characteristics. A more complicated situation may arise, particularly in solids, when the wave strikes at an angle, or at oblique incidence. What may occur, as shown in Fig. 3.1b, is that two types of waves are reflected for a single incident wave. This phenomenon is

known as mode conversion, and is illustrated for the case of a longitudinal wave generating both longitudinal and shear waves. Yet another aspect is involved when waves encounter edges. Complex scattering and diffraction of the waves may occur, similar to optics (figure 3.1c).

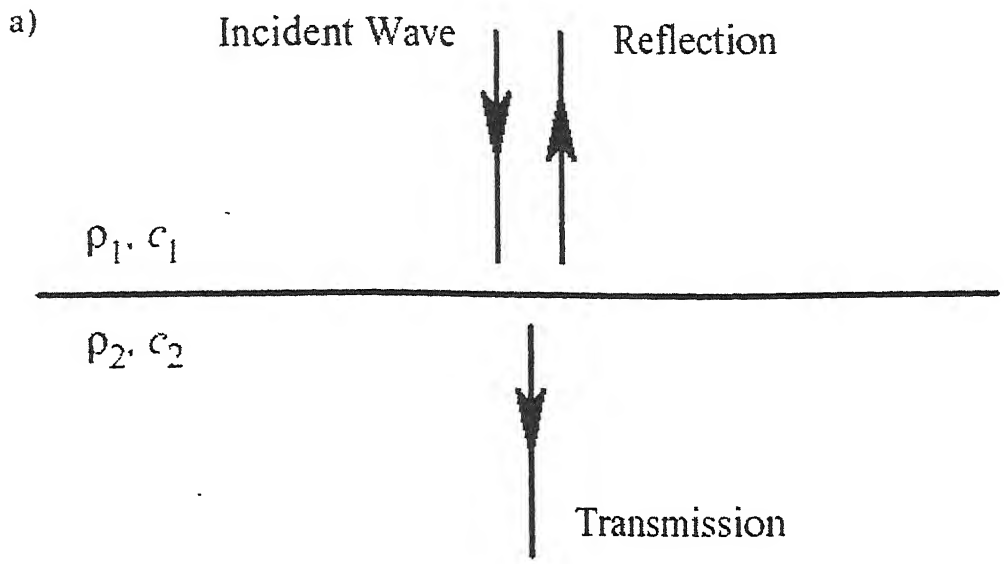

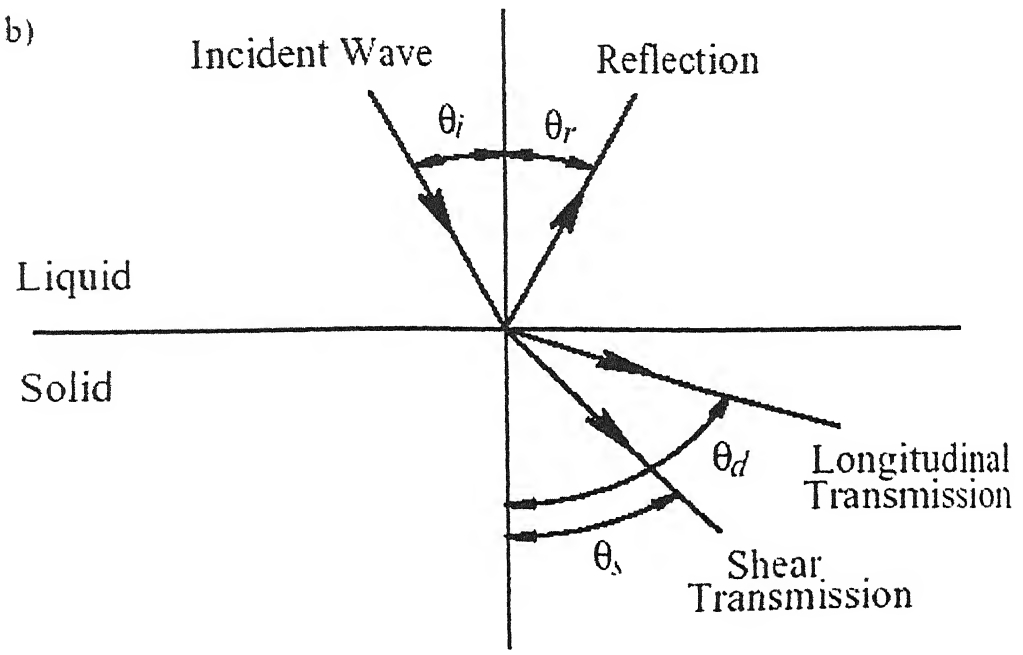

c)

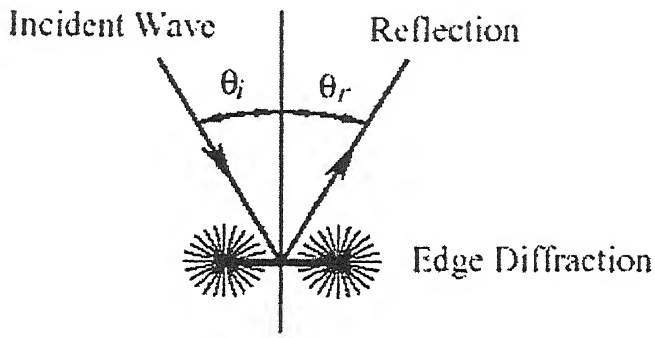

Figure 3.1 Different type of acoustic wave interaction with material discontinuties: (a) Normal Incidence (b) Oblique Incidence and Mode conversion (c) Diffraction and Scattering

3.3 Reflection and Refraction in Isotropic materials

3.3.1 Snell's Law (Isotropic case)

In the case of a plane interface between two isotropic elastic media in "welded" contact (rigid boundary conditions), imply continuity of all stresses and displacements across the interface. Figure 3.2 shows a schematic diagram of a plane wave with wavenumber k_i incident on the interface at angle ϕ_i. The parallel lines with spacing equal to the incident wave length λ_i correspond to equal-phase planes orthogonal to the incident plane. By definition, the wavenumber $k_i = 2\pi/\lambda_i$ is the magnitude of the wave vector $\vec{k}_i$. The incident wave is converted at the interface into reflected and transmitted waves. The refraction angle of the transmitted wave is ϕ_r and its wave number is k_t. The wave fronts of the transmitted and reflected waves should match that of the incident wave along the entire interface. This follows from the requirement that the interface continuity conditions be satisfied not only at one particular point (e.g., at the origin), but everywhere along the interface. Any mismatch among the phases of the incident, reflected, and transmitted waves, that together must satisfy the boundary conditions, would lead to an inevitable variation of their relative contributions along the interface and thereby would prevent them from perfectly balancing each other over the whole boundary.

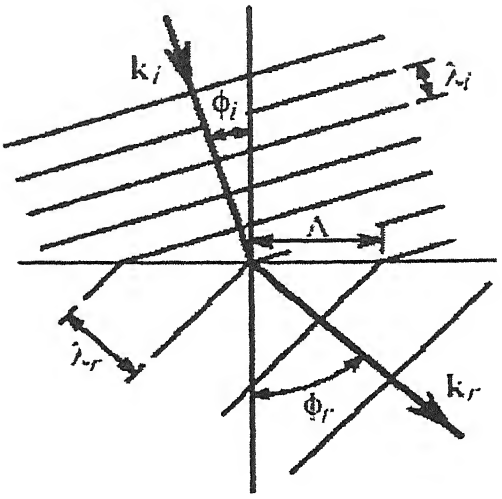

Figure 3.2 A schemetic diagram of a plane wave incident on the interface

From the universal phase matching requirement along the interface

$$\Lambda \sin \phi_i = \lambda_i \text{ and } \Lambda \sin \phi_r = \lambda_r \tag{3.1}$$

where λ_i and λ_r are the wavelengths for the incident and transmitted waves and Λ, as shown in Fig. 4.1, is the spatial period of the wave motion along the interface. Equation (3.1) is Snell's law that can be also written in terms of the wavelengths

$$\Lambda = \frac{\lambda_i}{\sin \phi_i} = \frac{\lambda_r}{\sin \phi_r}, \tag{3.2}$$

In terms of velocities

$$V = \frac{V_i}{\sin \phi_i} = \frac{V_r}{\sin \phi_r}, \tag{3.3}$$

In terms of wave number

$$K = k_i \sin \phi_i = k_r \sin \phi_r \tag{3.4}$$

Here, V_i and V_r are the phase velocities of the incident and refracted waves, respectively. Figure 3.3 shows the geometrical interpretation of Snell's law in terms of velocity vectors (a) and wave vectors (b), which can be summarized in the following way:

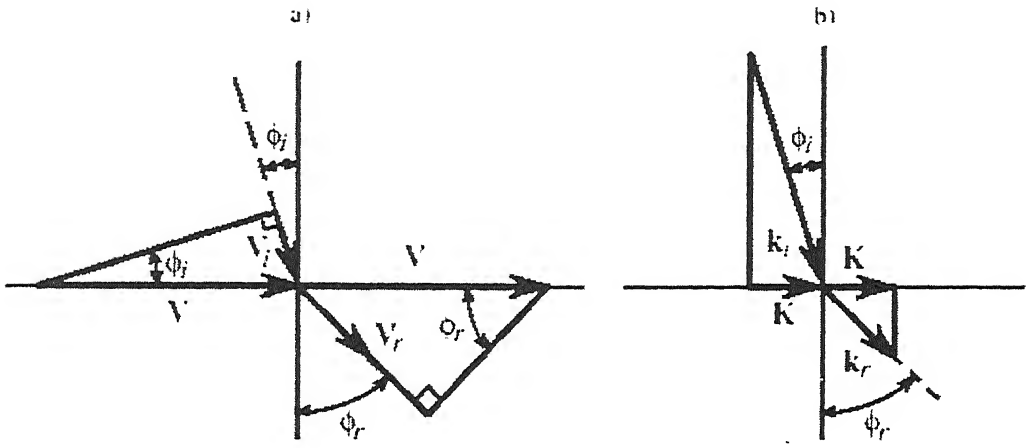

Figure 3.3 Geometrical interpretation of Snell's law in terms of (a) Velocity (b) wave vectors

1. The traces of the wavelengths (3.2) and velocities (3.3) of the incident, reflected and refracted waves on the interface are equal. The phase velocity trace V is shown in Fig. 3.2(a).
2. The projections of the wave vectors of the incident, reflected and refracted waves on the interface are equal. The wave vector projection K is shown in Fig. 3.2(b) ($K = \omega/V$).

The same conclusion holds for multilayered media. The projections on the interfaces of the transmitted and reflected wavenumbers always equals to that of the incident wave. In general at an interface, the incident wave is converted into longitudinal and transverse waves in such a way that Snell's law will hold for both types of waves, as shown in Fig. 3.4. Here, the incident wave k_i produces four waves, namely a reflected longitudinal wave k_{l1}, a reflected transverse wave k_{t1}, a transmitted longitudinal wave k_{l2}, and a transmitted shear wave k_{t2}.

According to Snell's law, all five (incident, two reflected, and two transmitted) waves have the same wave vector projection K on the interface. This is the basic concept on which reflection and refraction analysis of waves in the case of anisotropic and inhomogeneous materials can be based. In anisotropic case the incident wave is generally converted at the interface into three possible modes of elastic waves and Snell's law is similarly satisfied.

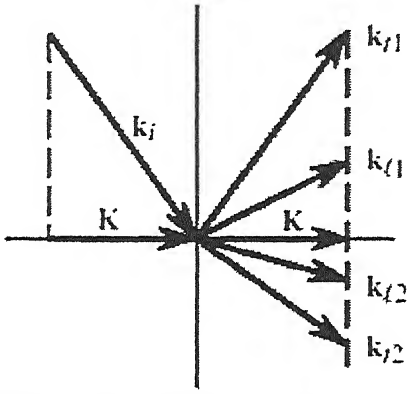

Figure 3.4 Reflected and Transmitted wave vectors produced at an isotropic solid/solid interface by an obliquely incident wave

3.3.2 Reflection/Refraction Analysis Using Slowness Surfaces

The concept of the slowness surface has been introduced previously. Since in isotropic materials the wave velocity is independent of the propagation direction the slowness surface is a sphere with radius m = 1/V. As an example, Fig. 3.5(a) illustrates the case of a plane wave incident from a faster to a slower medium (mode conversion is avoided for the sake of simplicity), i.e., V1 > V2. The wave vectors for the incident, reflected, and transmitted waves are k_i, k_1, and k_2, respectively, and ϕ_i is the incident angle. The wave vector of the incident wave originates on the slowness surface and is directed at angle ϕ_1 toward the origin as shown in the figure. Angles of the reflected ϕ_1 and transmitted ϕ_2 waves can be found by equating the projections on the interface of all wave vectors involved.

Figure 3.5(b) illustrates the case of incidence at grazing angle ($\phi_i = 90^0$). The refraction angle is clearly determined from the figure as $\sin\phi_2 = \frac{V_2}{V_1}$. The case of a wave arriving from a

slow to a fast medium at oblique incidence is illustrated in Fig. 3.5(c). Here the refraction angle is larger than the incident one, $\phi_2 > \phi_i$. An important phenomenon occurs when ϕ_1 reach the critical angle ϕ_{cr} as shown in Fig. 4.4(d). At the critical angle the refraction angle ϕ_2 becomes 90^0 and the refracted wave becomes evanescent, i.e., an inhomogeneous wave that exponentially decays into the lower medium. In the absence of attenuation this wave has only reactive power and does not carry energy, however it may affect the phase of the reflected signal.

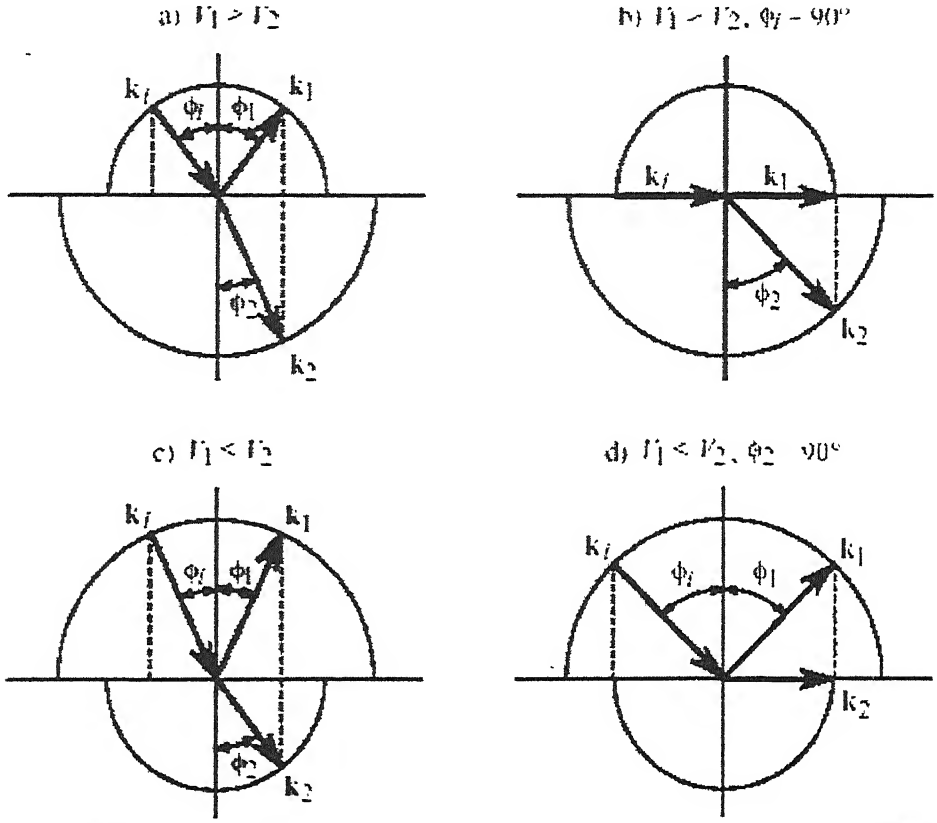

Figure 3.5 Use of slowness diagram in finding the reflected and refracted waves in different cases

There exist a "critical" incident angle which a wave makes with the traction free surface of an elastic half space and that as the incident angle passes through this critical value, the energy flux vector of the reflected or refracted wave passes through grazing incidence and emerges as a surface wave. This wave is like a Rayleigh wave in that the amplitude of motion decay exponentially away from interface, particle motions have an elliptical orbit, and the wave travels with a constant phase velocity

3.4 Reflection and Refraction at an Interface between two Anisotropic Media

3.4.1 Snell's Law (Anisotropic Case)

Application of Snell's law for anisotropic materials can be understand by considering a monochromatic plane wave incident on the interface between two anisotropic solids as shown in Fig. 3.6 the interface coincide with x_1x_2 plane and **b** is a unit vector parallel to the x_3

The displacement vector u_j of an elastic wave can be given as

$$u_j = A_0 p_j \exp[i(k_l x_l - \omega t)] \tag{3.5}$$

In terms of the previously defined slowness vector **m**, the displacement vector can be also written in the following alternative form

$$u_j = A_0 p_j \exp[i\omega(m_l x_l - t)] \tag{3.6}$$

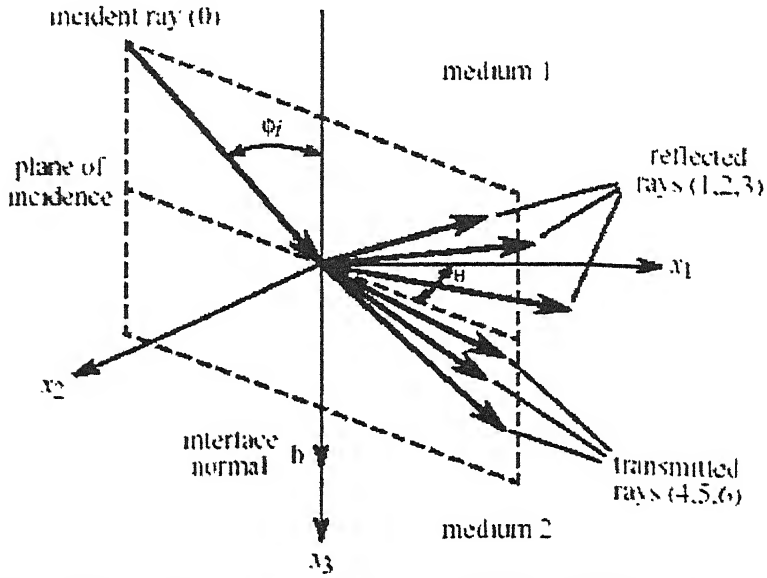

Figure 3.6 Acoustic wave incident on an interface betweeen two anisotropic media

Because of assumed rigid boundary conditions at the interface, it requires continuity of both displacements and tractions across the boundary. Then, continuity of the displacements and tractions at the boundary (x3 = 0) is given by

$$u_i^0 + \sum_{\alpha=1}^{3} u_i^\alpha = \sum_{\alpha=4}^{6} u_i^\alpha \tag{3.7}$$

and

$$\sigma_{i3}^0 + \sum_{\alpha=1}^{3} \sigma_{i3}^\alpha = \sum_{\alpha=4}^{6} \sigma_{i3}^\alpha. \tag{3.8}$$

The incident wave is marked with superscript 0, and the three reflected and three transmitted waves are marked with superscripts 1; 2; 3 and 4; 5; 6, respectively.

Using the relevant displacement-strain and constitutive relationships, the stress tensor can be expressed as

$$\sigma_{ik} = C_{ikjm} \frac{\partial u_j}{\partial x_m} = i\omega m_m A_0 p_j \exp[i\omega(m_l x_l - t)]. \tag{3.9}$$

Substituting Eq. (3.6) into (3.7) the displacement continuity (3.7) can be written as

$$A_0^0 p_j^0 \exp\left(i\omega m_l^0 x_l^0\right) = -\sum_{\alpha=1}^{3} A_0^\alpha p_j^\alpha \exp\left(i\omega m_l^\alpha x_l^\alpha\right) + \sum_{\alpha=4}^{6} A_0^\alpha p_j^\alpha \exp\left(i\omega m_l^\alpha x_l^\alpha\right), \tag{3.10}$$

Similarly Substituting Eq. (3.9) into (3.8) the stress continuity (3.7) can be written as

$$\begin{aligned} & m_m^0 C_{i3jm}^I A_0^0 p_j^0 \exp(i\omega m_l^0 x_l) \\ & = -\sum_{\alpha=1}^{3} m_m^\alpha C_{i3jm}^I A_0^\alpha p_j^\alpha \exp(i\omega m_l^\alpha x_l) + \sum_{\alpha=4}^{6} m_m^\alpha C_{i3jm}^{II} A_0^\alpha p_j^\alpha \exp(i\omega m_l^\alpha x_l), \end{aligned} \tag{3.11}$$

where C^{I}_{ikjm} and C^{II}_{ikjm}, are the elastic coefficients of the first and second media. The boundary conditions must be satisfied not only for all times t, which is a direct result of the common term $\exp(i\omega t)$ in all equations, but also at all points (x1, x2, x3 = 0) on the interface. Since the exponential functions $\exp(i\omega m_l^\alpha x_l)$ are linearly independent for α= 0, 1, . . , 6 Eq. (3.10) and Eq. (3.11) will be satisfied only if all seven exponential functions are

identically equal. Snell's law follows immediately from this simple fact since this condition requires that

$$m_l^0 x_l = m_l^1 x_l = m_l^2 x_l = m_l^3 x_l = m_l^4 x_l = m_l^5 x_l = m_l^6 x_l \tag{3.12}$$

Here the coordinate vector x lies on the interface plane therefore

$$\mathbf{b} \cdot \mathbf{x} = 0 \tag{3.13}$$

where **b** is normal to the interface as shown in Fig. 4.5. Another way of looking at Eq. (3.12) is that for any two different β and γ values from the set (0,1, . . ,6)

$$(\mathbf{m}^\beta - \mathbf{m}^\gamma) \cdot \mathbf{x} = 0. \tag{3.14}$$

Comparing Eqs. (3.13) and (3.14) shows that the difference $\mathbf{m}^\beta - \mathbf{m}^\gamma$ is always parallel to **b**, i.e., the plane defined by any two of the seven slowness vectors is always perpendicular to the interface. By definition, the slowness vector of the incident wave $\mathbf{m}^0$ lies in the plane of incidence, therefore all the other surface vectors must also lie in the plane of incidence. Since the direction of the slowness vector coincides with that of the wave vector, it can be conclude that the wave vector of the incident wave as well as all the other wave vectors of the reflected and refracted waves lie in the same plane which is normal to the interface, i.e., the plane of incidence. Furthermore,

$$\begin{aligned} &(\mathbf{m}^\beta - \mathbf{m}^\gamma) \times \mathbf{b} = \mathbf{0} \text{ or} \\ &\mathbf{m}^\beta \times \mathbf{b} = \mathbf{m}^\gamma \times \mathbf{b}, \end{aligned} \tag{3.15}$$

i.e., all vector products of $\mathbf{m}^\alpha$ are equal, which is an alternative form of Snell's law. This relationship can be converted into a more familiar form by introducing polar angles ϕ^α between the interface normal b and the different wave normals $\mathbf{n}^\alpha$ for the incident wave and all refracted and reflected waves so that $\mathbf{b} \cdot \mathbf{n}^\alpha = \cos \phi^\alpha$. Then, according to the definition of the vector product

$$\mathbf{m}^\alpha \times \mathbf{b} = m^\alpha \sin \phi^\alpha \tag{3.16}$$

Since **b** is a unit vector and α=1,2...,6 .

Equation (3.16) expresses generalized Snell's law for arbitrarily anisotropic media. It is important to note that the slowness values m^{α} in general depend on the angles θ^{α} due to anisotropy. Figure 3.7 illustrates the fundamental principle that slowness vector of the incident wave and all the other slowness vectors of the reflected and refracted waves lie in the same plane which is normal to the interface, i.e., the plane of incidence, and that they all have the same projection on the plane of the interface. The same conclusion holds for the projections of the wave vectors since $k^{\alpha} = m^{\alpha}\omega$. In terms of the wave vectors, we can summarize Snell's law as follows:

- The wave vectors for the incident and reflected/refracted waves all lies in a single plane, which also contains the interface normal and is called the incident plane.
- All their projections on the interface are equal.

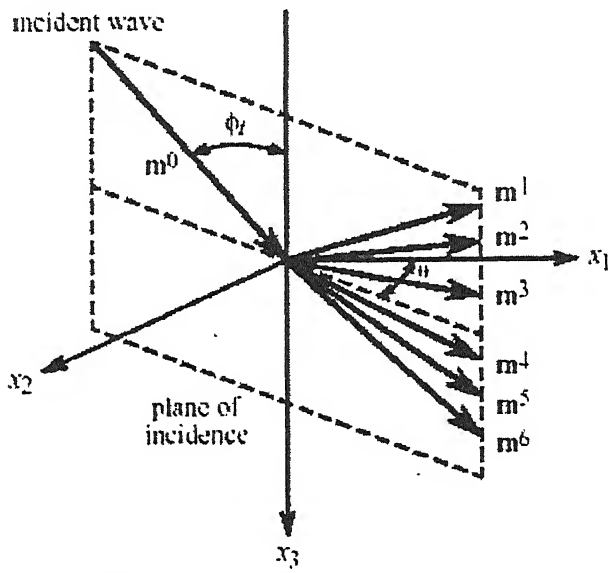

Figure 3.7 Generalized Snell's law for arbitrarily Anisotropic media

3.4.2 Reflection/Refraction Analysis Using Slowness Surfaces

As concluded in the previous article incident and all reflected and refracted waves lie in a single plane, i.e., in the incident plane. In a case where incident plane is x1 x3 as shown in

Fig. 3.8. In this "physical" coordinate system the slowness vector m^{α} has only two components; m_1^{α} and m_3^{α}, while the components m_2^{α} identically vanish. From Snell's law (3.16) the tangential components $m^{\alpha}{}_1$ in the plane of the interface are all equal to each other:

$$m_1^0 = m_1^1 = \ldots\ldots\ldots = m_1^6 = \frac{n_1^0}{V^0} \tag{3.17}$$

Here, $n^0_1 = \sin\phi^0$, where $\mathbf{n}^0$ is wave normal for incident wave, $\phi^0 = \phi^i$ is the incident angle, and V^0 is the phase velocity of the incident wave. Since m^0_1 for the incident wave is known, the tangential components of the slowness vectors $m^{\alpha}{}_1$ (i.e., the projections of the slowness vectors on the interface) are also known. Equation (3.17)) can be re-written in terms of the corresponding wave vector components as follows

$$k_1^0 = k_1^1 = \ldots\ldots\ldots = k_i \sin\phi_i . \tag{3.18}$$

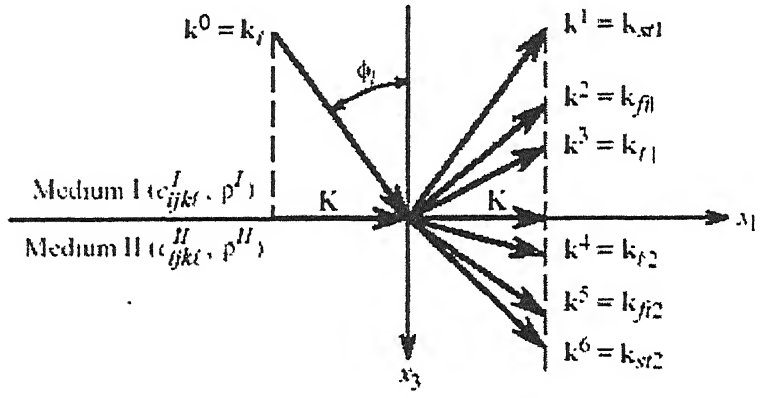

Figure 3.8 Reflected and transmitted wave vectors produced at an anisotropic solid/solid interface by an obliquely incident wave

From equation (4.19) only the tangential components $m^{\alpha}{}_1$ of the slowness vectors **m** are known and the normal slowness components $m^{\alpha}{}_3$ of the reflected and refracted waves are still unknown and must be determined.

To find the slowness vectors for the reflected and refracted waves Snell's law and one additional equation is needed. As shown in previously, the acoustic wave must satisfy the so-called Christoffel equation given as

$$\left(C_{ijkl}n_j n_k - \rho V^2 \delta_{im}\right)p_l = 0. \tag{3.19}$$

In terms of the slowness vector $m_j = n_j/V$, this equation can be re-written as follows

$$(C_{ijkl}m_j m_k - \rho\delta_{im})p_l = 0 \tag{3.20}$$

In order to have a nontrivial solution for p_l, the determinant of the coefficients this equation must vanish,

$$\left|C_{ijkl}m_j m_k - \rho\delta_{im}\right| = 0. \tag{3.21}$$

By introducing a tensor T_{il} as

$$T_{il} = C_{ijkl}m_j m_k - \rho\delta_{il} \tag{3.22}$$

Eq.(3.21) can be written as

$$\left|T_{il}\right| = 0 \tag{3.23}$$

In the chosen coordinate system, the plane of incidence coincides with the x1 x3 plane, therefore $m_2 = 0$ and Eq. (3.22) reduces to

$$T_{il} = \left[C_{i11l}(m_1^0) + (C_{i31l} + C_{i13l})m_3 m_1^0 + C_{i33l}m_3^2\right] - \rho\delta_{il}, \tag{3.24}$$

where m_1^0 is used for all modes instead of m_1 due to Snell's law. This is a second-order polynomial in the unknown normal component m_3 of the slowness vector and can be written as

$$T_{il} = a_{il} + b_{il} m_3 + d_{il} m_m^2, \tag{3.25}$$

where

$$\begin{aligned} a_{il} &= C_{i11l}(m_1^0)^2 - \rho\delta_{il}, \\ b_{il} &= (C_{i31l} + C_{i13l})m_1^0, \\ d_{il} &= C_{i33l}, \\ a_{il} &= a_{li}, b_{il} = b_{li}, d_{il} = d_{li}. \end{aligned} \tag{3.26}$$

3.4.3 Geometrical Considerations on Reflection and Refraction

As the projection of the group velocity vector V_g on the wave direction **n** is equal to the phase velocity V

$$V_{gi} n_i = V \tag{3.27}$$

The slowness vector **m** was defined as a vector parallel to the wave direction with a magnitude equal to the inverse of the phase velocity

$$m_i = \frac{1}{V} n_i, \tag{3.28}$$

which leads to

$$\mathbf{V}_g \cdot \mathbf{m} = 1. \tag{3.29}$$

Taking the exact differential of left side of Eq.(3.29) yields

$$d\mathbf{V}_g \cdot \mathbf{m} + \mathbf{V}_g \cdot d\mathbf{m} = 0, \tag{3.30}$$

where

$$d\mathbf{m} = \frac{\partial \mathbf{m}}{\partial n_i} dn_i. \tag{3.31}$$

Here, the partial derivative of $\mathbf{m}_j$ with respect to n_i can be calculated as

$$\frac{\partial m_j}{\partial n_i} = \frac{\partial}{\partial n_i}\left(\frac{n_j}{V}\right) = \frac{\delta_{ij}}{V} - \frac{n_j}{V^2}\frac{\partial V}{\partial n_i}. \tag{3.32}$$

Substituting Eq.(3.32) into Eq.(3.31) we will have

$$\mathbf{V}_g \cdot d\mathbf{m} = -V_{gi}\frac{\partial m_j}{\partial n_i} dn_i = -V_{gi}\left(\frac{\delta_{ij}}{V} - \frac{n_j}{V^2}\frac{\partial V}{\partial n_i}\right) dn_i = -\frac{1}{V}\left(V_{gi} - \frac{\partial V}{\partial n_i}\right) dn_i.$$

The right side of Eq. (3.33) is zero since from Eq. (3.27) $\partial V/\partial n_i = V_{gi}$, finally

$$\mathbf{V}_g \cdot d\mathbf{m} \equiv 0.$$

This means that V_g is always perpendicular to dm, i.e., to the slowness surface

The slowness diagram is very useful in the determination of the reflection and refraction slowness vectors by graphical means. Let us assume that a quasi-longitudinal wave impinges at the interface between these two solids at an angle of incidence ϕ_i and draw a line in the incident wave direction through the origin of the slowness diagram of the first medium. The slowness vector $\mathbf{m}^0$ of the incident wave is aiming at the origin from the intersection point of this line with the slowness curve of the quasi-longitudinal mode. According to Snell's law, the incident as well as all the reflected and transmitted waves will have the same tangential slowness vector component m^0_1, that is also indicated in Fig. 3.9. Now by drawing a vertical line on the opposite side of the origin at a distance m^0_1, the intersection of this line with the reflected and refracted slowness surfaces will determine the slowness vectors of the reflected and refracted waves. The group velocity vector (or ray direction) is normal to the slowness surface at these intersection points while the magnitude of the group velocity can

be determined from the fact that the projection of the group velocity to the wave propagation direction is equal to the phase velocity, i.e., to the inverse of the slowness.

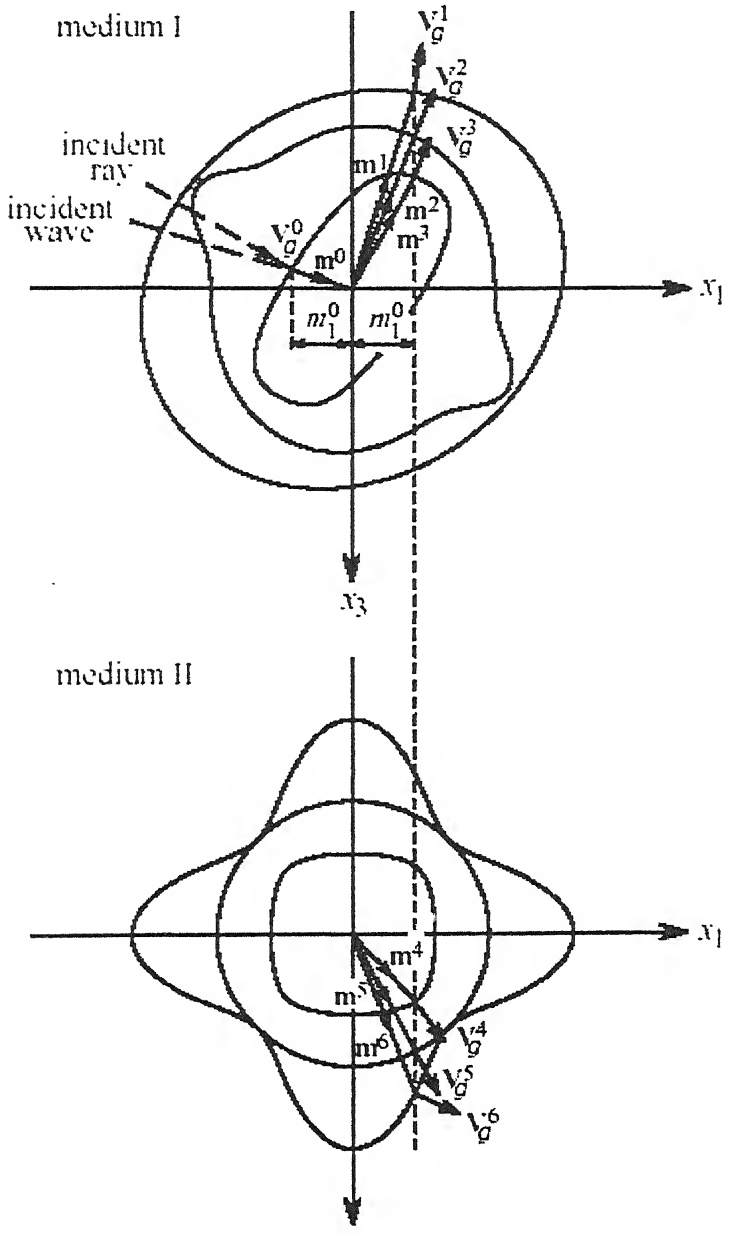

Figure 3.9 Analysis of wave reflection and refraction at an interface between two anisotropic materials based on the slowness surfaces

3.5 Closure

In this chapter refraction and reflection phenomena of ultrasonic waves at a planar interface has been discussed. The use of slowness diagrams in refraction / reflection analysis has been discussed.

Chapter 4

Wave propagation in Transversely Isotropic media

4.1 Introduction

In this chapter the mathematical modeling of ultrasonic wave propagation in transversely isotropic media with arbitrary orientation has presented. For this solution of the equation of motion is derived for transversely isotropic media such as fiber composites or ideally fiber textured austenitic steels. The corresponding wave vectors characterize plane elastic waves, making especially possible a quantitative evaluation of the deviation of wave propagation direction and energy flux, which is a basic characteristic of anisotropic materials. Reflection and refraction of plane waves at interfaces between two arbitrarily oriented transversely isotropic media is examined yielding an algorithm to trace the ultrasonic waves in anisotropic homogeneous or inhomogeneous material

A unidirectional composite material may be modeled to be linear, elastic, homogeneous, and transversely isotropic with five independent elastic constant: C_{1111}, C_{3333}, C_{2323}, C_{1212}, and C_{1133}. Figure 4.1 illustrates the symmetry characteristics of a transversely isotropic material. This symmetry class consists of an axis of symmetry normal to a plane of isotropy.

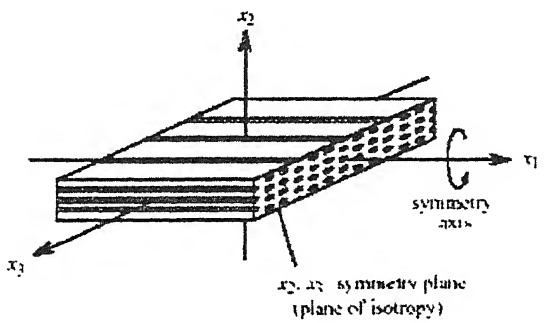

Figure 4.1 Transversely isotropic unidirectional composite material

4.2 Equation of motion

The plane wave equation in a linear elastic medium can be derived from the general equation of motion (2.7) and it can be expressed in tensorial notation as follows [19]

$$(\underline{\nabla}\cdot\underline{\underline{\underline{\underline{C}}}}\cdot\underline{\nabla})\cdot\underline{\mathbf{u}}(\underline{\mathbf{R}},\omega)+\rho\omega^2\underline{\mathbf{u}}(\underline{\mathbf{R}},\omega)=-\mathbf{f}(\underline{\mathbf{R}},\omega), \tag{4.1}$$

Where $\underline{\mathbf{u}}$ is the displacement vector at any point, $\underline{\nabla}$ is the gradient vector, ρ is the material density, $\underline{\mathbf{f}}$ accounts for the volume force density, $\underline{\underline{\underline{\underline{\mathbf{C}}}}}$ is the elastic stiffness tensor and ω denotes the frequency. In the absence of body forces the equation can be modified as

$$(\underline{\nabla}\cdot\underline{\underline{\underline{\underline{C}}}}\cdot\underline{\nabla})\cdot\underline{\mathbf{u}}(\underline{\mathbf{R}},t)+\rho\frac{\partial^2}{\partial t^2}(\underline{\mathbf{u}}(\underline{\mathbf{R}},t))=0 \tag{4.2}$$

This equation of motion explicitly depends upon space $\underline{\mathbf{R}}$ and time t.

The elastic stiffness tensor $\underline{\underline{\underline{\underline{\mathbf{C}}}}}$ for the general transversely isotropic materials has the following conventional relation,

$$\begin{Bmatrix}\sigma_x\\ \sigma_y\\ \sigma_z\\ \tau_{yz}\\ \tau_{zx}\\ \tau_{xy}\end{Bmatrix}=\begin{pmatrix}C_{1111} & C_{1133} & C_{1133} & 0 & 0 & 0\\ C_{1133} & C_{3333} & C_{3333}-2C_{2323} & 0 & 0 & 0\\ C_{1133} & C_{3333}-2C_{2323} & C_{3333} & 0 & 0 & 0\\ 0 & 0 & 0 & C_{2323} & 0 & 0\\ 0 & 0 & 0 & 0 & C_{2323} & 0\\ 0 & 0 & 0 & 0 & 0 & C_{1212}\end{pmatrix}\begin{Bmatrix}\varepsilon_x\\ \varepsilon_y\\ \varepsilon_z\\ \varepsilon_{yz}\\ \varepsilon_{zx}\\ \varepsilon_{xy}\end{Bmatrix} \tag{4.3}$$

In terms of Lame's elastic constant, elastic coefficients can be expressed as, $C_{1111} = \lambda_L + 2\mu_L$, $C_{3333}=\lambda_T + 2\mu_T$, $C_{2323}=\mu_T$, $C_{1212}=\mu_L$ and $C_{1133}=\nu$.

The stiffness tensor can also be written as

$$\underline{\underline{\underline{\underline{C}}}}(\underline{\mathbf{a}}) = \lambda_T \underline{\underline{\underline{\underline{I}}}}\underline{\underline{I}} + \mu_T[(\underline{\underline{\underline{\underline{I}}}}\underline{\underline{I}})^{1324} + (\underline{\underline{\underline{\underline{I}}}}\underline{\underline{I}})^{1342}] + (\nu - \lambda_T)[\underline{\underline{I}}\underline{\underline{a}}\underline{\underline{a}} + \underline{\underline{a}}\underline{\underline{a}}\underline{\underline{I}}] +$$
$$(\mu_L - \mu_T)[(\underline{\underline{I}}\underline{\underline{a}}\underline{\underline{a}})^{1324} + (\underline{\underline{a}}\underline{\underline{a}}\underline{\underline{I}})^{1324} + (\underline{\underline{I}}\underline{\underline{a}}\underline{\underline{a}})^{1342} + (\underline{\underline{a}}\underline{\underline{a}}\underline{\underline{I}})^{1342}] + \tag{4.4}$$
$$[\lambda_T + 2\mu_T + \lambda_L + 2\mu_L - 2(\nu + 2\mu_L)]\underline{\underline{a}}\underline{\underline{a}}\underline{\underline{a}}\underline{\underline{a}},$$

where unit vector $\underline{\mathbf{a}}$ indicates the orientation of the material's rotational symmetry axis, which will in the following be referred to as the "fiber direction." $\underline{\underline{I}}$ is the dyadic idemfactor, which can be decomposed, using dyadic products of the Cartesian unit vectors, according to

$$\underline{\underline{I}} = \underline{\mathbf{e}}_x\underline{\mathbf{e}}_x + \underline{\mathbf{e}}_y\underline{\mathbf{e}}_y + \underline{\mathbf{e}}_y\underline{\mathbf{e}}_y = \begin{pmatrix} 1 & 0 & 0 \\ 0 & 1 & 0 \\ 0 & 0 & 1 \end{pmatrix} \tag{4.5}$$

accordingly, the tetrad $\underline{\underline{\underline{\underline{I}}}}$ is the dyadic product of $\underline{\underline{I}}$ with itself. The upper indicial notation indicates transposition of elements in the tetrads;

The plane harmonic wave solutions of Eq. (4.1) with the stiffness tensor given by Eq. (4.2), i.e., the solutions to the homogeneous $(\underline{\mathbf{f}} = \underline{\mathbf{0}})$ equation of motion, are in the form

$$\underline{\mathbf{u}}_\alpha(\underline{\mathbf{R}}, \omega) = U\underline{\hat{\mathbf{u}}}_\alpha \exp[jK_\alpha \underline{\hat{\mathbf{K}}} \cdot \underline{\mathbf{R}}], \tag{4.6}$$

where $\underline{\hat{\mathbf{K}}}$ is the propagation direction.

In terms of slowness vector ($\mathbf{m}$) Eq. (4.6) can be written as

$$\underline{\mathbf{u}}_\alpha(\underline{\mathbf{R}}, \omega) = U\underline{\hat{\mathbf{u}}}_\alpha \exp[j\omega \mathbf{m}_\alpha \cdot \underline{\mathbf{R}}] \tag{4.7}$$

where $\mathbf{m}_\alpha = \hat{\mathbf{m}}/V_\alpha$ is the slowness vector.

Solving the corresponding linear algebra problem leads to two dispersion relations

$$m_S^2[\mu_T + (\mu_L - \mu_T)(\underline{\mathbf{a}} \cdot \underline{\hat{\mathbf{K}}})^2] = \rho, \tag{4.8}$$

$$m_{qS,qL}^2 = \rho(B \pm (B^2 - 4A)^{1/2})/(2A), \tag{4.9}$$

where

$$A=\mu_L(\lambda_T+2\mu_T)+(\underline{\mathbf{a}}\cdot\hat{\underline{\mathbf{K}}})^2(\lambda_L(\lambda_T+2\mu_T)-\nu(\nu+2\mu_L))+(\underline{\mathbf{a}}\cdot\hat{\underline{\mathbf{K}}})^4[(\lambda_L+2\mu_L)(\mu_L-(\lambda_T+2\mu_T))+(\nu+\mu_L)^2], \tag{4.10}$$

$$B=\mu_L+\lambda_T+2\mu_T+(\underline{\mathbf{a}}\cdot\hat{\underline{\mathbf{K}}})^2(\lambda_L+2\mu_L-(\lambda_T+2\mu_T)). \tag{4.11}$$

The abbreviations α=S, qS, qL denote Pure shear wave, quasi shear wave and quasi-longitudinal wave.

The direction of energy transport or the group velocity can be given as

$$(\underline{\mathbf{V}}_g)_\alpha=V_\alpha\hat{\underline{\mathbf{K}}}+F_\alpha V_\alpha(\underline{\mathbf{a}}\cdot\hat{\underline{\mathbf{K}}})(\underline{\underline{\mathbf{I}}}-\hat{\mathbf{K}}\hat{\mathbf{K}})\cdot\underline{\mathbf{a}} \tag{4.12}$$

where

$$F_S=\frac{\mu_L-\mu_T}{\mu_T+(\mu_L-\mu_T)(\underline{\mathbf{a}}\cdot\hat{\underline{\mathbf{K}}})^2} \tag{4.13}$$

$$F_{qS,qL}=\frac{1}{2}\left(y_A+2(\underline{\mathbf{a}}\cdot\hat{\underline{\mathbf{K}}})^2 z_A\pm\frac{F_1-(\underline{\mathbf{a}}\cdot\hat{\underline{\mathbf{K}}})^2F_2}{\sqrt{B^2-4A}}\right) \tag{4.14}$$

$$y_A=\lambda_L(\lambda_T+2\mu_T)-\nu(\nu+2\mu_L) \tag{4.15}$$
$$z_A=(\lambda_L+\mu_L)(\mu_L-(\lambda_T+\mu_T))+(\nu+\mu_L)^2$$

$$F_1=[\mu_L^2-(\lambda_L+2\mu_L)(\lambda_T+2\mu_T)][\mu_L-(\lambda_L+2\mu_T)]-(\nu+\mu_L)^2(\mu_L+\lambda_T+2\mu_T) \tag{4.16}$$

$$F_2=F_1+[\mu_L^2-(\lambda_L+2\mu_L)(\lambda_T+2\mu_T)][\mu_L-(\lambda_L+2\mu_L)]-(\nu+\mu_L)^2(\mu_L+\lambda_L+2\mu_L) \tag{4.17}$$

The group velocity can be given by the phase velocity $\mathbf{V}_\alpha=V_\alpha\hat{\underline{\mathbf{K}}}$ plus an additional term, which depends on wave propagation direction $\hat{\underline{\mathbf{K}}}$ and the fiber direction $\underline{\mathbf{a}}$. This shows the

deviation of energy flow from propagation direction, which is known as beam skewing. It vanishes when $\hat{\underline{\mathbf{K}}}$ points in to symmetry directions.

4.3 Refraction of plane waves at an Interface

For understanding the refraction/reflection in the transversely isotropic medium the orientation of medium is taken such that the fiber direction is variable but parallel to the surface. Thus the unit vector $\underline{\mathbf{a}}$ lies in the $[\underline{\mathbf{a}} = (a_x, a_y, 0)]$, as shown in fig.4.2.

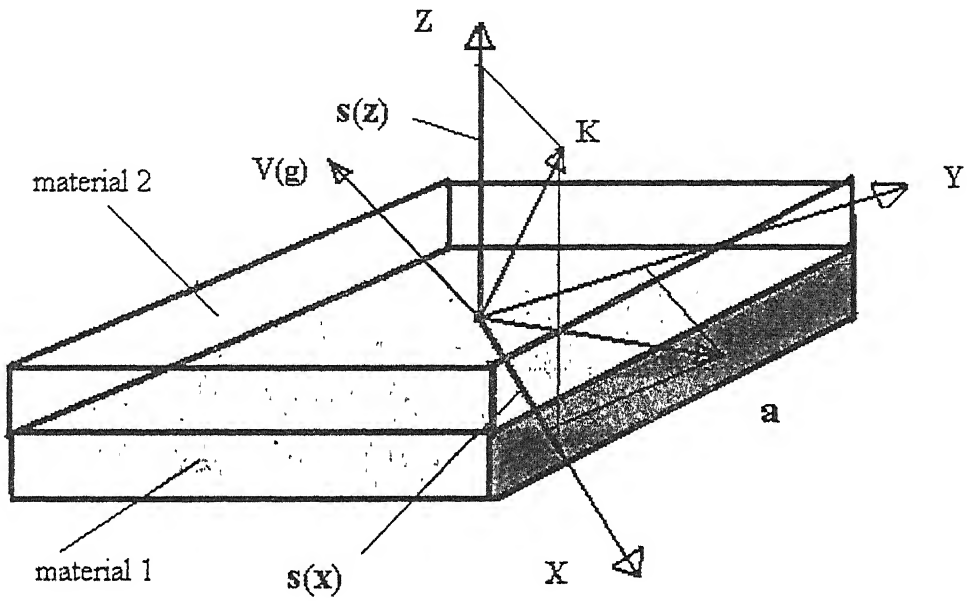

Figure 4.2 Fiber orientation , phase velocity and group velocity direction relative to cartesian coordinate system

The plane wave solution (4.7) for the incident and the reflected/transmitted waves can be given as

$$\underline{\mathbf{u}}^{I}(\underline{\mathbf{R}},\omega) = U^{I}\hat{\underline{\mathbf{u}}}^{I}\exp(j\omega\underline{\mathbf{s}}^{I}\cdot\underline{\mathbf{R}}), \tag{4.18}$$

$$\underline{\mathbf{u}}^{R,T\alpha}(\underline{\mathbf{R}},\omega) = U^{R,T\alpha}\hat{\underline{\mathbf{u}}}^{R,T\alpha}\exp(j\omega\underline{\mathbf{m}}^{R,T\alpha}\cdot\underline{\mathbf{R}}), \tag{4.19}$$

where for the problem in hand the slowness $\underline{\mathbf{m}}^{R,T\alpha}$ is to be determined. Assuming ideal rigid contact between two media requires the continuity of the particle displacement and the normal tractions according to

$$U^I \underline{\mathbf{u}}^I + \sum_\alpha U^{R\alpha} \underline{\mathbf{u}}^{R\alpha} = \sum_\alpha U^{T\alpha} \underline{\mathbf{u}}^{T\alpha}, \tag{4.20}$$

$$\underline{\mathbf{e}}_z \cdot \underline{\underline{\mathbf{T}}}^I + \sum_\alpha \underline{\mathbf{e}}_z \cdot \underline{\underline{\mathbf{T}}}^{R\alpha} = \sum_\alpha \underline{\mathbf{e}}_z \cdot \underline{\underline{\mathbf{T}}}^{T\alpha}, \tag{4.21}$$

where $\mathbf{T}$ designates the stress tensor.

Considering the wave propagation in the xz plane, Snell's law requires all projection of the $\underline{\mathbf{m}}$ vectors onto the interface to be identical

$$m_x^I = m_x^{R\alpha} = m_x^{T\alpha}, \tag{4.22}$$

and the y components of the slownesses to vanish

$$m_y^I = m_y^{R\alpha} = m_y^{T\alpha} = 0, \tag{4.23}$$

with these conditions, the m_z-components can be determined from the dispersion relations. Using dispersion relations (4.8) and (4.9) for refracted and reflected SH waves the m_z component can be given as

$$m_z^{R,TS} = (-b_S \pm \sqrt{(b_S^2 - a_S c_S)})/a_S \tag{4.24}$$

where

$$a_S = \mu_T + (\mu_L - \mu_T) a_z^2 \tag{4.25}$$

$$b_S = (\mu_L - \mu_T) a_x a_z^2 s_x \tag{4.26}$$

$$c_S = [\mu_T + (\mu_L - \mu_T) a_x^2] s_x^2 - \rho \tag{4.27}$$

For qS and qL waves, the $m_z^{R,Tq\beta}$ $(\beta = S, L)$ components of the slowness vector are defined as the roots of a fourth order polynomial,

$$
\begin{aligned}
&(m_z^{q\beta})^4(a_q + b_q a_z^2 + c_q a_z^4) + (m_z^{q\beta})^3 \cdot 2a_x a_z m_x (b_q + 2c_q a_z^2) \\
&+ (m_z^{q\beta})^2 (m_x^2[2a_q + b_q(a_x^2 + a_z^2) + 6c_q a_x^2 a_z^2] + d_q + e_q a_z^2) \\
&+ (m_z^{q\beta}) \cdot 2a_x a_z m_x (m_x^2 (b_q + 2c_q a_x^2) + e_q) \\
&+ m_x^4 (a_q + b_q a_x^2 + c_q a_x^4) + m_x^2 (d_q + e_q a_x^2) + f_q = 0
\end{aligned} \tag{4.28}
$$

where

$$
\begin{aligned}
a_q &= \mu_L(\lambda_T + 2\mu_T) \\
b_q &= \lambda_L(\lambda_T + 2\mu_T) - \nu(\nu + 2\mu_L) \\
c_q &= (\lambda_L + \mu_L)(\mu_L - (\lambda_T + 2\mu_T)) + (\nu + \mu_L)^2 \\
d_q &= -\rho(\mu_L + \lambda_T + 2\mu_T) \\
e_q &= -\rho(\lambda_L + 2\mu_L - (\lambda_T + 2\mu_T)) \\
d_q &= \rho^2
\end{aligned} \tag{4.29}
$$

The Eq. (4.28) will give four values of m_z values (two for reflection and two for refraction). In the present work HQR algorithm has been used for finding the roots of polynomial. The detail of HQR algorithm is given in Appendix-A.

To separate the roots corresponding to qS and qL wave the dispersion relation (4.9) is transformed with two conditions

$$
\frac{2A}{\rho} m_{qS}^2 - B \geq 0 \tag{4.30}
$$

$$
\frac{2A}{\rho} m_{qL}^2 - B \leq 0 \tag{4.31}
$$

The corresponding group velocity vector for the refracted and reflected waves has to be point from the interface into the respective material. If a root's pair is complex, a surface wave will occur and $m_z^{R\alpha} = 0$.

4.4 Closure

In this Chapter the mathematical formulation ultrasonic wave propagation in transversely isotropic media with arbitrary orientation have been presented. Reflection and refraction analysis of a plane waves at interfaces between two arbitrarily oriented transversely isotropic media have been presented.

Chapter 5
Ray Tracing

5.1 Introduction

The growing need for the proper non-destructive testing of composites/composite laminates has raised considerable interest in studying elastic wave propagation in anisotropic media. The ray-tracing model developed in the present work deals with the propagation of ultrasonic energy through anisotropic and/or inhomogeneous materials. Energy is assumed to behave as bundles of rays, each ray acting independently from its neighbors. As mentioned in previous Chapters, for anisotropic material, direction of energy propagation associated with each ray is generally not parallel to the phase velocity direction, the phase velocity defines the orientation of the phasefront associated with each ray. Furthermore, if a material is inhomogeneous then a ray path is likely to bend because of the continuous refraction as the ray experiences changing material properties.

The model can be applied to the study of energy propagation in composite structures, to identify the regions that might be difficult to inspect because of poor penetration of energy in these regions. Such regions usually arise due to presence of inhomogeneities, or from the inherent nature of the material. As expected, the model has highlighted the complicated nature of energy flow in these structures.

5.2 Assumptions

1. A plane wave solution of the wave equation has been assumed throughout.

2. It has been assumed that a geometrical construction for the ray path is valid i.e. no diffraction effects are allowed in passing through an inhomogeneous or homogeneous anisotropic medium.

3. Boundaries between regions of different elastic properties are assumed to be perfectly smooth.

4. Fiber composite materials are considered to be homogeneous anisotropic material.

5. For a boundary between two media, one or both of which is inhomogeneous, it has been implicitly assumed that the stresses along the boundary can be calculated using the local elastic constants appropriate to the point at which ray impinges on the boundary.

6. The waves are essentially monochromatic and continuous. Changes in ray parameters (i.e. phase and group velocities) due to adjacent rays in a beam have not been quantified.

Validation of the Assumptions

1. In general, for an ultrasonic beam not in the nearfield (N) of the probe, plane wave approximation is reasonable. For a probe crystal diameter d and ultrasonic wavelength λ

$$N \sim \frac{d^2}{4\lambda} \tag{5.1}$$

Using values appropriate to typical austenite inspection, d ~ 12.5 mm, λ ~ 1-5 mm, N ~ 10-40 mm.

For inspection of components whose dimensions are more then N, the assumption of plane wave propagation reasonable.

2. For a geometrical construction to be valid,

$$\lambda << d \tag{5.2}$$

where d is the dimension of any object which may cause diffraction. At typical NDT frequency of a few MHz, the ultrasonic wavelength is around 1-5mm. Which is much smaller than the typical specimen or its defect dimensions.

3. For material system of continuous parallel fiber, fiber spacing and the wavelength of propagating wave is of concern. For the worst case it has been verified that the shortest wavelength is 350 μm (at 5 MHz) compared with the longest fiber spacing that can exist in a composite materials (≈15 μm). Hence our material appeared to be a well-mixed continuum of anisotropic material with respect to practically used frequencies. So for the sake of simplicity we can leave the matrix – fiber interface in our analysis for reflection and refraction.

4. For a boundary between two regions, neither of which has been formed by a weld process. Here surface roughness will be on the tens of micrometer scale and hence apparently smooth for a wavelength of few millimeters.

5. In deriving the boundary conditions satisfied between two media, certain conditions on stress and displacement is specified. These were to be satisfied everywhere along the boundary. Here it has been implicitly assumed that the stress due to a wave of given displacement and slowness vector is the same at any point over the part of boundary covered by the beam width. Strictly this is not so, due to change in elastic properties along the boundary.

5.3 Two Point Ray tracing Method

Two point ray tracing method consists of finding the path of that ray which will travel between two given points in a material. The two points generally represent transmitter and receiver position. For example, if a defect is situated in a inhomogeneous material as shown in fig. 5.1, then determination of the ray path that reaches the defect edge will require two point ray tracing. The ray1, emanating from transmitter in a straight path towards the defect will not reach the defect edge, because of refraction at interfaces and bending in inhomogeneous material. As shown in Fig.5.1, a 60^0 (angle measured from surface normal) ray aimed at the top of a defect is skewed, refracted and bent away from the required

endpoint. So for determining the route by which, energy will reach the defect requires the solution of a non-linear boundary value problem, (the boundary values being the required initial and final ray position, the non-linearity arising from the distortion of ray path within the material). As there is no general analytical technique exists for solving this problem. Numerical iterative techniques have to be employed to find an adequate solution to this problem. Although the use of iterative techniques are computationally intensive, they are generally versatile in the sense that arbitrary inhomogeneity may be considered and as many arbitrary combination of different materials can be taken.

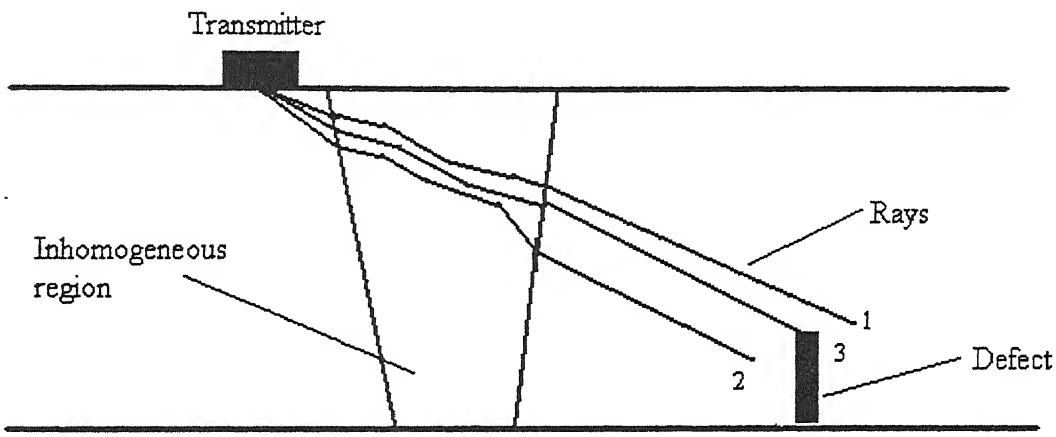

Figure 5.1 An example showing various iterations in two point ray ray tracing

5.4 Shooting Method

The shooting technique developed in the present work is a kind of 'two point iterative ray tracing scheme'. Application of this shooting scheme allows calculation of the route that ultrasonic energy takes from a source to the diffracting edge of a defect and to receiver.

In "Two point iterative ray tracing" the start and end point (i.e. the transducer and the receiver locations) are specified by the user and the program determines the ray which passes through those two specified points. In two point iterative scheme there is no user intervention after the start and end points have been specified.

In shooting technique developed here for a given transducer position, a conical shape fan beam of definite cone angle is sent in to the material and this beam is received at the other side. Here visualizing the path of the beam, the user can either increase or decrease the probe angle, such that rays can reach the desired receiver position. This shooting technique, coupled with the opportunity of user intervention, is far more efficient than its counterpart, namely, two point ray-tracing scheme, which requires large computation time because of its inherent iterative nature. Although the shooting technique also seems to be iterative, but is more efficient than the former as with this technique the user can interpret the effect of probe angle on ray path for a given anisotropic and inhomogeneous material.

5.4.1 Applicability of the technique

The success of the iterative technique relies upon the assumption that a sensible relation exists between initial slowness vector direction of a ray and its final location. This means that the change in initial direction of the slowness vector should lead to a corresponding change in final ray position, where the direction of these changes should not vary from one ray to a nearby ray. This will be true unless the ray paths cross each other in a non-uniform manner. Even if one spurious path is present, then it will slow down the convergence rate as well as generally impede successful solution. If large number of ray paths crosses each other in such a manner that the relationship between initial slowness vector and final ray position is not a smoothly varying function, then the technique will fail.

The likelihood of misbehaving ray paths depends on the types of material used and on the ray mode. The presence of many ray paths of this nature suggests that the energy propagation is incoherent and will be widely scattered. Furthermore, amplitude will be reduced because of the loss of coherence. The ray tracing approach is not appropriate in the vicinity of incoherent propagation.

A cause of difficulty, but not generally of failure, in the technique arises when small changes of slowness vector are accompanied by large changes in group velocity (energy direction). When this happens, the technique will be highly sensitive to the initial choice of slowness vector, as slight change in the initial direction of slowness vector will lead to large changes in

ray endpoint, reducing greatly the chance of reaching the desired endpoint within a reasonable number of iterations.

5.5 Basic steps of the program

The model is capable of predicting the propagation of ultrasonic waves within any component made up of one or more regions whose elastic properties and fiber orientations are known. The interface between two different regions is treated as a planar boundary such that reflection and refraction angles can be calculated using the elastic equivalent of Snell's law.

For tracing the path of different waves in a component, after specifying the size of component, the whole domain is discretized in to number of square elements. In the present work the size of element has been taken as 2×2 mm. In the case where an element has partially defect properties and partially base material properties, it is necessary to find the actual ('edge') interface normal direction for the sake of refraction and reflection analysis. For the sake of display purpose an element is shown to belong to one type material depending upon to which the major fraction of element area belongs as shown in Fig 5.2. Fig. 5.2 shows the meshing for a square block of side 200 mm.

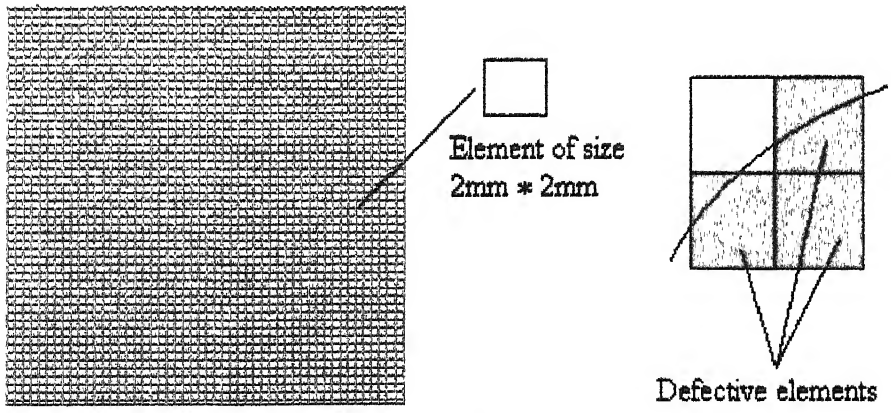

Figure 5.2 Meshing of a square block of size 200mm *200 mm

Ray paths are calculated using a discrete stepping process. A ray travels a small distance in the current group velocity direction and the material properties at the start and end points of the step are found. The ray is then assumed to have crossed a boundary separating two regions with different material properties. This is implemented in the program by considering the refraction at a boundary between two regions. The elastic equivalent of Snell's law is used to determine the new wavevector direction, which is dependent on the old direction and on the change in material properties across the interface (i.e. the properties at each end of a small ray step). The new ray parameters, such as group velocity and group angle etc, are determined using the theory of waves in anisotropic materials.

Figure 5.2 is a flow diagram showing the basic steps involved in the program. In addition to checks shown in the flow diagram, there are numerous other error checks at each decision stage. There are however three principal steps in the algorithm:

Step 1. Solution of the elastic wave equation for a general anisotropic medium leading to wave energy direction and associated particle displacement direction.

Step 2. Stepping forward of the ray path in the direction of group velocity (energy direction) with, for inhomogeneous media, solution of appropriate boundary conditions across the step.

Step 3. Calculation of refracted rays at a boundary between two regions of different material by applying appropriate boundary conditions.

The combination of these principal steps, together with appropriate data storage and plotting routines, leads to simulation of ultrasonic wave paths.

The program is written in Visual C++ having about 55 subroutines. In total there are about 8000 lines of executable statements. A detailed documentation of the program and various subroutines is given in Appendix-C.

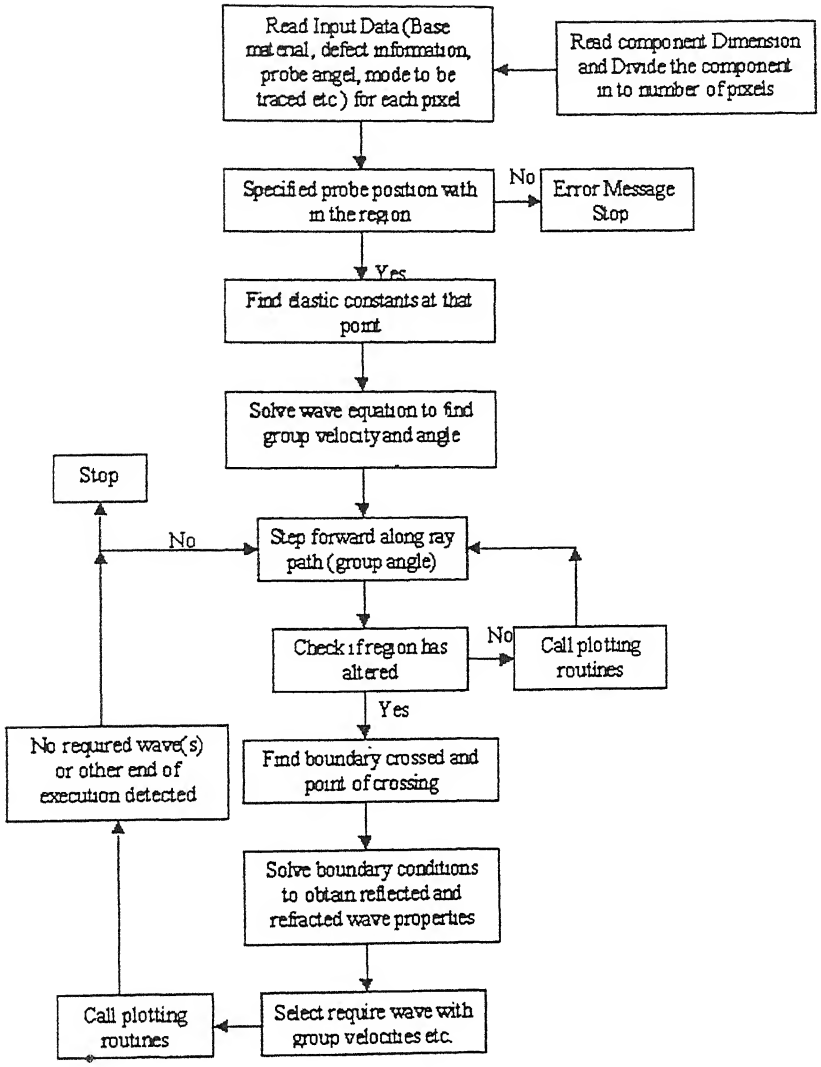

Figure 5.3 Flow diagram of Ray tracing program

5.5.1 Case I: Homogeneous anisotropic media

In the present model the medium is assumed to be non-dispersive. A ray traveling in some direction will continue in this direction until it reaches a boundary. Stepping forward is therefore relatively trivial as no new calculation of velocities is required after every step. It follows the ray through the medium, checking after each step that the ray is within the same region. This procedure continues until a change in region is detected. After a change in region has been detected, the exact location of crossing is found, together with the other

details such as direction of normal etc. This information, with the ray velocities and direction is then used for refraction analysis.

5.5.2 Case II: Inhomogeneous media

For any inhomogeneous medium the elastic constants alters along a ray path. This leads to change in phase velocity and the group velocity. These effects will lead to a beam path, which is not a straight line but a curved one, the curvature of this path being dependent on the variation of elastic constants over the region.

In the program the whole region is divided in to number of elements and for each element elastic properties is specified. So for every new element in the path of the ray, the program compares the elastic properties of the new and the previous element and if there is any change in elastic properties, refraction at the interface between the new and the previous pixel will take place. Due to refraction there will be a alteration in wavevector direction and group velocity. The ray path is therefore composed of a set of lines showing alteration in direction.

5.5 Closure

In this Chapter various assumption used in the ray-tracing model and their validation have been presented. The basic steps involved in the algorithm have been also discussed. The difference in the analysis for homogeneous and inhomogeneous have been presented.

Chapter 6
Results and Discussions

In this Chapter, the results of wave propagation in inhomogeneous and anisotropic materials are presented. The results consist of ray paths developed by ray tracing model, slowness diagram, group velocity diagram for different modes and effect of the various fiber angle on various ray parameters.

A two- dimensional model has been developed which allows for the tracing of ultrasonic rays within a component, which may be inhomogeneous and anisotropic. The model also analyzes the reflection and refraction phenomena in anisotropic and inhomogeneous media.

The effect of fiber angle and phase angle on wave propagation parameters like phase velocity, group velocity, group angle is presented. The effect of phase angle on beam divergence and beam skewing is also studied. The model also predicts the strength of signal received by the receiver of a given dimension. The results predicted by the model developed here are also compared with the experimentally obtained results.

For the purpose of wave propagation analysis in anisotropic material, the following properties corresponding to Graphite/Epoxy composite are considered:

C_{11} = 145.8 GPa, C_{33} = 13.5 GPa, C_{44} = 3.4 GPa, C_{66} = 6.8 GPa, C_{13} = 10.6 GPa and density =1.6 g cm^{-3}

6.1 Wave propagation characteristic in Graphite/Epoxy Composite

6.1.1 Phase and Group velocity

In anisotropic materials the direction of wave vector (phase velocity) and the direction of energy flow (group velocity) are not the same and the magnitude of the phase velocity and

in the wave vector direction. So phase velocity is in general less then the group velocity.

The variation of group velocity / phase velocity with phase angle has been plotted for Graphite/Epoxy composite with various fiber angles (Fig.6.1-6.4). The behavior of the curve and the values of group and phase velocity are quite matching with the experimentally obtained results by Degtyar et al [21] Fig. (6.5-6.6).

Figure 6.1 shows the variation of group and phase velocity with the phase angle for quasi-longitudinal (QL) and quasi-shear (QS) wave in graphite epoxy specimen with 0^0 fiber angle.

Figure 6.2 shows the variation of group and phase velocity with the phase angle for quasi-longitudinal and quasi-transverse wave in graphite epoxy specimen with 90^0 fiber angle. It can be very clearly seen that the behavior of 90^0 specimen is exactly reverse to that of 0^0 specimen which was expected.

It is also clear that the velocity for quasi-longitudinal wave is generally largest when the wave vector (i.e. phase angle) is in the direction parallel to fiber direction.

Figure 6.3 shows the variation of group and phase velocity with the phase angle for quasi-longitudinal in graphite epoxy specimen with 40^0 fiber angle.

Figure 6.4 shows the variation of group and phase velocity with the phase angle for quasi-shear in graphite epoxy specimen with 40^0 fiber angle

Here also it can be seen that for quasi-shear waves velocity is minimum when wave vector is parallel to the direction of fibers.

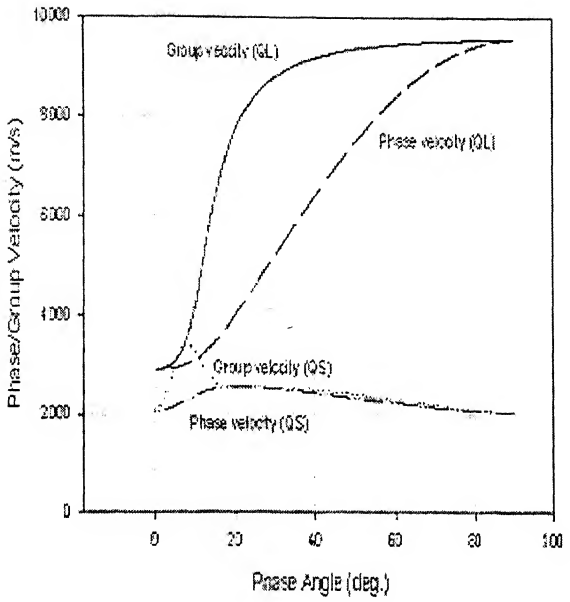

Figure 6.1 variation of Phase/Group velocity with Phase angle for Graphite/Epoxy composite having fiber angle 0 deg.

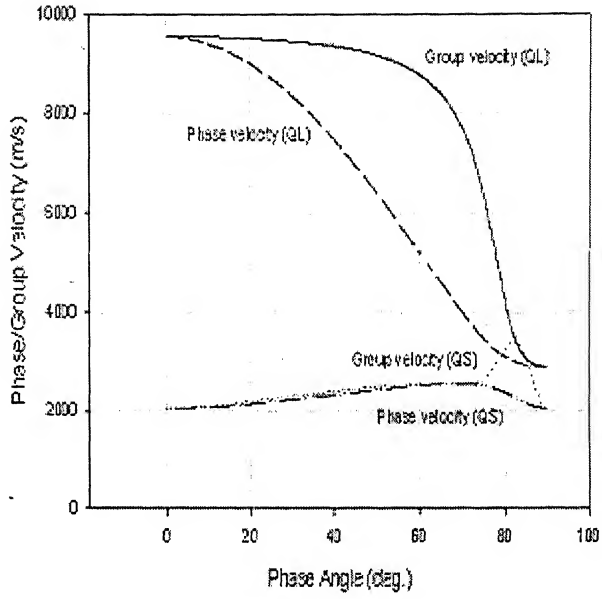

Figure 6.2 Variation of Phase/Group velocity with Phase angle for Graphite/Epoxy composite having fiber angle 90 deg.

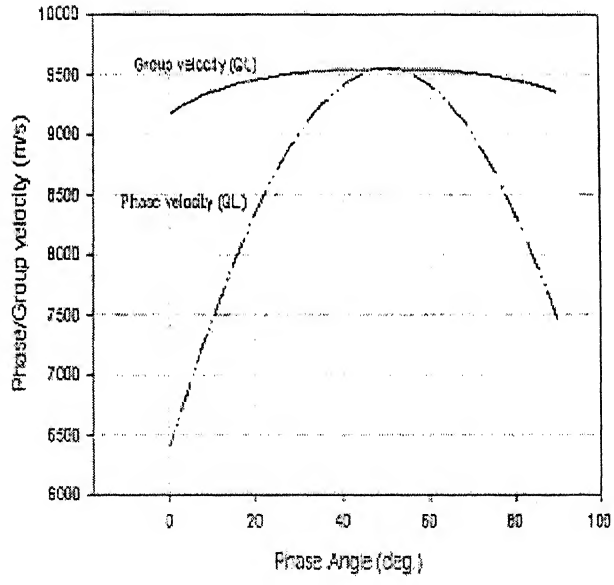

Figure 6.3 Variation of QL Phase/Group velocity with Phase angle for Graphite/Epoxy composite having fiber angle 40 deg.

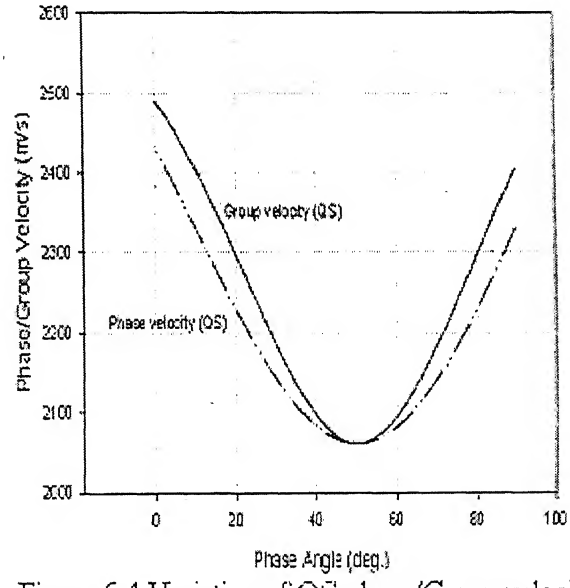

Figure 6.4 Variation of QS phase/Group velocity with Phase angle for Graphite/Epoxy composite having fiber angle 40 deg.

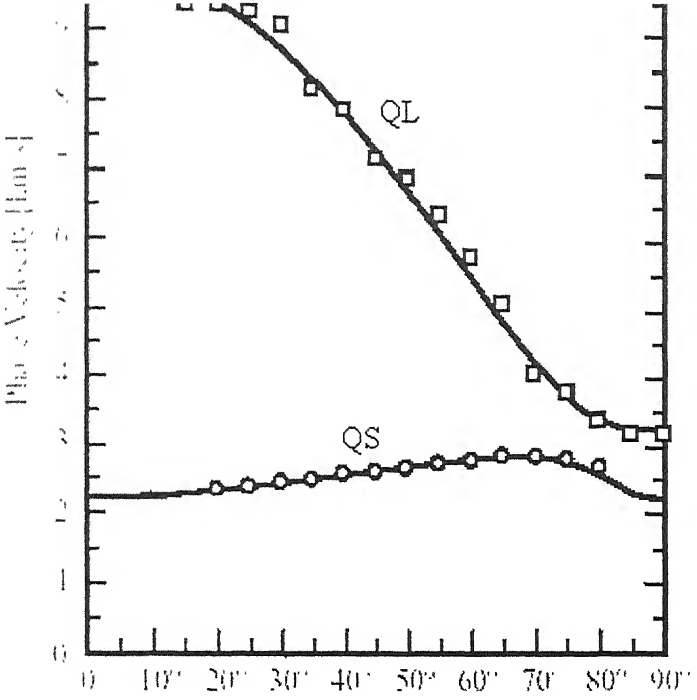

Figure 6.5 Experimentally obtained variation of phase velocity with phase angle for 90-deg. graphite epoxy composite [21]

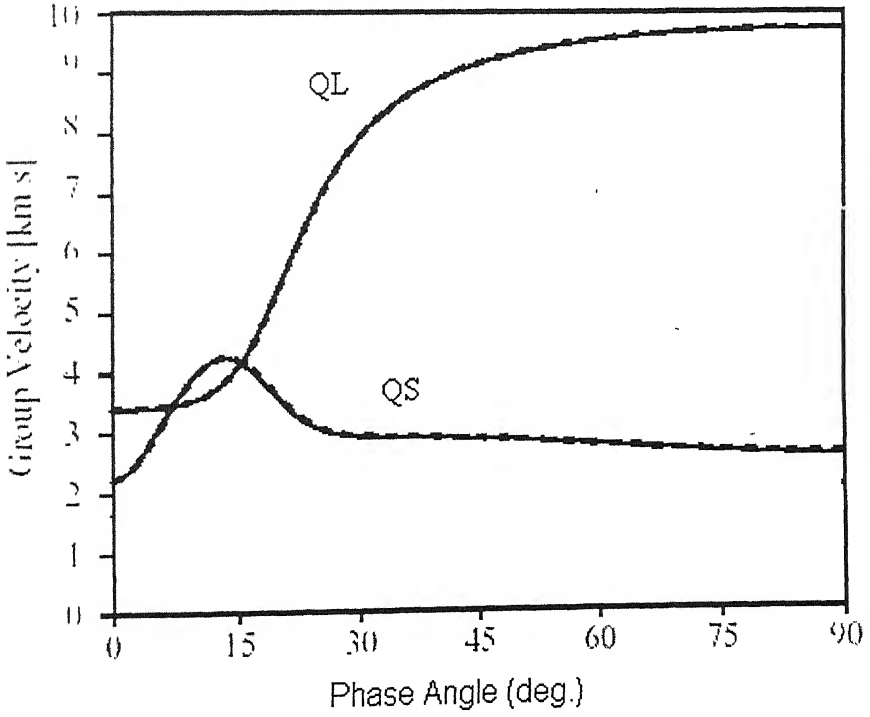

Figure 6.6 Expermentally obtained variation of group velocity with phase angle for 0 deg.Graphite/Epoxy Composite [21]

Figure 6.7 shows the variation of group velocity with the group angle for quasi-shear and quasi-longitudinal wave in graphite epoxy composite with 0^0 fiber angle.

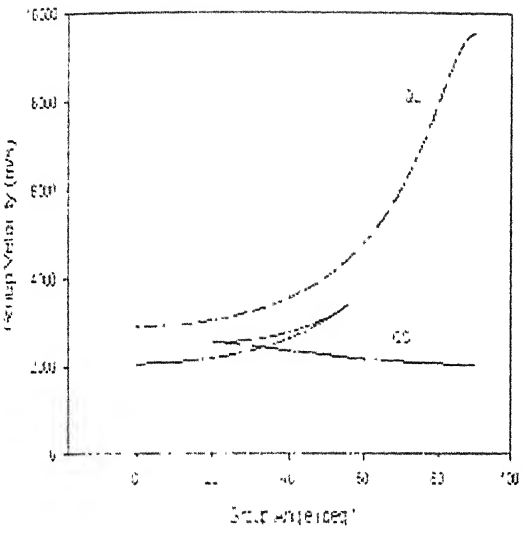

Figure 6.7 Variation of group velocity with group angle for graphite/epoxy composite having 0 deg. fiber angle

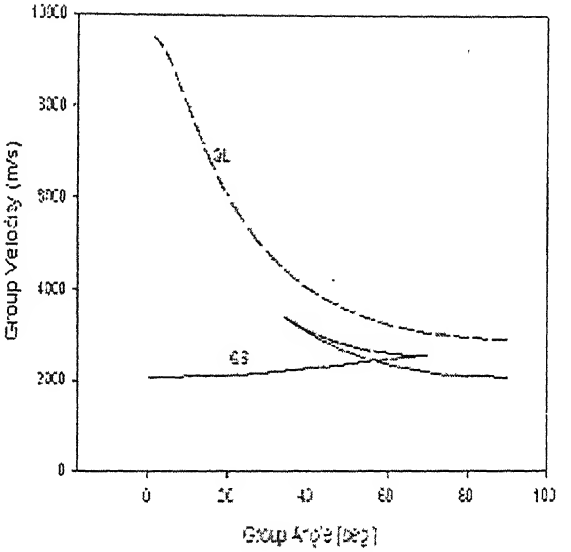

Figure 6.8 Variation of group velocity with group angle for graphite/epoxy composite having 90 deg. fiber angle

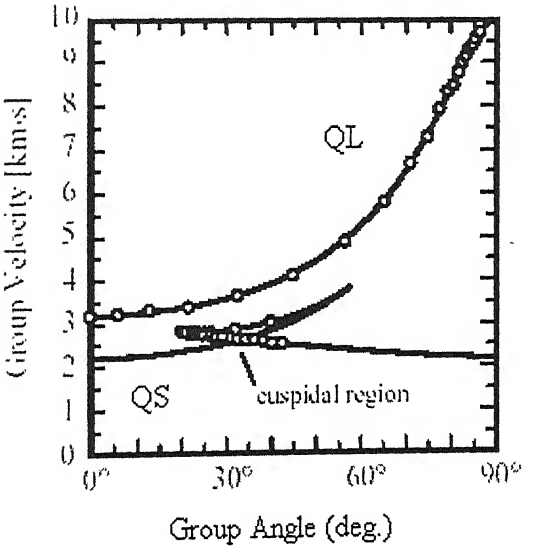

Figure 6.9 Expermentally obtained variation of group velocity with group angle for 0 deg. Grpahite/Epoxy composite [21]

Figure 6.8 shows the variation of group velocity with the group angle for quasi-longitudinal and quasi-shear wave in graphite epoxy specimen with 90^0 fiber angle.

Figure 6.9 shows the experimental obtained variation of group velocity with the group angle for quasi-longitudinal and quasi-shear wave in graphite epoxy specimen with 0^0 fiber angle by Degtyar et al [21].

It can be seen that the behavior of 90^0 fiber is exactly reverse to that of 0^0 fiber specimen. It can also be noted that the variation of quasi-shear waves of both 0^0 fiber and 90^0 fiber includes a cuspidal region. This is due to fact that for waves at two different phase angle can have the same group velocity direction.

Figure 6.10 shows the variation of group velocity with the group angle for quasi-longitudinal wave in graphite epoxy specimen with 40^0 fiber angle.

Here it can be seen that for 0^0 to 90^0 phase angle variation the group angle varies only from 45.7^0 to 53.1^0 which shows that quasi-longitudinal waves in 40^0 fiber specimen has much less beam divergence than in 0^0 fiber or 90^0 fiber specimen.

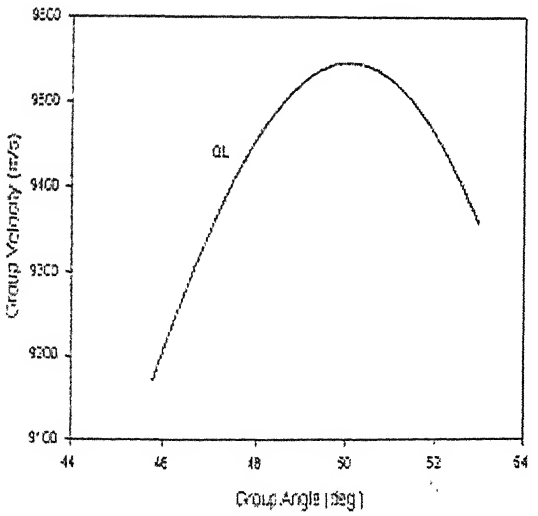

Figure 6.10 Variation of group velocity with group angle for graphite/epoxy composite having 40 deg. fiber angle

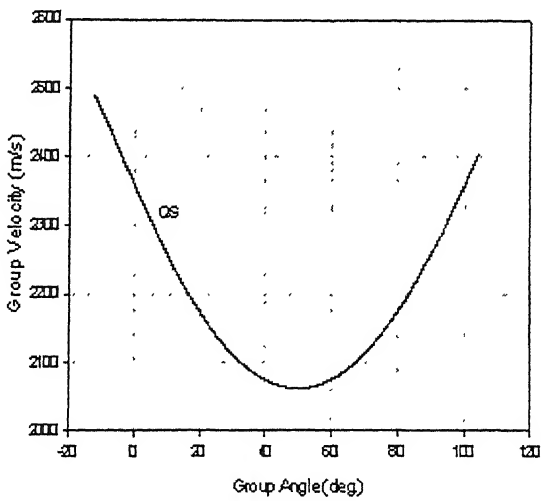

Figure 6.11 Variation of QS group velocity with group angle for graphite/epoxy composite having 40 deg. fiber angle

Figure 6.11 shows the variation of group velocity with the group angle for quasi-longitudinal wave in graphite epoxy specimen with 40^0 fiber angle.

6.1.2 Slowness Diagrams

An extremely useful insight into the effects of anisotropy can be obtained by examination of the slowness surfaces of a material. Slowness diagram for graphite/epoxy composite specimen has been plotted. These diagrams are compared with the experimentally obtained by Spies [22]. The results obtained by the present model are quite similar to those obtained by Spies.

Figure 6.12 and 6.13 shows the slowness diagram for quasi-longitudinal and quasi-shear waves in graphite/epoxy specimen with 0^0 fiber angle and 90^0 fiber angle specimen respectively.

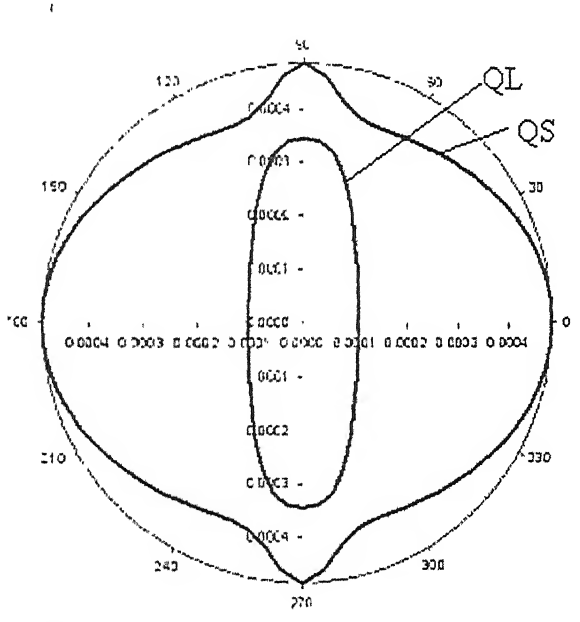

Figure 6.12 Slowness diagram for 0 deg. graphite/epoxy composite

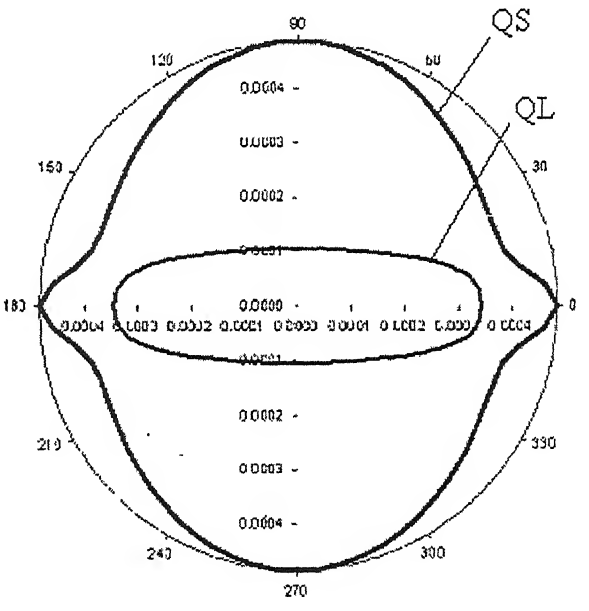

Figure 6.13 Slowness diagram for 90 deg. graphite/epoxy composite

Figure 6.14 and shows the slowness diagram for quasi-longitudinal and quasi-shear waves in graphite epoxy specimen with 40^0 fiber angle.

It can be noted that group velocity direction is almost same between $0\text{-}90^0$ of phase angle.

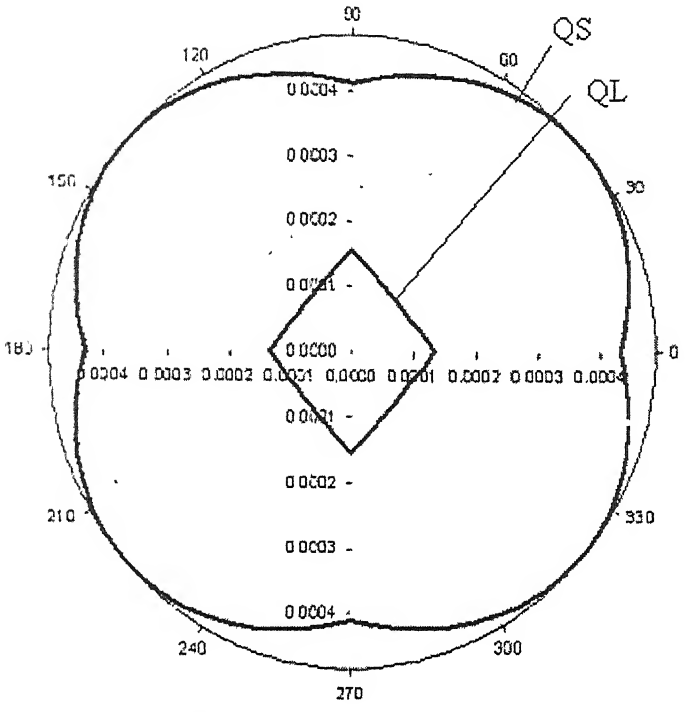

Figure 6.14 Slowness diagram for 40 deg. graphite/epoxy composite

By closely observing the slowness diagram for quasi-longitudinal wave it can be seen that normal to the slowness diagram is in the direction of wave vector for most of the time and as the direction of energy propagation (i.e. group angle) is given by the normal to the slowness surface. So from just observing the slowness surface of a material direction of energy propagation for a given wave vector direction can be predicted.

6.1.3 Group velocity Diagrams

Group velocity diagram for graphite epoxy composite specimen has been plotted. These are compared with the experimentally obtained by Spies [22]. The results obtained by the present model are quite similar to those obtained by Spies.

Figure 6.15(a), (b) and 6.16(a),(b) shows group velocity diagram for quasi-longitudinal and quasi-shear waves respectively in graphite epoxy specimen with 0^0 fiber angle.

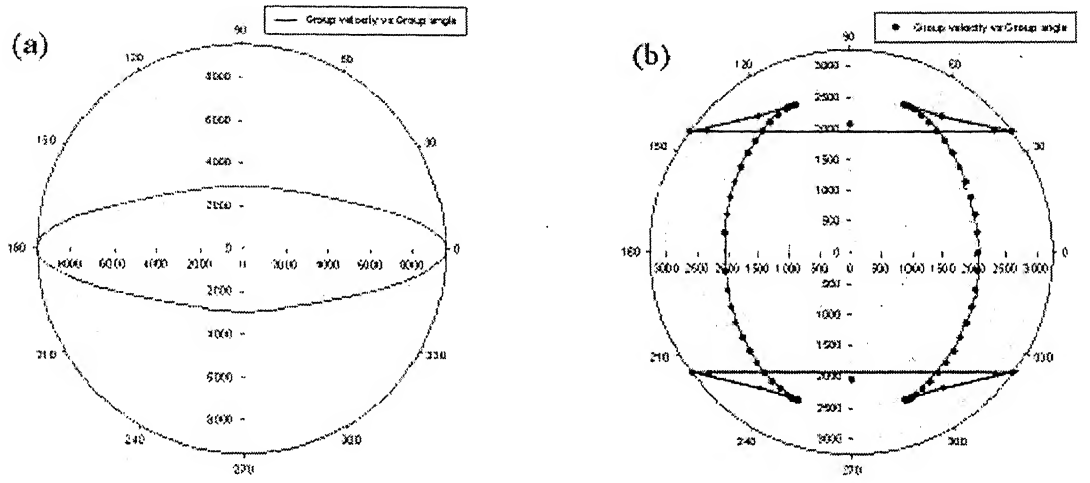

Figure 6.15 Group velocity diagram for graphite epoxy specimen with 0^0 fiber angle (a) QL wave (b) QS wave

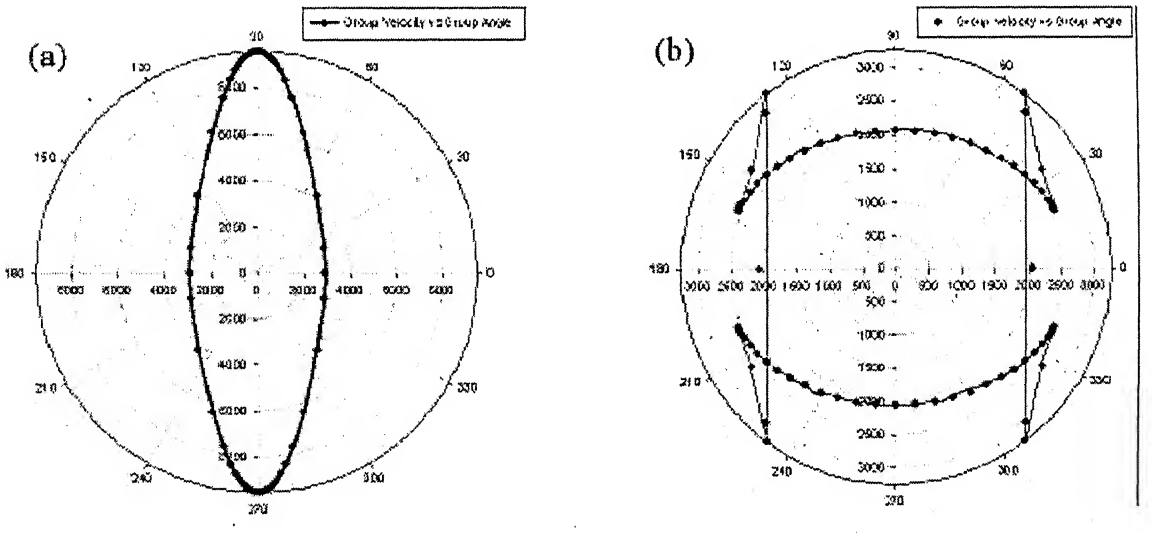

Figure 6.16 Group velocity diagram for graphite epoxy specimen with 90^0 fiber angle (a) QL wave (b) QS wave

6.1.4 Beam Skewing

The deviation between wave propagation and energy direction, known as beam skewing, is presented in Fig 6.17 and 6.18 for quasi-shear and quasi-longitudinal wave in graphite epoxy specimen with 0^0 fiber angle and 90^0 fiber angle.

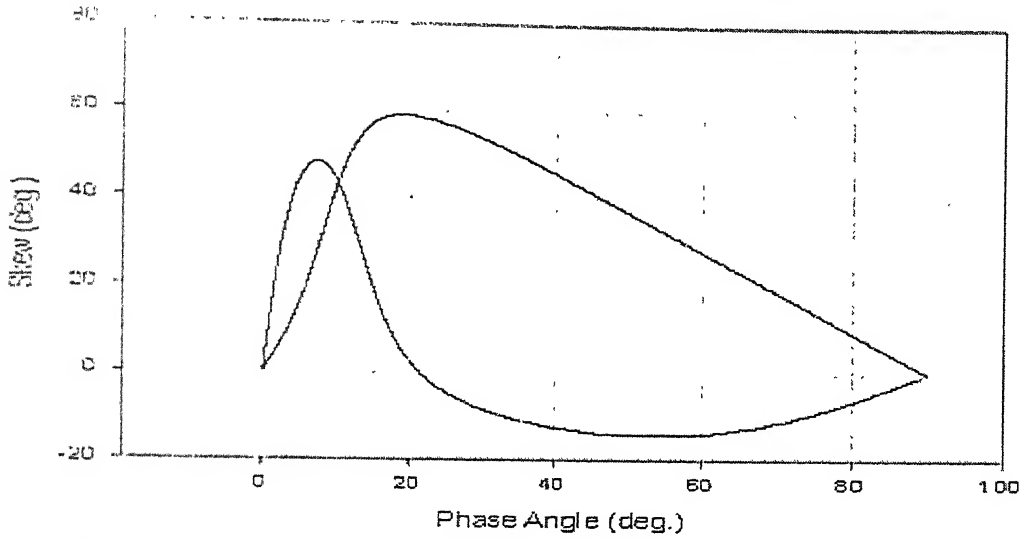

Figure 6.17 Variation of skew with phase angle for graphite/epoxy composite having fiber angle 0 deg.

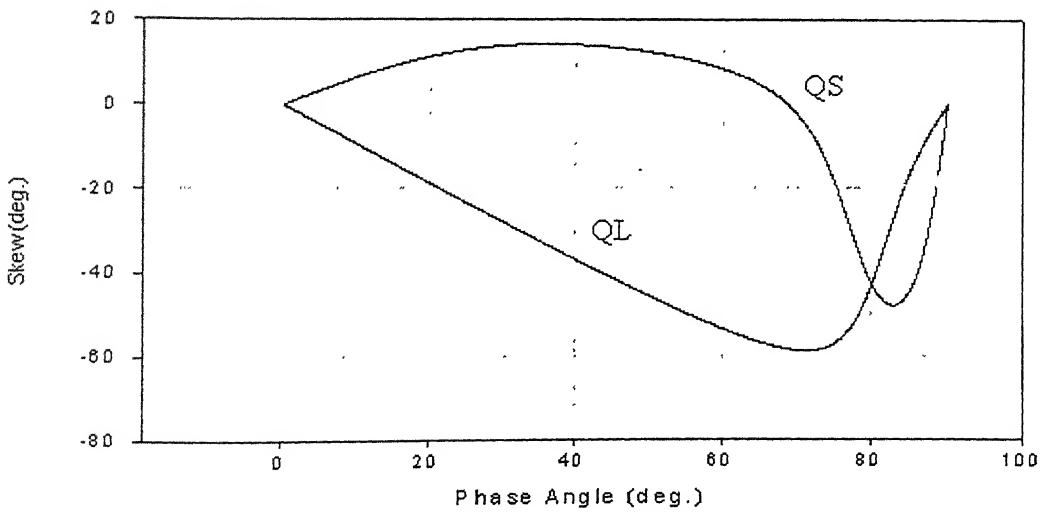

Figure 6.18 Variation of skew with phase angle for graphite/epoxy composite having fiber angle 90 deg.

From the curve obtained for 0^0 fiber it can be predicted that between phase angles 16-30^0 the beam skewing is very high around 45-60^0.

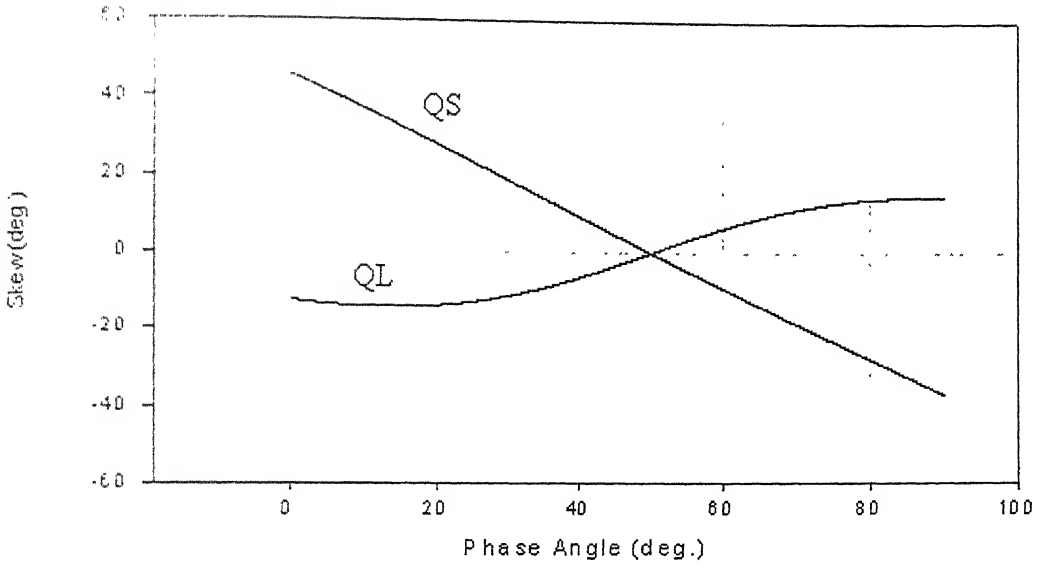

Figure 6.19 Variation of skew with phase angle for graphite/epoxy composite having fiber angle 40 deg.

Figure 6.19 shows variation of beam skewing for quasi-shear and quasi-longitudinal wave in graphite epoxy specimen with 40^0 fiber angle.

It can be seen that the beam skewing vanishes in both the symmetry direction, i.e., along the fibers and normal to fibers.

6.1.5 Beam Divergence

Beam divergence is a measure of how fast the energy within beam is spreading as the beam travels. A plot between beam divergences against phase angle is shown in fig. 6.20,6.21 and 6.22 for 0, 90 and 40^0 graphite/epoxy composite.

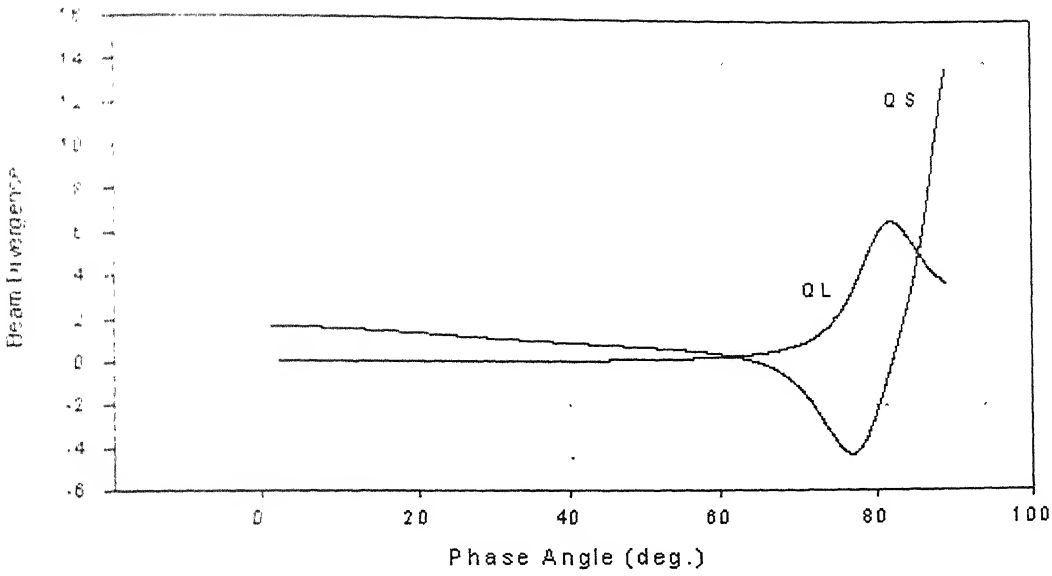

Figure 6.20 Variation of Beam divergence with phase angle for graphite/epoxy composite having fiber angle 0 deg

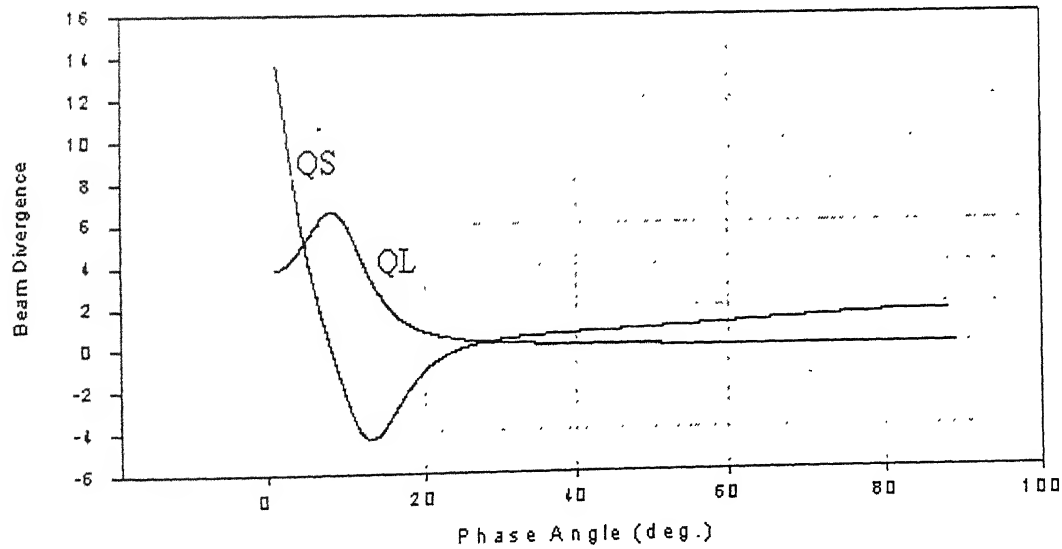

Figure 6.21 Variation of Beam divergence with phase angle for graphite/epoxy composite having fiber angle 0 deg.

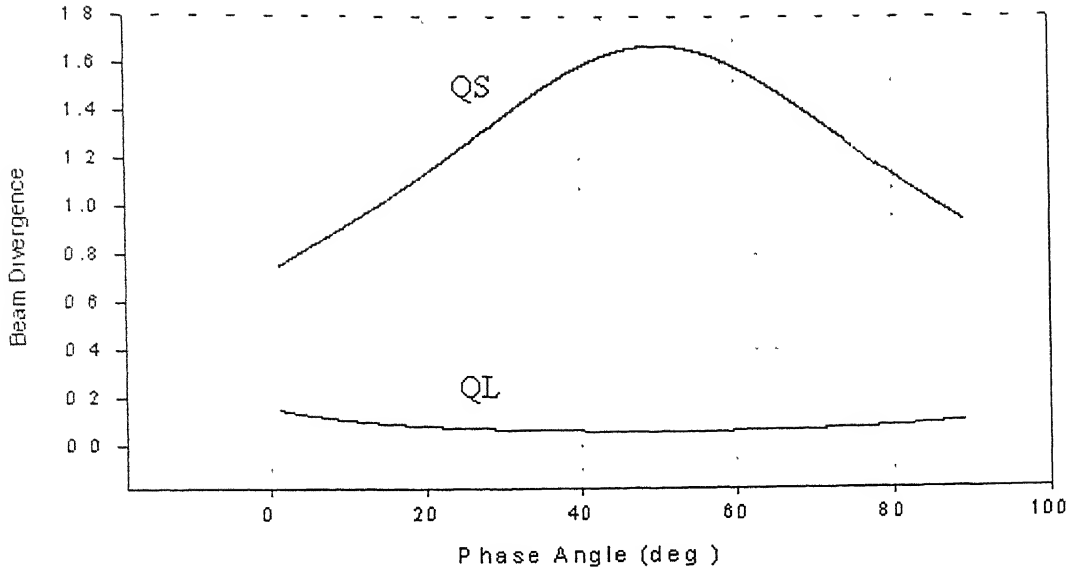

Figure 6.22 Variation of Beam divergence with phase angle for graphite/epoxy composite having fiber angle 40 deg.

By observing the various plots beam divergence and phase angle it is seen that the beam divergence is highest when wave vector is in the direction parallel to the fiber direction.

6.2 Ray propagation in Graphite/Epoxy Composite with defects

6.2.1 Ray Paths

For tracing the path of different waves in a component the whole domain (200×200 mm) is discretized into a number of square elements each of 2×2 mm (Fig. 5.2). In the present analysis, three shapes of the defect are analyzed namely rectangular, circular and elliptical. All of these inputs are given in a visual interactive manner as shown in Appendix-B.

The input parameter for tracing the ray paths are:

- Base Material properties (i.e. elastic constants, density, fiber angle).
- Defect location, size and shape.
- Defect properties (i.e. elastic constants, density, fiber angle).
- Initial Ray angle.

- Scanner position.
- Receiver dimension and location
- Wave mode to be traced. The option is provided to trace the same mode in the whole component or tracing different modes in different regions.

Fig. 6.23 shows the basic layout of the software developed in the present work, which include component, ray paths, axes and various controls for analysis.

The model can trace two types of beams, one is parallel beam and other one is fan rays (cone shape). For the present model the cone angle of 5^0 has been taken. The model can trace both the quasi-shear and quasi-longitudinal wave and also different modes in different regions.

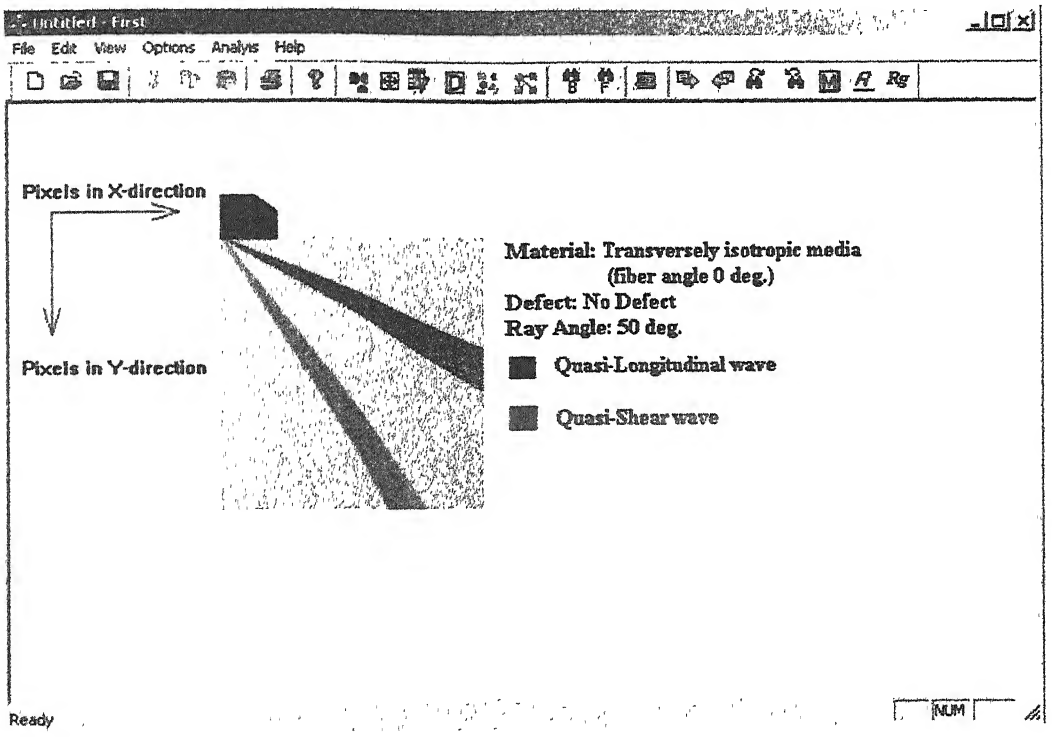

Figure 6.23 Basic layout of the model

6.2.1.1 Rectangular Defect

Fig 6.24 shows both quasi-longitudinal and quasi-shear wave paths for 60^0 ray angle in graphite epoxy composite specimen having a rectangular defect. The size of the defect is 40×40 mm and the defect properties are taken to be C_{11} =60 GPa, C_{33} = 30 GPa, C_{44} = 3.7 GPa, C_{66} = 7.5 GPa, C_{13} = 15 GPa and density =2.6 g/ cm^3

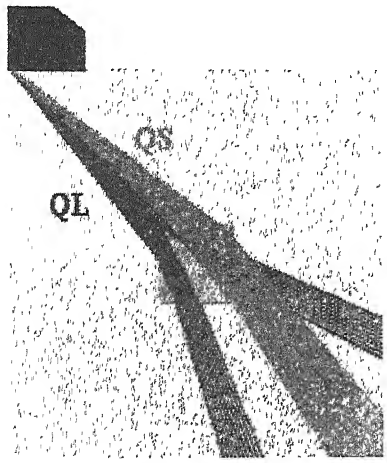

Figure 6.24 Ray paths in graphite/epoxy composite having a rectangular defect

In this figure it can be that for a given phase angle 60^0 both quasi-longitudinal and quasi-shear wave have different energy propagation directions. Quasi-shear wave's group angle 37.30^0 while quasi-longitudinal wave's is 44.47^0

6.2.1.2 Circular Defect

Fig 6.25 shows quasi-shear wave paths for 78^0 ray angle in graphite epoxy composite specimen having a circular defect of radius 40mm.The fiber angle of the base material is 0^0 while the defect has 90^0 fiber angle. Scanner is positioned at 35mm from the origin (i.e. upper left corner of block). The defect properties are same as in 6.2.1.1.

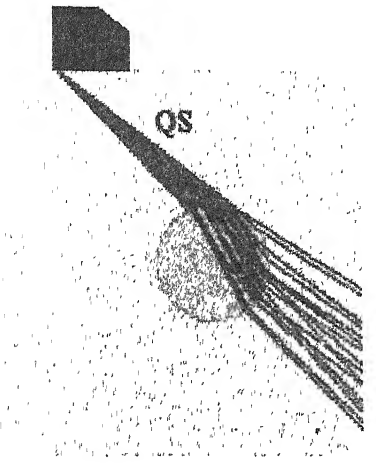

Figure 6.25 Ray paths in graphite/epoxy composite having a circular defect

6.2.1.3 Elliptical Defect

Fig 6.26 shows quasi-shear wave paths for 65^0 ray angle in graphite epoxy composite specimen having a elliptical hole. The base material is 40^0 – graphite/epoxy composite.

Hole's minor radius =30mm,
Hole's major radius =50mm,
Hole's center = (110,130)
Scanner is located at 20 mm from origin.

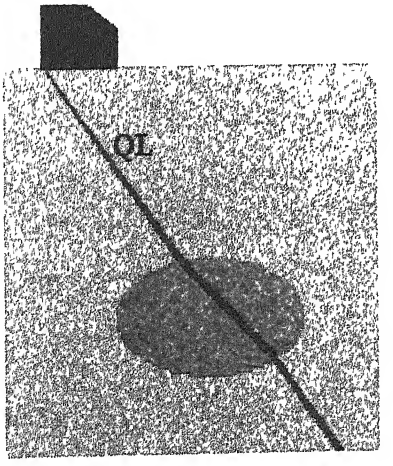

Figure 6.26 Ray paths in graphite/epoxy composite having a elliptical defect

Here it is clear that beam divergence for a 40^0 fiber composite is very less than those having 0^0 and 90^0 fibers.

6.2.1.4 Mixed modes

In this a ray is analyzed where in a quasi-longitudinal mode before ray is input, converted into quasi-shear mode in defect region and quasi-longitudinal mode after defect. Fig 6.27 shows both mixed mode propagations for 67^0 ray angle in graphite epoxy specimen having a square defect. The side of the square defect is 50 mm. Scanner is located at 20mm from the left edge of block.

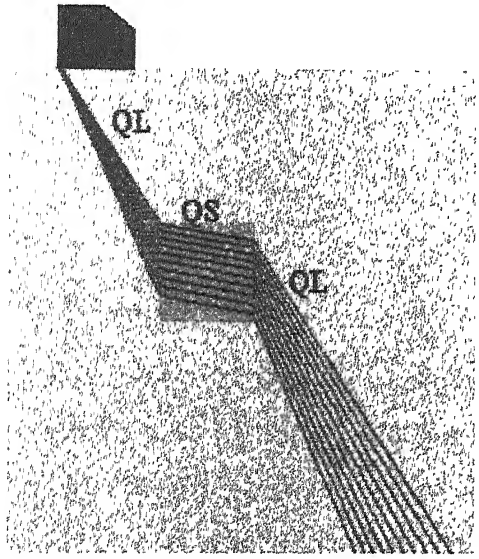

Figure 6.27 Mixed modes wave propagation

Figure 6.28 shows the beam type ray tracing in which a parallel beam of rays instead of a cone passes through the specimen. In this case base material has a rectangular defect of size 80×40mm.

It can be seen here that for 60^0 angle quasi-longitudinal wave passes through the defect but quasi shear waves just misses the defect.

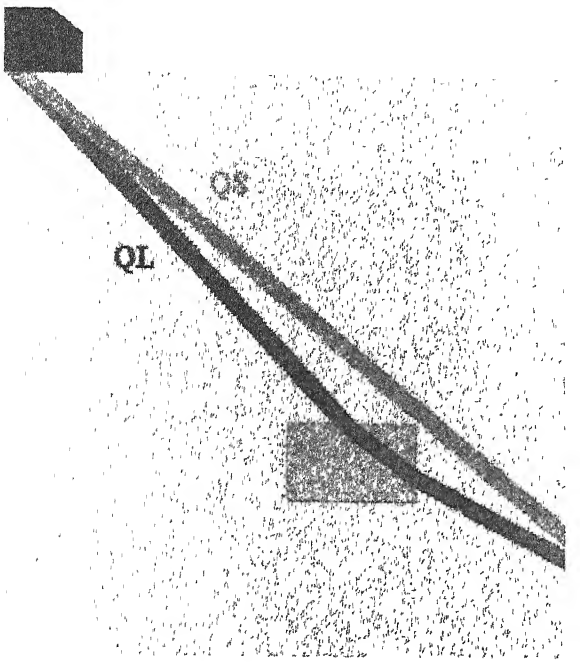

Figure 6.28 Ray tracing in the form of a parallel beam

6.2.2 Signal Strength at Receiver

Signal strength is evaluated by means that for a given number of rays in a fan beam what percentage of rays send reaches a receiver position. Although there are various attenuation effects which came in to effect while a ray travels passes through a material but in the present work concentration is just made on the percentage of rays reaching to a particular position.

Figure 6.29 (a) and (b) shows the signal strength at horizontal face for a given rectangular defect in a composite material. The receiver dimension is 25mm. Here it can be see that no rays can be collecting by putting the receiver on vertical face.

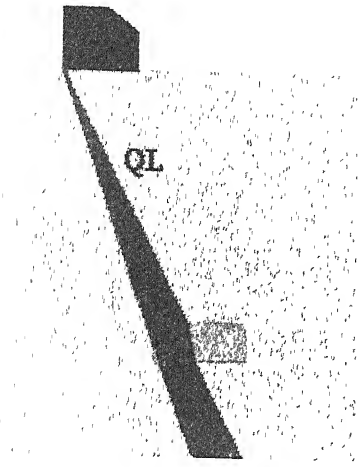

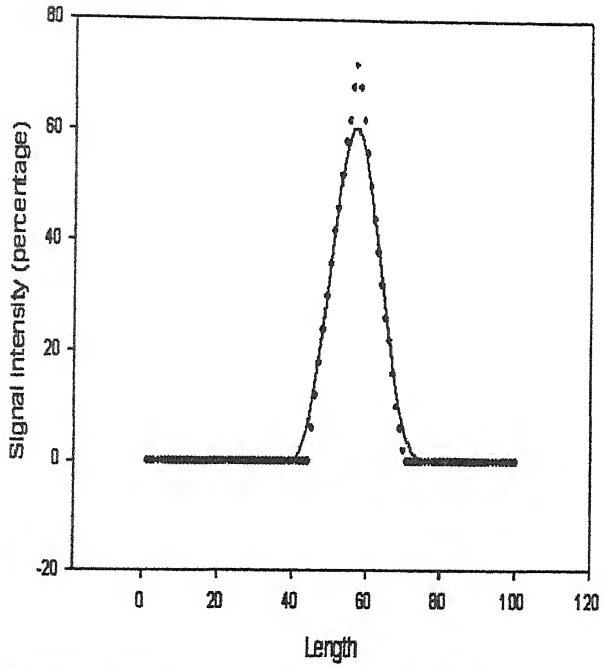

Figure 6.29 (a) Quasi-longitudinal ray path in a graphite/epoxy composite having a rectangular defect (b) Signal strength at various receiver position

Figure 6.30 (a) shows a path of a fan beam in a material having a circular defect. After refraction from the interface some of the rays goes to horizontal and some to vertical face. Figure 6.30 (b) and (c) shows variation of the signal at horizontal and vertical face respectively.

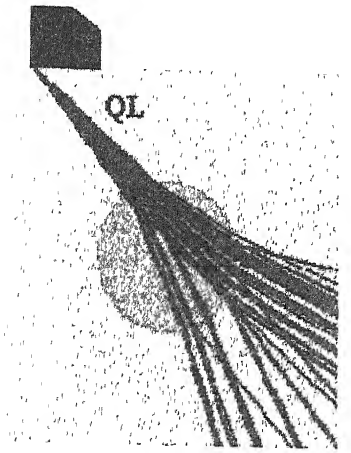

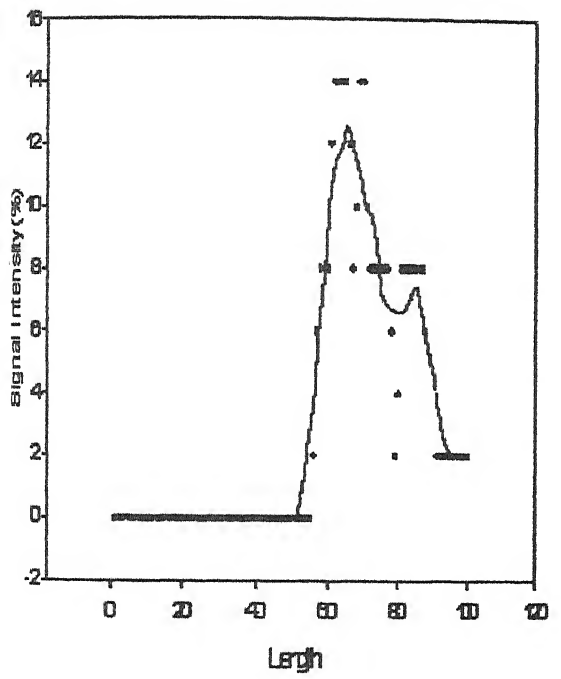

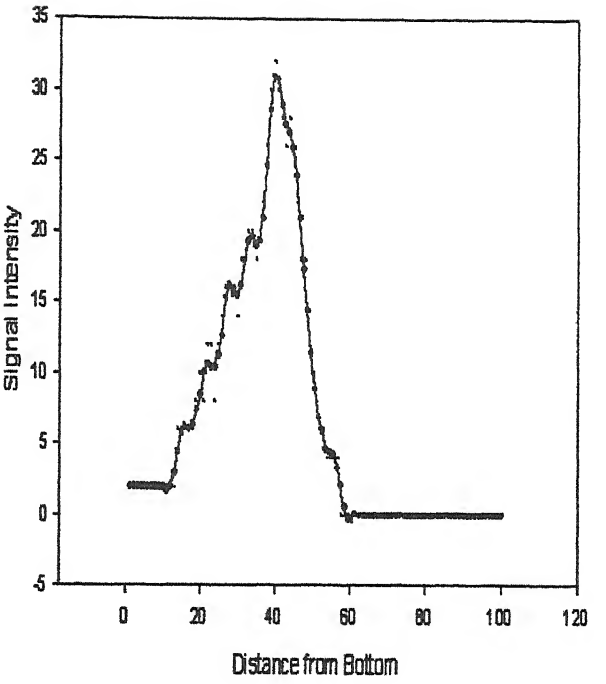

Figure 6.30(a) Quasi-longitudinal ray path in a graphite/epoxy composite having a circular defect (b) Signal strength at various receiver position on horizontal face (c) Signal strength at various receiver position on vertical face

6.2.3 Critical Angle Phenomena

As explained previously that there exists a "critical" incident angle, which a wave makes with the traction free surface of an elastic half space and that as the incident angle passes

through this critical value, the energy flux vector of the reflected or refracted wave passes through grazing incidence and emerges as a surface wave.

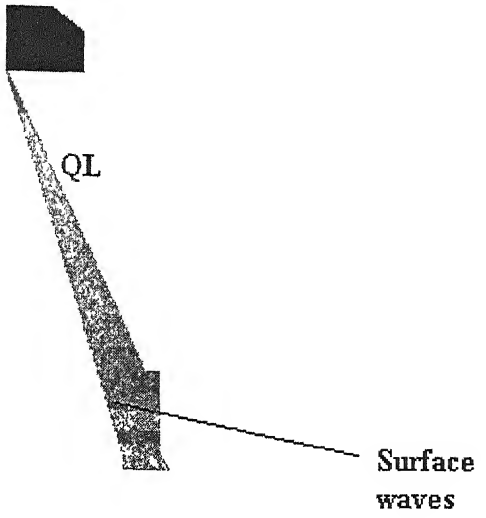

Figure 6.31 Critical angle phenomena

Figure 6.31 shows 71^0 quasi-longitudinal ray paths in a composite having a rectangular defect. The rays which incident on the vertical face of the defect (because of the critical angle phenomena) converted in to surface waves and stops penetrating.

6.9 Time of Flight

The time taken by a ray to pass through a material is called time of flight. While traveling the ray will get reflected from various interfaces it encounters in its path. Time of flight is a very useful data in the sense, which can be used for reconstructing the defect images by tomographic algorithm. Here in present work a fan beam of 50 quasi-longitudinal rays is send in to the specimen and monitored on the other sides of specimen.

Figure 6.32 (a) and (b) shows the 70^0 ray paths in a composite having a rectangular defect and the time of flight for each ray of the fan beam. The rays having incidence angle above 70.8^0 do not reach the other face as they converted in to surface wave at the defect interface.

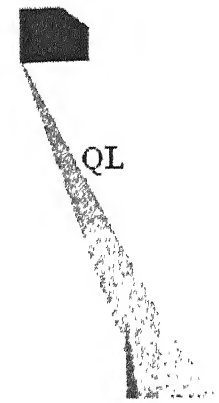

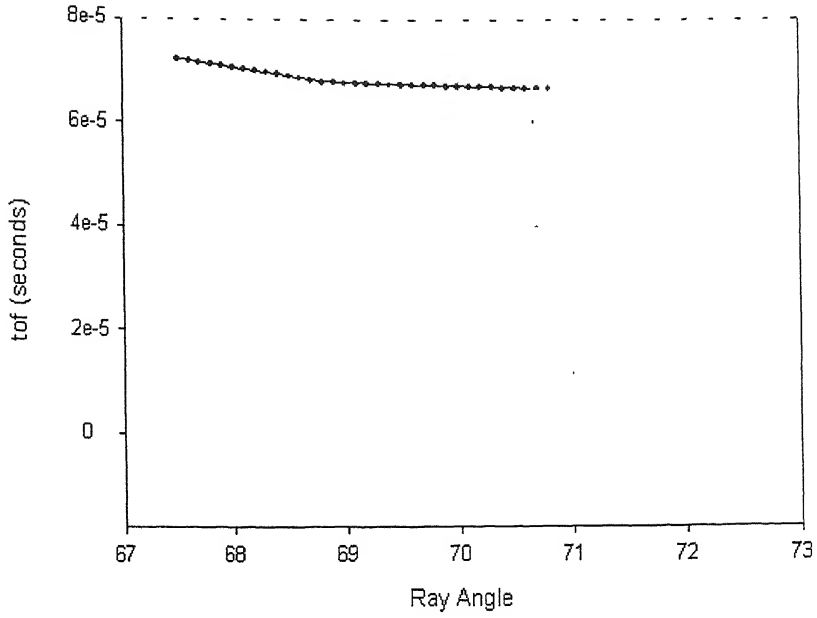

Figure 6.32 Time of flight data for a fan beam incident on a rectangular defect

Figure 6.30 (a) and (b) shows the 60^0 ray paths in a composite having a circular defect and the time of flight for each ray of the fan beam. It can be observed that between phase angle 61.8 to 62^0 there is no ray reaching to the opposite face and thus no time of flight recorded.

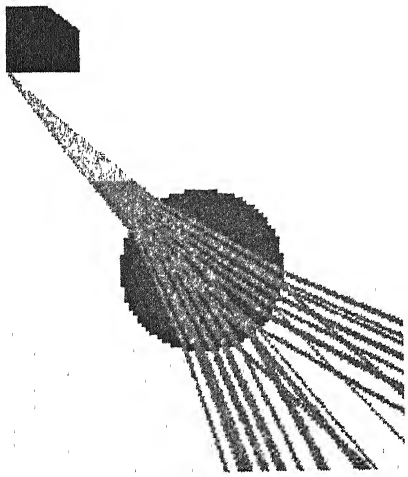

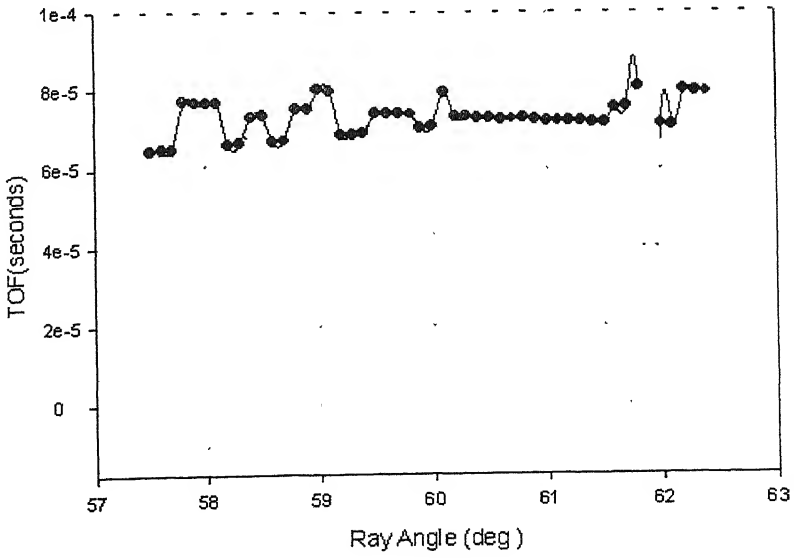

Figure 6.33 Time of flight data for a fan beam incident on a circular defect

Chapter 7
Conclusions and Scope for Future work

7.1 Conclusions

A two - dimensional numerical model has been developed which allows for the tracing of ultrasonic rays within a component, all or part of which may be inhomogeneous and anisotropic. From this model an understanding of physical reasons for the difficulties associated with ultrasonic inspection through composite materials has been gained. The model seems to be very useful to predict and understand the effects leading to beam distortion in anisotropic media. From the model developed in the present work following conclusions can be drawn.

- The direction of energy flow in general does not coincide with wave vector direction when an elastic wave propagates in anisotropic media. Therefore, it is possible that the incident wave vector can be directed towards the interface but the energy can propagate outward from the interface.
- Unlike isotropic case incident wave transformed into the three possible reflected and transmitted modes (i.e. pure shear, quasi-longitudinal and quasi shear).
- The wave propagation velocities (i.e. phase and group velocity) are maximum when wave propagates in a direction parallel to the fiber direction.
- It has been found that if a specimen is scanned across a surface at constant beam angle, there is a possibility that ultrasonic ray energy may not penetrate certain regions. Therefore in such cases to ensure that the whole component can be examined, more than one probe angle may be needed.
- The model is found to be a powerful tool in the numerical simulation of elastic wave propagation in transversely isotropic media. From the results it is found that the technique clearly models the special behavior of ultrasonic waves in such media.

7.2 Scope for Future work

- In the present model although calculation of reflection angles is done but only the refracted waves has been plotted. The model can be extended so that it can also plot reflected waves.
- Calculation of reflection and refraction coefficients can be incorporated in the model.
- Automatic change of step size for a ray path depending on then local rate of change of material properties. This should make the model more efficient when an inhomogeneous region has widely differing properties in different parts of the region.

References

1. Chen H.C, "Theory of Electromagnetic Waves-A coordinate free approach (McGraw-Hill, New York, 1983)
2. Synge, J. L, "Elastic waves in anisotropic media", *J. Math. and Phys.*, Vol.35, 1957, pp 323-334
3. Musgrave M.J.P, "Crystal Acoustics", Holden Day, 1970
4. Silk, "A computer model for ultrasonic propagation in complex orthotropic structure", Ultrasonics, Vol. 19, 1981, pp 208-212
5. Ogilvy J.A, " A model for ultrasonic inspection of composite plates", Ultrasonics Vol. 33, No. 2, 1995, pp 85-93
6. Leander J.L, "On the relation between wavefront speed and the group velocity concept", Journal of Acoustical society of America, Vol. 100, No. 6, December 1996, pp 3503-3507
7. Crandall S.H, "On the use of Slowness diagrams to represent wave reflections", Journal of Acoustical society of America, Vol. 47, No. 5, 1970, pp 1338-1342
8. Fedorov F.I, "Theory of Elastic Waves in Crystals", Plenum Press, 1968
9. Auld B.A, "Acoustic Fields and Waves in Solids", Vols. I and II, Wiley-Interscience, 1973.
10. Henneke E.G, "Reflection – Refraction of a stress wave at a plane boundary between anisotropic media", Journal of Acoustical society of America, Vol. 51, No. 2, August 1972, pp 210-217
11. McNiven H.D, Mengi Y, " Critical angles associated with the reflection-refraction of elastic waves at an interface", Journal of Acoustical society of America, Vol. 44,No. 6, 1968, pp 1658-1663
12. Vandenbossche B, Kriz R.D, Oshima T, " Stress-Wave displacement and attenuation in unidirectional composites: Theory and Experiment", Res. Nondestructive Evaluation, Vol. 8, 1996, pp 101-123

13. Rokhlin S.I, Bolland T.K, Adler L, "Reflection and Refraction of elastic waves on a plane interface between two generally anisotropic media", Journal of Acoustical society of America, Vol. 79, No. 4, April 1986, pp 210-217

14. Ogilvy J.A, "The influence of Austenitic weld geometry and manufacture on ultrasonic inspection of welded joints" British Jr. of NDT, V29, 1987, pp 147-155

15. Ogilvy J.A, "Computerized ultrasonic ray tracing in austenitic steel ", NDT International, Vol. 18, No. 2, April 1985, pp 67-77

16. Ogilvy J.A,"An iterative ray tracing model for ultrasonic nondestructive testing", NDT & E International, Vol. 25, 1992, pp 3-9

17. Schmitz V, Walte F, Chaklov S.V, "3D ray tracing in austenite materials", NDT & E International, Vol. 32, 1999, pp 201-213

18. Harker A.H, Ogilvy J.A, " Coherent wave propagation in inhomogeneous materials: a comparison of theoretical models", Ultrasonics, Vol. 29, 1991, pp 235-243

19. Spies M, "Elastic wave propagation in general transversely isotropic media. I. Green's function and elastodynamic holography", Journal of Acoustical society of America, Vol. 96, No. 2, August 1994, pp 1144-1157

20. Kishore N.N, Jaleel K.M.A, Sundararajan V, " Finite element simulation of elastic wave propagation in Orthotropic composite materials", Materials Evaluation, July 1993

21. Degtyar A.D, Rokhlin S.I, "Comparison of elastic constant determination in anisotropic materials from ultrasonic group velocities data", Journal of Acoustical society of America, Vol. 102, No. 6, December 1997, pp 3458-3466

22. Spies M, "Elastic waves in homogeneous and layered transversely isotropic media: Plane waves and Gaussian wave packets. A general approach", Journal of Acoustical society of America, Vol. 95, No. 4, April 1994, pp 1748-1760

23. Karal F.C, Keller J.B, "Elastic wave propagation in homogeneous and inhomogeneous media", Journal of Acoustical society of America, Vol. 31, No. 6, June 1959, pp 694-705

24. Mandal B, " Reflection and transmission properties of elastic waves on a plane interface for general anisotropic media", Journal of Acoustical society of America, Vol. 90 (2), August 1991, pp 1106-1118

25. Graff K.F, " Wave motion in elastic solids", Oxford University Press, 1975

26. Achenbach J.D, " Wave Propagation in elastic solids", North-Holland Publishing Co, 1973

Appendix – A

This appendices will describe the numerical technique used for the solution of the forth order characteristic polynomial, the roots of which will give the z- component of slowness vectors. The polynomial is given by Eq. (4.28)

$$\begin{aligned}&(m_z^{q\beta})^4(a_q + b_q a_z^2 + c_q a_z^4) + (m_z^{q\beta})^3 \cdot 2a_x a_z m_x (b_q + 2c_q a_z^2)\\&+ (m_z^{q\beta})^2 (m_x^2[2a_q + b_q(a_x^2 + a_z^2) + 6c_q a_x^2 a_z^2] + d_q + e_q a_z^2)\\&+ (m_z^{q\beta}) \cdot 2a_x a_z m_x (m_x^2(b_q + 2c_q a_x^2) + e_q)\\&+ m_x^4(a_q + b_q a_x^2 + c_q a_x^4) + m_x^2(d_q + e_q a_x^2) + f_q = 0\end{aligned} \qquad \text{(a-1)}$$

The Eigen value method has been used for solving the above polynomial.

Eigen value Methods

The eigen values of a matrix **A** are the roots of the "characteristic polynomial" P(x) =det[**A** - x**I**]. This method is very efficient in terms of convergence and order of error. It can be easily verified that characteristic polynomial of the special $m \times n$ matrix

$$\begin{pmatrix} -\frac{a_{m-1}}{a_m} & -\frac{a_{m-1}}{a_m} & \cdots & -\frac{a_1}{a_m} & -\frac{a_0}{a_m} \\ 1 & 0 & \cdots & 0 & 0 \\ \vdots & \vdots & & \vdots & \vdots \\ 0 & 0 & \cdots & 1 & 0 \\ 0 & 0 & \cdots & 0 & 1 \end{pmatrix} \qquad \text{(a-2)}$$

is equivalent to the general polynomial

$$P(x) = \sum_{i=0}^{m} a_i x^i \qquad \text{(a-3)}$$

If the coefficients a_i are real, rather than complex, then the eigen values of **A** can be found using the routines "balance" and "hqr". It is a more robust technique, largely because of the fairly sophisticated convergence methods embodied in "hqr" routine.The method is to construct an upper Hessenberg matrix whose eigenvalues are the desired roots, and then use the routines balanc and hqr.

Reduction to Hessenberg Form

The strategy for finding the eigen system of a general matrix parallels that of the symmetric case. First the matrix is reduced to a simpler form, and then an iterative procedure is perfomed on the simplified matrix. The simpler structure we use here is called Hessenberg form. An upper Hessenberg matrix has zeros everywhere below the diagonal except for the first sub diagonal row. For example, in the 6×6 case, the nonzero elements are:

$$\begin{bmatrix} \times & \times & \times & \times & \times & \times \\ \times & \times & \times & \times & \times & \times \\ & \times & \times & \times & \times & \times \\ & & \times & \times & \times & \times \\ & & & \times & \times & \times \\ & & & & \times & \times \end{bmatrix}$$

Such a structure can be achieved by a sequence of Householder transformations.Householder reduction to Hessenberg form is in fact an accepted technique. An alternative, however, is a procedure analogous to Gaussian elimination with pivoting. This elimination procedure has been used in present work since it is about a factor of 2 more efficient than the Householder method.

Before the rth stage, the original matrix A has become A_r , which is upper Hessenberg in its first r - 1 rows and columns. The rth stage then consists of the following sequence of operations:

- Find the element of maximum magnitude in the rth column below the diagonal. If it is zero the stage is done. Otherwise, suppose the maximum element was in row r'
- Interchange rows r' and r + 1. This is the pivoting procedure. To make the permutation a similarity transformation, also interchange columns r' and r + 1.
- For i = r+2, r+3,……,N, compute the multiplier

$$n_{i,r+1} = \frac{a_{ir}}{a_{r+1,r}} \qquad \text{(a-4)}$$

Subtract $n_{i,r+1}$ times row r+1 from row i. To make the elimination a similarity transformation, also add $n_{i,r+1}$ times column i to column r+1. A total of N - 2 such stages are required.

When the magnitudes of the matrix elements vary over many orders, try should be done to rearrange the matrix so that the largest elements are in the top left-hand corner. This reduces the roundoff error, since the reduction proceeds from left to right.

Balancing

The sensitivity of eigen values to rounding errors during the execution of some algorithms can be reduced by the procedure of balancing. The errors in the eigen system found by a numerical procedure are generally proportional to the Euclidean norm of the matrix, that is, to the square root of the sum of the squares of the elements. The idea of balancing is to use similarity transformations to make corresponding rows and columns of the matrix have comparable norms, thus reducing the overall norm of the matrix while leaving the eigen values unchanged. A symmetric matrix is already balanced.

Balancing is a procedure with of order N^2 operations. Thus, the time taken by the procedure of balancing, should never be more than a few percent of the total time required to find the eigen values. It is therefore recommended always to balance nonsymmetric matrices. It never

hurts, and it can substantially improve the accuracy of the eigen values computed for a badly balanced matrix.

The actual algorithm consists of a sequence of similarity transformations by diagonal matrices D. The output is a matrix that is balanced in the norm given by summing the absolute magnitudes of the matrix elements. This is more efficient than using the Euclidean norm, and equally effective: A large reduction in one norm implies a large reduction in the other.

The QR Algorithm for Real Hessenberg Matrices

The QR algorithm with shifts can be given as

$$\mathbf{Q}_s \cdot (\mathbf{A}_s - k_s \mathbf{I}) = \mathbf{R}_s \qquad \text{(a-5)}$$

where **Q** is orthogonal and **R** is upper triangular, and

$$\begin{aligned} \mathbf{A}_{s+1} &= \mathbf{R}_s \cdot \mathbf{Q}_s + k_s \mathbf{I} \\ &= \mathbf{Q}_s \cdot \mathbf{A}_s \cdot \mathbf{Q}_s^T \end{aligned} \qquad \text{(a-6)}$$

The *QR* transformation preserves the upper Hessenberg form of the original matrix **A=A1**, and the workload on such a matrix is $O(n^2)$ per iteration as opposed to $O(n^3)$ on a general matrix. As $s \longrightarrow \infty$, $\mathbf{A}_s$ converges to a form where the eigen values are either isolated on the diagonal or are eigen values of a 2×2 submatrix on the diagonal.

A key difference here is that a nonsymmetric real matrix can have complex eigenvalues. This means that good choices for the shifts k_s may be complex, apparently necessitating complex arithmetic.

Complex arithmetic can be avoided, however, by a clever trick. The trick depends on a lemma which states that if **B** is a nonsingular matrix such that

$$\mathbf{B} \cdot \mathbf{Q} = \mathbf{Q} \cdot \mathbf{H} \qquad \text{(a-7)}$$

where $\mathbf{Q}$ is orthogonal and $\mathbf{H}$ is upper Hessenberg, then $\mathbf{Q}$ and $\mathbf{H}$ are fully determined by the first column of $\mathbf{Q}$.

The lemma is used in practice by taking two steps of the *QR* algorithm, either with two real shifts k_s and k_{s+1}, or with complex conjugate values k_s and $k_{s+1} = k_s^*$. This gives a real matrix $\mathbf{A}_{s+2}$, where

$$\mathbf{A}_{s+2} = \mathbf{Q}_{s+1} \cdot \mathbf{Q}_s \cdot \mathbf{A}_s \cdot \mathbf{Q}_s^T \cdot \mathbf{Q}_{s+1}^T \qquad \text{(a-8)}$$

The $\mathbf{Q}$'s are determined by

$$\mathbf{A}_s - k_s \mathbf{I} = \mathbf{Q}_s^T \cdot \mathbf{R}_s \qquad \text{(a-9)}$$

$$\mathbf{A}_{s+1} = \mathbf{Q}_s \cdot \mathbf{A}_s \cdot \mathbf{Q}_s^T \qquad \text{(a-10)}$$

$$\mathbf{A}_{s+1} - k_{s+1} \mathbf{I} = \mathbf{Q}_{s+1}^T \cdot \mathbf{R}_{s+1} \qquad \text{(a-11)}$$

Using Eq. (a-10), Eq. (A-11) can be rewritten

$$\mathbf{A}_{s+1} - k_{s+1} \mathbf{I} = \mathbf{Q}_s^T \cdot \mathbf{Q}_{s+1}^T \cdot \mathbf{R}_{s+1} \cdot \mathbf{Q}_s \qquad \text{(a-12)}$$

Hence, if

$$\mathbf{M} = (\mathbf{A}_s - k_{s+1} \mathbf{I}) \cdot (\mathbf{A}_s - k_s \mathbf{I}) \qquad \text{(a-13)}$$

Equations (a-9) and (a-12) gives

$$\mathbf{R} = \mathbf{Q} \cdot \mathbf{M} \qquad \text{(a-14)}$$

where

$$\mathbf{Q} \doteq \mathbf{Q}_{s+1} \cdot \mathbf{Q}_s \qquad \text{(a-15)}$$

$$\mathbf{R} = \mathbf{R}_{s+1} \cdot \mathbf{R}_s \qquad \text{(a-16)}$$

Hence Eq.(a-8) can be rewritten as

$$\mathbf{A}_s \cdot \mathbf{Q}^T = \mathbf{Q}^T \cdot \mathbf{A}_{s+2} \qquad \text{(a-17)}$$

Thus suppose there is an upper Hessenberg matrix $\mathbf{H}$ such that

$$\mathbf{A}_s \cdot \overline{\mathbf{Q}}^T = \overline{\mathbf{Q}}^T \cdot \mathbf{H} \qquad \text{(a-18)}$$

where $\overline{\mathbf{Q}}$ is orthogonal. If $\overline{\mathbf{Q}}^T$ has the same first column as $\mathbf{Q}^T$ (i.e. $\overline{\mathbf{Q}}$ has the same first row as Q), then $\overline{\mathbf{Q}} = \mathbf{Q}$ and $\mathbf{A}_{s+2} = \mathbf{H}$.

The first row of $\mathbf{Q}$ is found as follows. Equation (a-14) shows that $\mathbf{Q}$ is the orthogonal matrix that triangularizes the real matrix **M**. any real matrix can be triangularized by premultiplying it by a sequence of Householder matrices $\mathbf{P}_1$ (acting on the first column), P2 (acting on the second column), ... , $\mathbf{P}_{n-1}$. Thus $\mathbf{Q} = \mathbf{P}_{n-1} \ldots\ldots \mathbf{P}_2 \cdot \mathbf{P}_1$, and the first row of $\mathbf{Q}$ is the first row of $\mathbf{P}_1$ since $\mathbf{P}_1$ is an $(i-1)\times(i-1)$ identity matrix in the top left-hand corner. Now $\mathbf{Q}$ must be find satisfying (a-17) whose first row is that of $\mathbf{P}_1$.

The Householder matrix $\mathbf{P}_1$ is determined by the first column of **M**. Since $\mathbf{A}_s$ is upper Hessenberg, Eq.(a-13) shows that the first column of **M** has the form $[p_1, q_1, r_1, 0, \ldots, 0]$, where

$$\begin{aligned} p_1 &= a_{11}^2 - a_{11}(k_s + k_{s+1}) + k_s k_{s+1} + a_{12} a_{21} \\ q_1 &= a_{21}(a_{11} + a_{22} - k_s - k_{s+1}) \\ r_1 &= a_{21} a_{32} \end{aligned} \qquad \text{(a-19)}$$

Hence

$$\mathbf{P}_1 = 1 - 2\mathbf{w}_1 \cdot \mathbf{w}_1^T \qquad \text{(a-20)}$$

where $\mathbf{w}_1$ has only its first 3 elements nonzero. The matrix $\mathbf{P}_1 \cdot \mathbf{A}_s \cdot \mathbf{P}_1^T$ is therefore upper Hessenberg with 3 extra elements:

$$\mathbf{P}_1 \cdot \mathbf{A}_s \cdot \mathbf{P}_1^T = \begin{bmatrix} \times & \times & \times & \times & \times & \times & \times \\ \times & \times & \times & \times & \times & \times & \times \\ \mathbf{x} & \times & \times & \times & \times & \times & \times \\ \mathbf{x} & \mathbf{x} & \times & \times & \times & \times & \times \\ & & & \times & \times & \times & \times \\ & & & & \times & \times & \times \\ & & & & & \times & \times \end{bmatrix} \qquad \text{(a-21)}$$

This matrix can be restored to upper Hessenberg form without affecting the first row by a sequence of Householder similarity transformations. The first such Householder matrix, $\mathbf{P}_2$, acts on elements 2, 3, and 4 in the first column, annihilating elements 3 and 4. This produces a matrix of the same form as (a-21), with the 3 extra elements appearing one column over:

$$\begin{bmatrix} \times & \times & \times & \times & \times & \times & \times \\ \times & \times & \times & \times & \times & \times & \times \\ & \times & \times & \times & \times & \times & \times \\ & \mathbf{x} & \times & \times & \times & \times & \times \\ & \mathbf{x} & \mathbf{x} & \times & \times & \times & \times \\ & & & & \times & \times & \times \\ & & & & & \times & \times \end{bmatrix}$$

Proceeding in this way up to $\mathbf{P}_{n-1}$, it is seen that at each stage the Householder matrix $\mathbf{P}_r$ has a vector $\mathbf{w}_r$ that is nonzero only in elements r, $r + 1$, and $r + 2$.These elements are determined by the elements r, $r + 1$, and $r + 2$ in the $(r - 1)$st column of the current matrix. Note that the preliminary matrix $\mathbf{P}_1$ has the same structure as $\mathbf{P}_2,\ldots,\mathbf{P}_{n-1}$.

The result is that

$$\mathbf{P}_{n-1} \cdots \mathbf{P}_2 \cdot \mathbf{P}_1 \cdot \mathbf{A}_S \cdot \mathbf{P}_1^T \cdot \mathbf{P}_2^T \cdots \mathbf{P}_{n-1}^T = \mathbf{H} \qquad \text{(a-22)}$$

where $\mathbf{H}$ is upper Hessenberg. Thus

$$\overline{\mathbf{Q}} = \mathbf{Q} = \mathbf{P}_{n-1} \cdots \mathbf{P}_2 \cdot \mathbf{P}_1 \qquad \text{(a-23)}$$

and

$$\mathbf{A}_{s+2} = \mathbf{H} \qquad \text{(a-24)}$$

The shifts of origin at each stage are taken to be the eigenvalues of the 2×2 matrix in the bottom right-hand corner of the current $\mathbf{A}_s$. This gives

$$\begin{aligned} k_s + k_{s+2} &= a_{n-1,n-1} + a_{n,n} \\ k_s k_{s+1} &= a_{n-1,n-1} a_{n,n} - a_{n-1,n} a_{n,n-1} \end{aligned} \qquad \text{(a-25)}$$

Substituting Eq.(a-25) in Eq.(a-19) gives

$$p_1 = a_{22}\{[(a_{nn} - a_{11})(a_{n-1,n-1} - a_{11}) - a_{n-1,n}a_{n,n-1}]/a_{21} + a_{12}\}$$
$$q_1 = a_{21}[a_{22} - a_{11} - (a_{nn} - a_{11}) - (a_{n-1,n-1} - a_{11})] \qquad \text{(a-26)}$$
$$r_1 = a_{21}a_{32}$$

here terms are judiciously grouped to reduce possible roundoff when there are small off-diagonal elements. Since only the ratios of elements are relevant for a Householder transformation, we can omit the factor a_{21} from Eq.(a-26)

In summary, to carry out a double QR step we construct the Householder matrices $\mathbf{P}_r$, r = 1,....,n-1. For $\mathbf{P}_1$ we use p_1, q_1, and r_1 given by Eq.(a-26). For the remaining matrices p_r, q_r, and r_r are determined by the (r, r+1), (r+1,r+1), and (r+2,r-1) elements of the current matrix.

There are two possible ways of terminating the iteration for an eigen value. First, if $a_{n,n-1}$ become negligible then a_{nn} is an eigen value. Then delete the n^{th} row and column of the matrix and look for the next eigen value. Alternatively, $a_{n-1,n-2}$ may become negligible. In this case the eigen values of the 2×2 matrix in the lower right-hand corner may be taken to be eigen values. Then delete the n^{th} and $(n-1)^{th}$ rows and columns of the matrix and continue.

Appendix – B

This appendix shows the various user interfaces provided for input the data like component size, material elastic properties, fiber angle, probe angle and wave modes etc.

Basic View

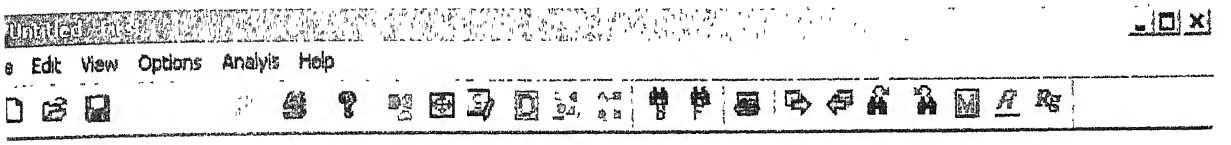

Component size

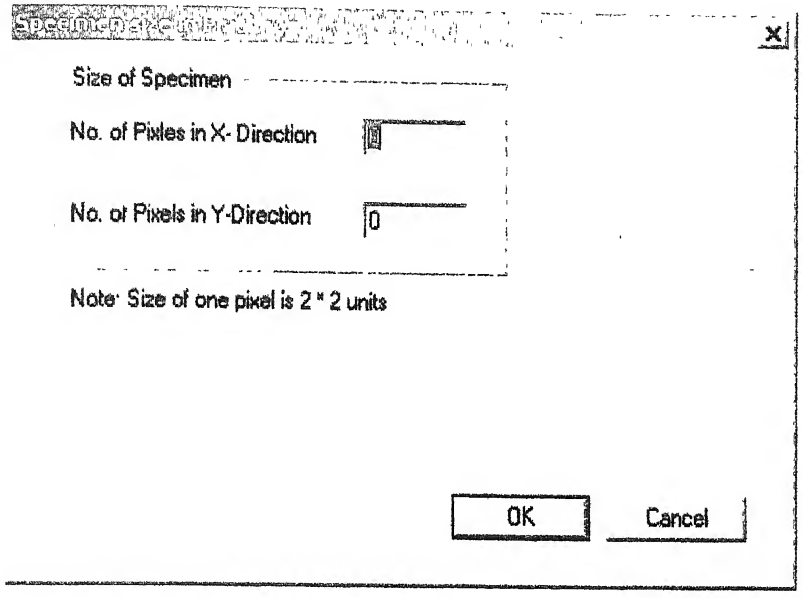

Probe Angle

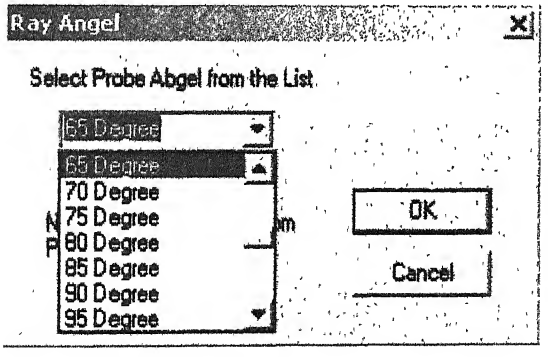

Base Material

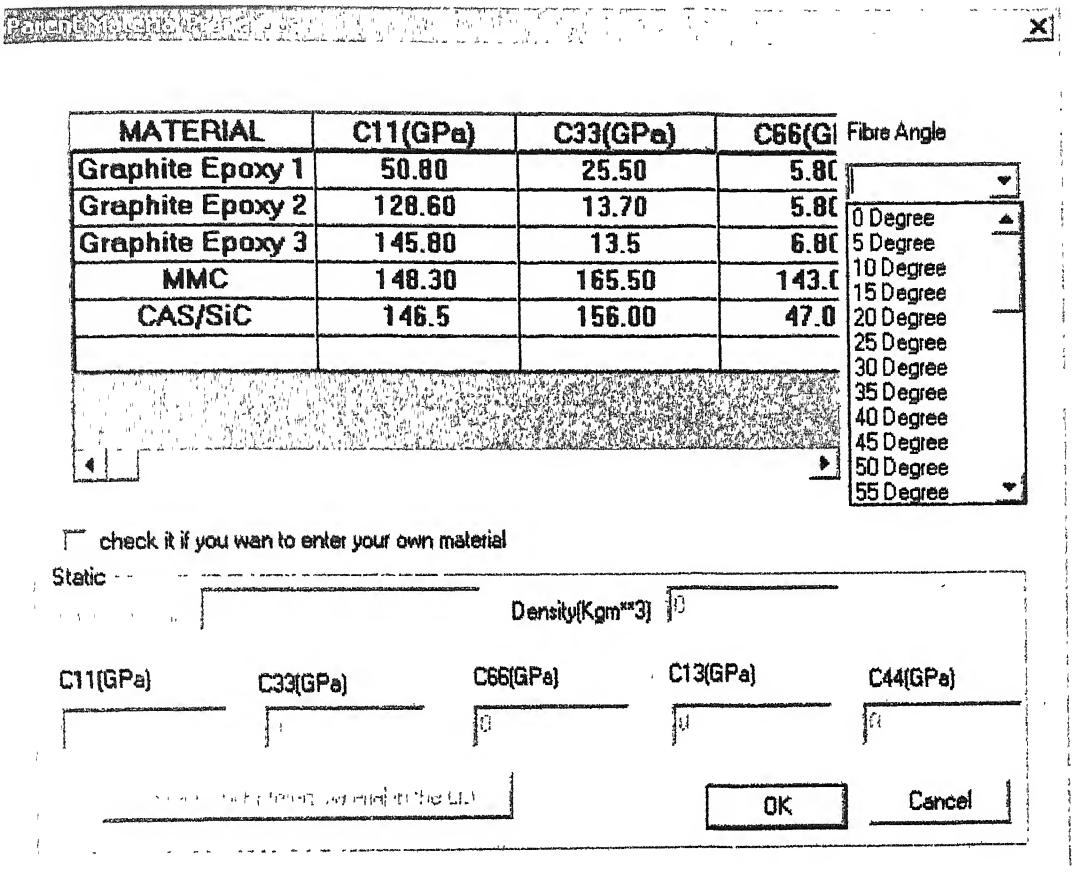

Defect Shape

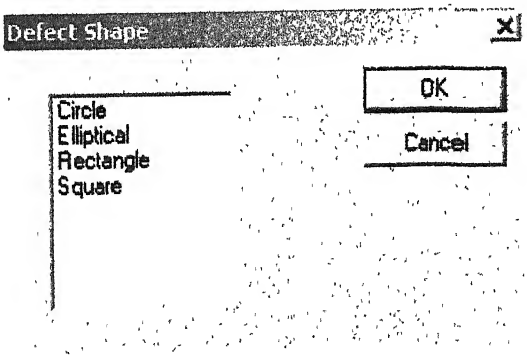

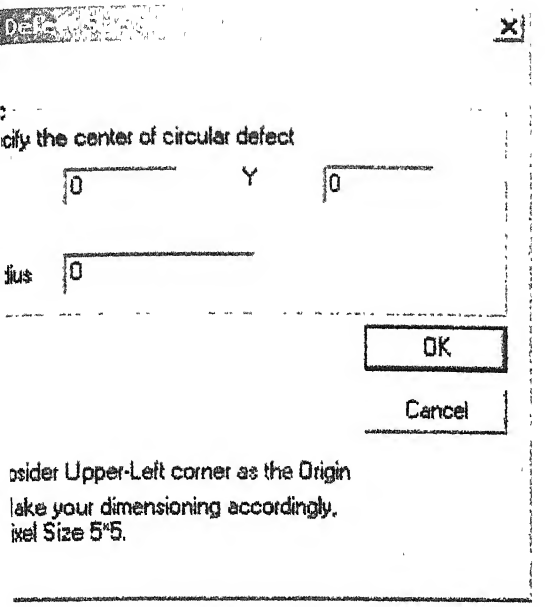
cify the center of circular defect
0
Y
0
dius
0
OK
Cancel
sider Upper-Left corner as the Origin
lake your dimensioning accordingly.
ixel Size 5*5.

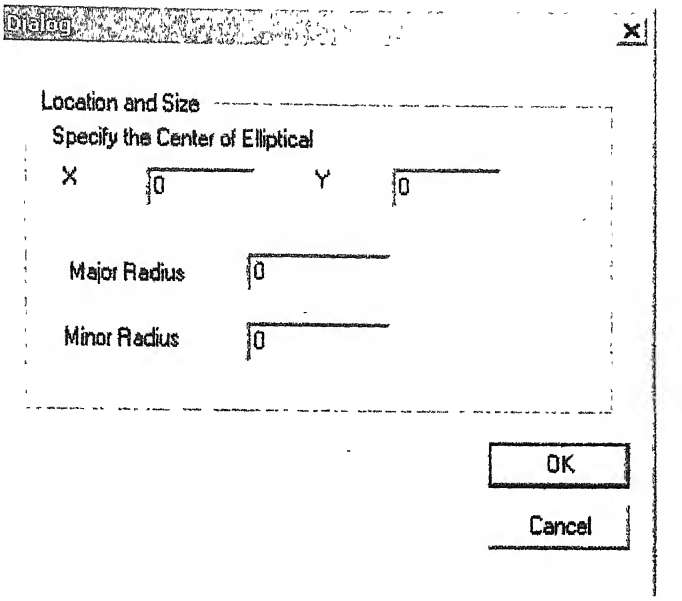
Dialog
Location and Size
Specify the Center of Elliptical
X
0
Y
0
Major Radius
0
Minor Radius
0
OK
Cancel

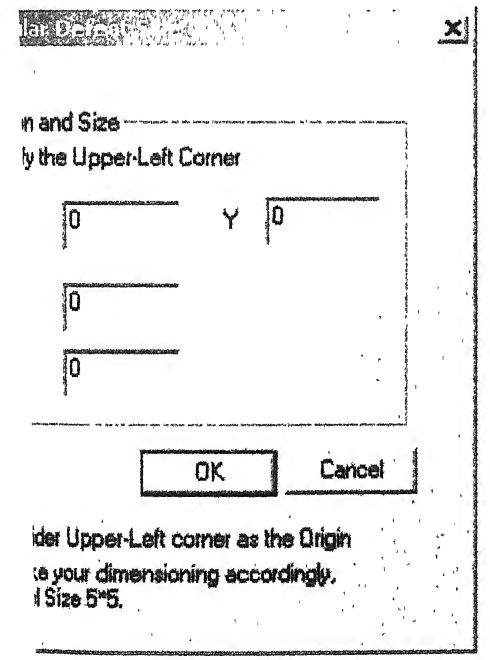
n and Size
ly the Upper-Left Corner
0
Y
0
0
0
OK
Cancel
ider Upper-Left corner as the Origin
e your dimensioning accordingly.
l Size 5*5.

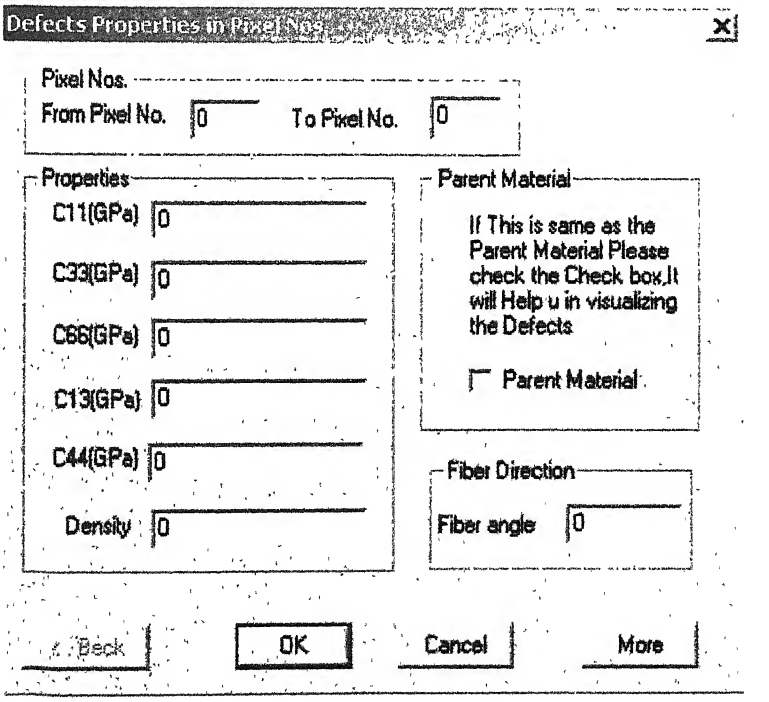
Defects Properties in Pixel Nos
Pixel Nos.
From Pixel No.
0
To Pixel No.
0
Properties
C11(GPa)
0
C33(GPa)
0
C66(GPa)
0
C13(GPa)
0
C44(GPa)
0
Density
0
Parent Material
If This is same as the Parent Material Please check the Check box,It will Help u in visualizing the Defects
Parent Material
Fiber Direction
Fiber angle
0
Back
OK
Cancel
More

Analysis for ray paths

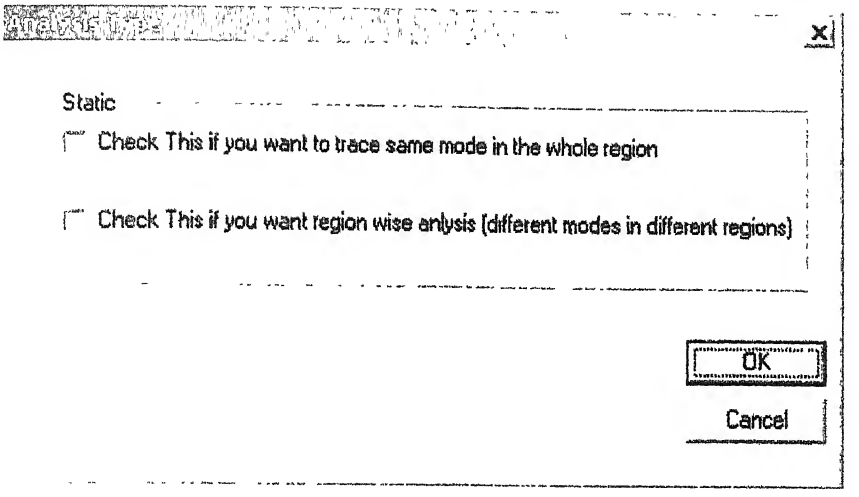

Wave modes

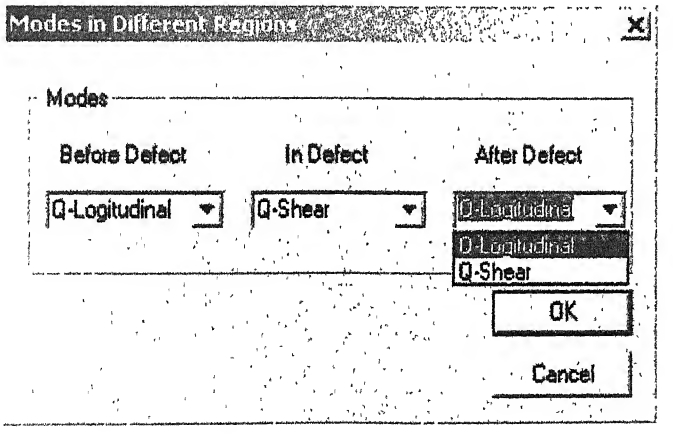

Scanner position

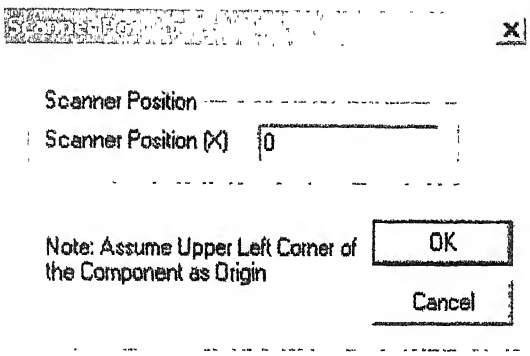

Receiver Information

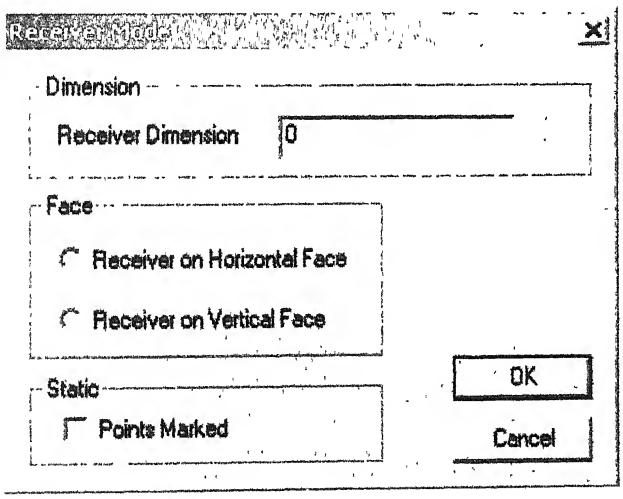

Appendix-C

This appendix will describe the file structure of the program developed in the present work and it will discuss the various subroutines used in the program.

File Structure

In whole about 30 source code files and 25 header file are there in the program. Each file performs a specific task. The basic structure of the whole program based on these files is iven in the flow chart below.

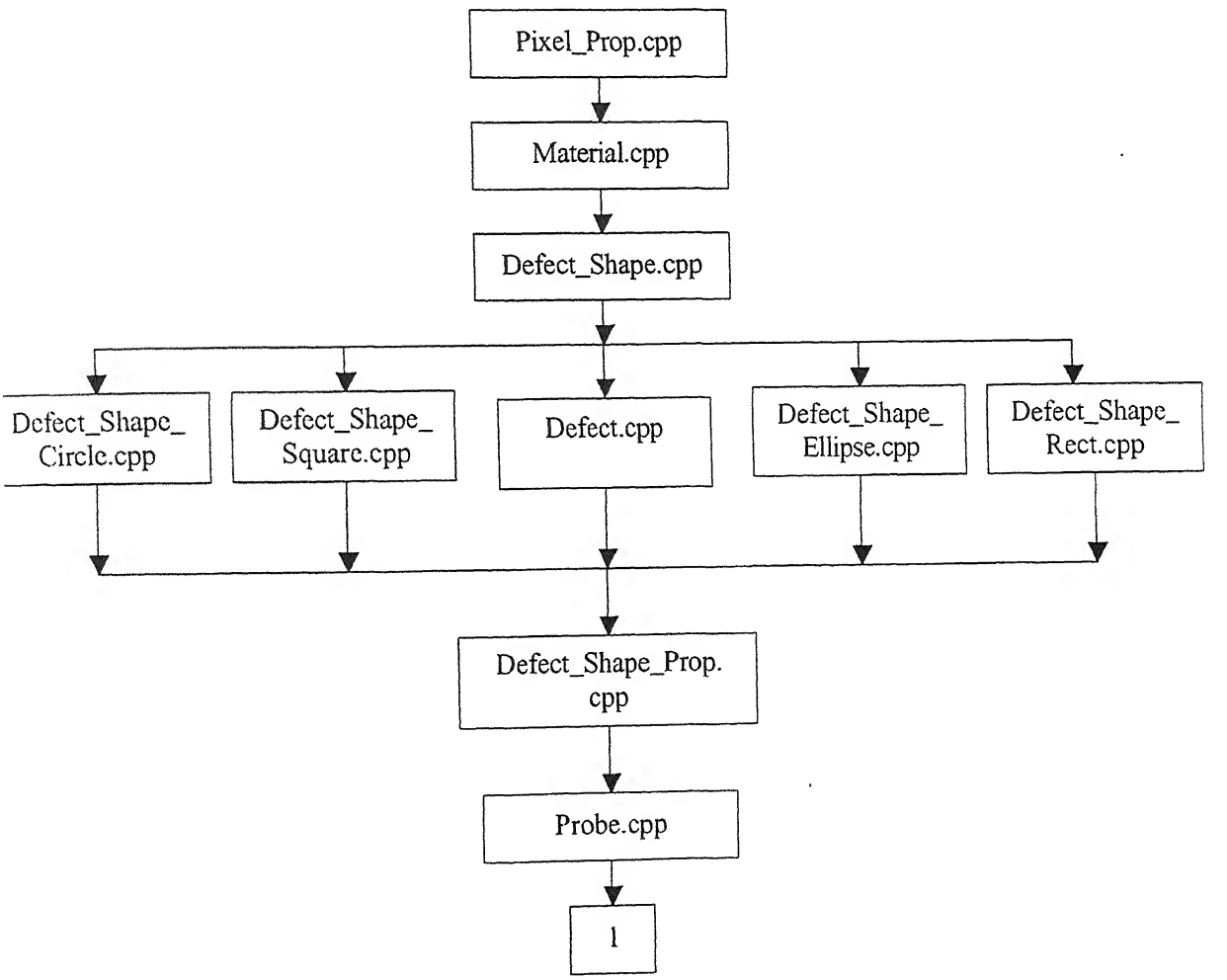

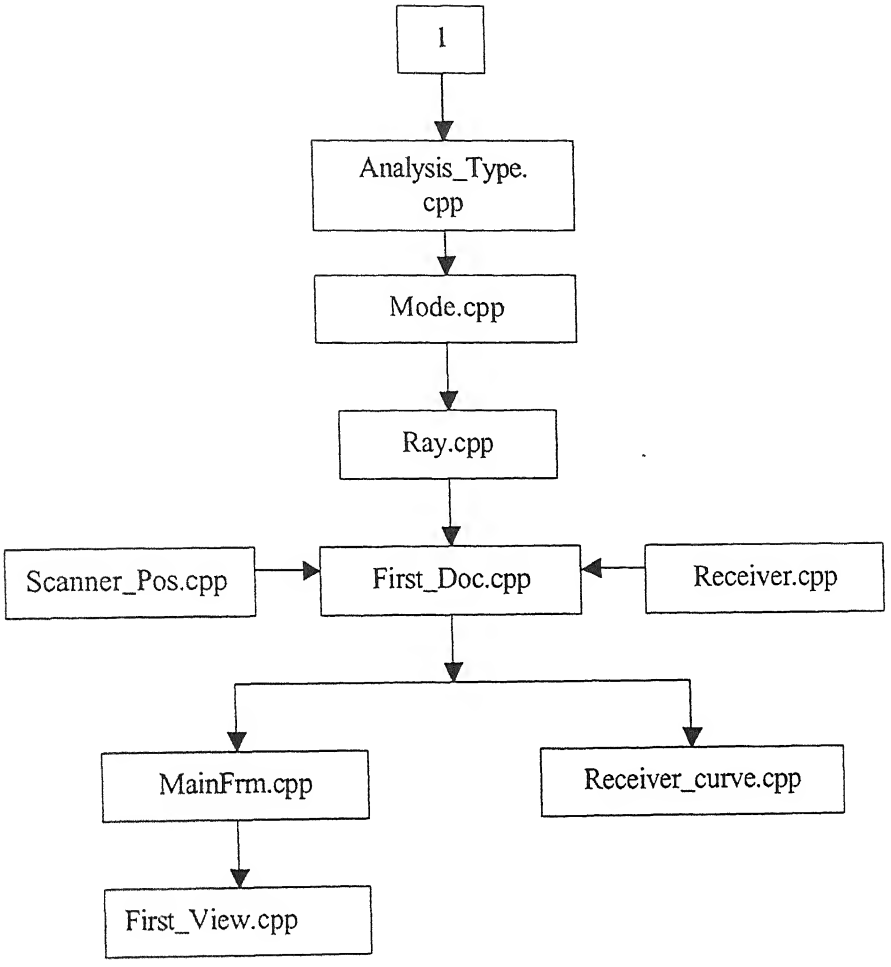

Function of various files

Pixel_Prop.cpp: It gathers the component size information from user and sends it for analysis

Material.cpp: It gathers the base material propaerties from user and sends it for analysis.

Defect_Shape.cpp: It determines the shape of the defect.

Defect_Shape_Circle.cpp: It gathers the size and location information of circular defect and sends it for analysis.

Defect_Shape_Rect.cpp: It gathers the size and location information of elliptical defect and sends it for analysis.

Defect_Shape_Ellipse.cpp: It gathers the size and location information of rectangular defect and sends it for analysis.

Defect.cpp: It takes care if there is any particular pixel or group of pixels defective.

Defect_Shape_Prop.cpp: It collects the defect properties for any shape or pixel.

Probe.cpp: It gathers the probe angle information from user and sends it for analysis.

Analysis_Type.cpp: It finds out that user is interested to do fanbeam or parallel beam analysis.

Mode.cpp: It gathers the wave mode for analysis.

Ray.cpp: It stores the starting point etc. data for each ray.

Scanner_Pos.cpp: It gathers the scanner position for analysis.

Receiver.cpp: It collects the receiver size location etc. information.

First_Doc.cpp: This file contains all the analysis subroutines. This is the mind of the whole program.

First_View.cpp: This file contains all the plotting subroutines. This is the heart of the whole program.

Receiver_curve: It calculates the data for signal strength at different faces and plots the curve.

Subroutines

There are around 55 subroutines in the whole code. The main subroutines and their functions are as follows:

main_beam: It analyses the input data for parallel beam of rays.

main_fanrays: It analyses the input data for fan beam of rays.

christoffel_soln: It solves the Christoffel's equation. It finds the group velocity and group angles for every step.

ray_tracing: It calculates the ray path for the given group velocity and angle.

ray_tip_in_pixel: It calculates the pixel nos. in which tip and tail of pixel lies for a particular step.

find_slowness_parallel: It calculates the parallel component of slowness vector.

zrhqr, balance and hqr: This are numerical techniques used for solving the fourth order polynomial.

look_for_realroots: It calculates the normal component of slowness vector

group_vel_spies: It calculates the group velocity.

step_forward: It forward the ray by the stepsize defined previously.

check_for_crossing: It checks whether the ray has cross any boundary or not.

reduced_stepsize: It sends back the ray to interface if ray has crossed any interface.

output: It stores the coordinates of complete path of the ray and send it for plotting.

OnDraw: It plots the ray paths.